Graz University of Technology

Masterthesis

Calibration of 2D pre-relaxation factors in tunnelling with 3D Finite element calculations

Submitted at the

Institute of

Soil Mechanics and Foundation Engineering

Graz University of Technology

July 2012

Author: Johanna Zelger, BSc

Examiners: Ao. Univ.-Prof. Dipl. Ing. Dr. techn. M. Sc. tit. Univ.-Prof. Helmut F. Schweiger

Dipl. Ing. Franz Tschuchnigg

EIDESSTATTLICHE ERKLÄRUNG

Ich erkläre an Eides statt, dass ich die vorliegende Arbeit selbstständig und ohne fremde Hilfe verfasst, andere als die angegebenen Quellen nicht benutzt und die den benutzten Quellen wörtlich und inhaltlich entnommenen Stellen als solche erkenntlich gemacht habe.

Graz, Juli 2012

Johanna Zelger

DANKSAGUNG

An dieser Stelle bedanke ich mich bei den Mitarbeitern des Instituts für Bodenmechanik und der Grundbau für die hervorragende Betreuung beim Verfassen dieser Arbeit, insbesondere bei Franz Tschuchnigg und Bert Schädlich, welche immer ein offenes Ohr für Fragen hatten.

Weiter möchte ich mich bei meinen Eltern bedanken, welche mir das Studium überhaupt erst ermöglicht haben.

Ein großes Dankeschön geht an meine *Hennen* zu Hause, welche mich immer unterstützt haben, sowie an meine Freunde in Graz, ohne die meine Zeit hier nicht so schön gewesen wäre.

ABSTRACT

Due to increasing computing capacities over the past years the use of 3D Finite element analysis in underground design has become more common. Nevertheless, 3D calculations are time consuming and the necessary numerical tools may not always be available. In engineering practice empirical methods and 2D Finite Element analysis are used for tunnel design. The development of stresses and deformations due to tunnelling, however, is a complex three-dimensional problem. Reliable approximations are necessary.

In this thesis tunnel induced settlements and internal lining forces are investigated for a non-circular tunnel in clay-/siltstone. The tunnel is constructed according to the principles of the New Austrian Tunnelling Method. 3D FE-analyses are compared with frequently used empirical methods and 2D FE-analyses. To account for three-dimensional stress redistribution in 2D the stress reduction method is used.

The load reduction factor β is determined by calibration with 3D FE-analysis. Different reference values, constitutive models and stiffness parameters are compared. The obtained values are mainly influenced by the used reference value, ground water conditions and drainage type. Furthermore, the initial stress state and the soil model are shown to have an impact on the load reduction factor.

KURZFASSUNG

In den letzten Jahren hat die Anwendung von 3D Finite Elemente Berechnungen aufgrund höherer Rechenleistungen zugenommen. 3D Berechnungen bleiben aber weiterhin sehr zeitintensiv. In der Praxis sind empirische Methoden und 2D FE-Verfahren für die Bemessung im Tunnelbau weiterhin Standard. Die Verteilung der Spannungen und Verformungen ist jedoch ein dreidimensionales Phänomen.

In dieser Arbeit werden die durch den Bau eines NATM – Tunnels in Ton-/Sandstein hervorgerufenen Setzungen und Schnittkräfte in der Tunnelschale untersucht. Die Überlagerung beträgt im Schnitt 25 Meter. Die Ergebnisse der 3D FE- Berechnungen werden mit gängigen empirischen Methoden und 2D FE-Berechnungsverfahren verglichen. Zur Berücksichtigung der dreidimensionalen Spannungsumlagerung wird das Lastreduktionsverfahren in der 2D-Berechnung verwendet.

Der Lastreduktionsfaktor β wird durch Anpassung an das 3D Model bestimmt. Verschiedene Kalibrierungswerte, Stoffgesetze und Steifigkeitsparameter werden verglichen. Die erhaltenen Faktoren sind in erster Linie vom verwendeten Referenzwert, Grundwasserbedingungen sowie dem Drainagetyp abhängig. Zusätzlich haben die verwendeten Stoffgesetze und Initialspannungszustände Einfluss auf den ermittelten Lastreduktionsfaktor.

TABLE OF CONTENTS

1 Introduction 1
2 Soil models 2
2.1 Mohr-Coulomb model 2
2.2 Hardening soil model 3
2.2.1 Deviatoric yield Surface 4
2.2.2 Volumetric yield Surface 5
2.3 Hardening soil-small model 6
3 Numerical model 8
3.1 Tunnel geometry 8
3.2 Ground conditions 9
3.3 Soil parameters 10
3.3.1 Parameters for drained calculation 12
3.3.2 Parameters for undrained calculation 12
3.4 Initial stress state 12
3.4.1 Constant K_0 13
3.4.2 Variable K_0 due to loading history (POP) 13
3.4.3 The influence of POP on initial yield surfaces 14
3.5 Support means 16
3.5.1 Material parameters of the lining 16
3.5.2 Anchors 16
3.6 Mesh generation and quality 17
3.6.1 Plaxis 3D 2011 17
3.6.2 Plaxis 2D 2011 18
3.7 Construction stages for 3D calculation 19
3.8 Construction stages for 2D calculation 20
4 “Wished-in-place” calculations in 2D and 3D 21
4.1 Performed calculations 21
4.1.1 Calculations without groundwater (drained) 21
4.1.2 Calculations with groundwater (undrained) 21
4.2 Settlements 22
4.2.1 Influence of the initial stress state 23
4.2.2 Influence of small-strain stiffness 23
4.3 Influence of pre-overburden pressure on the development of plastic points 24
4.4 Distribution of excess pore pressures in undrained analysis 25
4.4.1 Linear-elastic model 26
4.4.2 Mohr-Coulomb model 26

4.4.3 Hardening soil and HS-small model 28
5 Drained 3D calculations 30
5.1 Performed calculations 30
5.2 Influence of tolerated error in HS-small calculations 30
5.3 Surface settlements 31
5.3.1 Transversal settlement trough 32
5.3.2 Longitudinal settlement profile 32
5.4 Lining forces and deformations 33
5.4.1 Crown settlement 33
5.4.2 Lining forces 35
6 Undrained 3D calculations 37
6.1 Modelling undrained behaviour in Plaxis 37
6.2 Performed calculations 38
6.3 Influence of tolerated error in HS-small calculations 39
6.4 Surface settlements 39
6.4.1 Transversal settlement trough 40
6.4.2 Longitudinal Settlement profile 41
6.5 Lining forces and deformations 41
6.5.1 Crown settlements 41
6.5.2 Lining forces 43
6.6 Influence of consolidation 45
6.6.1 Performed calculations 46
6.6.2 Dissipation of excess pore pressures 46
6.6.3 Settlements 47
7 Calibration of 2D calculations 52
7.1 Three-dimensional effects in tunnelling 52
7.2 Stress reduction method 52
7.3 Determination of the load reduction factors 53
7.3.1 Determination of β using crown settlements 54
7.3.2 Determination of β using surface settlements 64
7.3.3 Determination of β using axial forces in the lining 67
7.3.4 Conclusion 69
8 Comparison with analytical methods 73
8.1 Transversal surface settlement trough 74
8.2 Longitudinal surface settlement trough 78
9 Comparison with field measurements 81
10 Conclusion 83

11 References I
12 List of figures III
13 List of tables VI

1 INTRODUCTION

In tunnel design the stability of the ground, but also surface settlements, deformations of the cavity and the resulting forces on the lining are of main interest. The development of stresses and deformations is a complex three-dimensional problem. However, in engineering practice commonly simple empirical methods and 2D FE-analyses are used. To account for the effects of three-dimensional stress-redistribution in 2D calculations approximation methods have to be used. [1]

In open face tunnelling no support is applied on the tunnel face. It includes shield tunnelling without a pressurized face support and conventional tunnelling. Conventional tunnelling is characterized by an altering excavation and support sequence using shotcrete, anchors and steel arches as support means. Conventional tunnelling is often referred to as sprayed concrete method or New Austrian Tunnelling Method (NATM). The support can be adjusted to current ground conditions. Therefore, its use is very flexible. Over the last years the use of conventional tunnelling techniques in hard soil/soft rock (HSSR) increased. It includes hard, over-consolidated clays and soft sedimentary rocks (claystone, siltstone, weak limestone, etc.) The ground response is between that of rock and soil. Due to lower stability and larger deformations for tunnelling in HSSR ground the demands on support means are high. A fast ring-closure of the sprayed concrete lining and short round length help reducing settlements. The most common approximation method for modelling conventional tunnelling in 2D FE-analysis is the stress-reduction method. [1]

In this thesis numerical calculations for a non-circular tunnel constructed in hard soil/soft rock using NATM are carried out with the commercial Finite Element code “PLAXIS 2D 2011” and “PLAXIS 3D 2011”. The results of the 3D calculations are compared to the suggested approximation procedure in 2D, empirical methods and field data.

The main focus is on the prediction of surface settlements, deformations of the tunnel and internal forces of the lining. The purpose is to achieve a better understanding of the influencing factors for the determination of the stress-reduction factor β to account for three-dimensional effects in 2D FE-analysis.

2 SOIL MODELS

To mathematically represent the stress-strain-strength behaviour of soil a set of constitutive equations is used. Soil behaviour can be modelled with different degrees of accuracy. The simplest material model is linear-elastic and isotropic with only 2 input parameters. However, to obtain realistic results stress- and strain-dependent material properties of soil have to be considered. A reasonable number of input parameters, which are physically relevant and can be measured, have to be chosen. In this thesis calculations with the Mohr-Coulomb, Hardening Soil and HS-small model in PLAXIS are carried out.

2.1 MOHR-COULOMB MODEL

The Mohr-Coulomb model is a linear-elastic, perfectly plastic model. Perfectly plastic models have a fixed yield surface *f*, which separates admissible and inadmissible states in stress space. Within the yield surface soil behaviour is purely elastic. The stress-strain relation is a bi-linear curve.

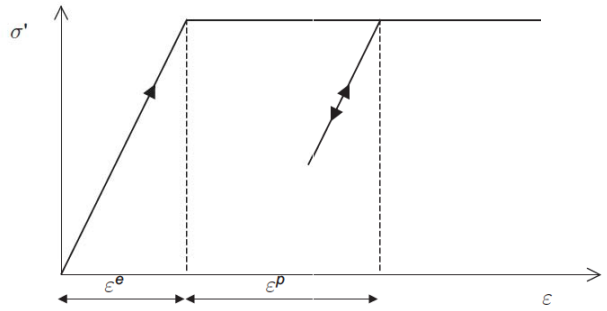

FIGURE 1: STRESS-STRAIN RELATION OF AN LINEAR-ELASTIC PERFECTLY PLASTIC MODEL [2]

No stress- and stress path dependency of stiffness is taken into account. The chosen soil stiffness *E*, which in reality is known to be stress dependent, should be consistent with the developing stress level and stress path. Effective stress states near failure are described well by the model. The Mohr-Coulomb failure criterion is characterized by effective strength parameters, friction angle φ' and cohesion *c*'. In total five parameters are required: [2]

- Young's modulus: *E* [kN/m²]
- Poisson ratio: *v* [-]
- Cohesion: *c* [kN/m²]
- Friction angle: φ [°]
- Dilatancy angle: *ψ* [°]

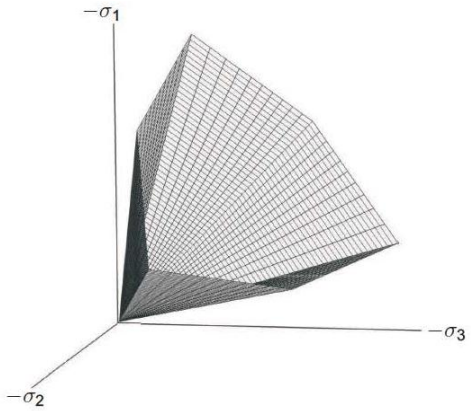

FIGURE 2: MOHR-COULOMB YIELD SURFACE IN PRINCIPAL STRESS SPACE FOR COHESIONLESS SOIL [2]

The Mohr-Coulomb model allows tensile stresses to develop in cohesive soils when shear stresses are small. However, experience shows that soil may fail in tension instead of in shear. In PLAXIS this can be considered by selecting the *Tension cut-off*. In this case no positive principal stresses are allowed. [2]

2.2 HARDENING SOIL MODEL

The Hardening Soil model is an isotropic hardening model. The yield surface is not fixed, but expands with plastic straining. Two types of hardening can be distinguished. Shear hardening due to deviatoric loading is governed by the secant stiffness modulus E_{50} at 50% strength in triaxial testing. Compression hardening due to compression in oedometric and isotropic loading is governed by the oedometric stiffness E_{oed}. If no yield surface is active, soil behaviour is elastic. For un- and reloading the stress path is modelled as elastic using the higher stress-dependent stiffness E_{ur}. [3]

Input parameters for soil stiffness are:

- Secant stiffness in standard drained triaxial test E_{50}^{ref} [kN/m²]
- Tangent stiffness for primary oedometer loading E_{oed}^{ref} [kN/m²]
- Power for stress-level dependency of stiffness m [-]
- Un-/reloading stiffness E_{ur}^{ref} [kN/m²]
- Poisson's ratio for un-/reloading v_{ur} [-]
- Reference stress for stiffness's p^{ref} [kN/m²]
- Coefficient for lateral earth pressure at rest for normal consolidation K_0^{nc} [-]
- Failure ratio (default value: 0.9) R_f [-]

Stress dependency of stiffness is considered in the Hardening Soil model. The input stiffness parameters are defined for a reference stress level. E_{50}^{ref} and E_{ur}^{ref} are related to the minor principal stress σ'_3. E_{oed}^{ref} is related to the vertical stress σ'_1. The stress dependent stiffness is calculated by the relation $E = E^{ref} \cdot \left(\frac{\sigma'}{p^{ref}}\right)^m$. [2]

One of the main advantages of the Hardening Soil model is the hyperbolic stress-strain curve for drained triaxial tests. The relationship between vertical strain ε_1 and deviatoric stress q in primary triaxial loading is described by a hyperbolic curve as shown in Figure 3. The curve is representative for a fixed value of σ_3. [2]

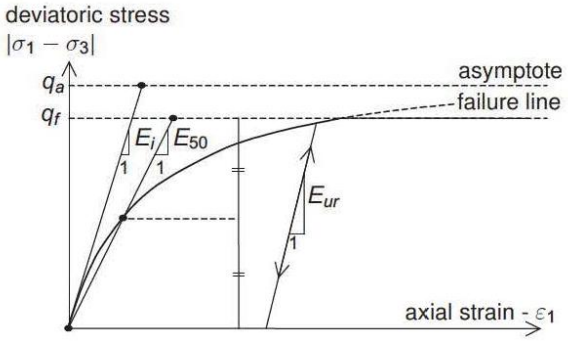

FIGURE 3: HYPERBOLIC STRESS-STRAIN RELATION IN A STANDARD DRAINED TRIAXIAL TEST [2]

$$\varepsilon_1 = \frac{q_a}{2 \cdot E_{50}} \cdot \frac{q}{q_a - q} \quad \text{for } q < q_f \tag{2.1}$$

With

Ultimate deviatoric stress

$$q_f = \frac{2 \cdot \sin\varphi}{1 - \sin\varphi} \cdot (c \cdot \cot\varphi - \sigma'_3) \tag{2.2}$$

Asymptotic value for shear strength $q_a = \frac{q_f}{R_f}$ **(2.3)**

In Figure 4 the yield surfaces of the Hardening Soil model in twodimensional *p'-q* plane is shown. Within the elastic region no yield surface is active and no plastic strains occur. In the blue marked region 1 the deviatoric yield surface is active. In region 2, displayed in green, the volumetric yield surface is active. In region 3 both yield surfaces are active and both volumetric and deviatoric hardening occur. The mobilization of the deviatoric yield surface is restricted by the Mohr-Coulomb failure criterion. If $q = q_f$ the Mohr-Coulomb failure criterion is satisfied.

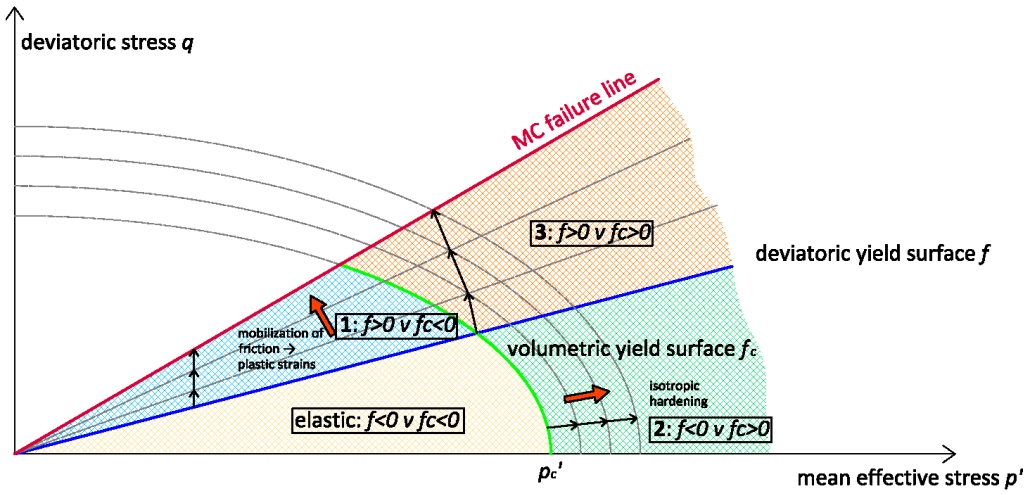

FIGURE 4: YIELD SURFACES OF THE HARDENING SOIL MODEL IN TWO-DIMENSIONAL P'-Q PLANE - ACTIVATION OF DEVIATORIC AND VOLUMETRIC YIELD SURFACE

2.2.1 DEVIATORIC YIELD SURFACE

The position of the deviatoric hardening surface *f* is related to mobilizied friction and governed by E_{50}. It represents lines of equal shear strains in triaxial tests with a constant hardening parameter γ^p. γ^p can be considered as the plastic shear strain related to the mobilized shear resistance. The shape depends on the power *m* and is a slighly curved line for values $m < 1$. The relationship between plastic shear strain γ^p and plastic volumetric strain $\dot{\varepsilon}_v^p$ is given by the linear non-associated shear hardening flow rule [3]:

$$\dot{\varepsilon}_v^p = \sin\psi_m \, \dot{\gamma}^p \quad \textbf{(2.4)}$$

The mobilised dilatancy angle ψ_m is

$$\sin\psi_m = \frac{\sin\varphi_m - \sin\varphi_{cv}}{1 - \sin\varphi_m \cdot \sin\varphi_{cv}} \quad \textbf{(2.5)}$$

With

φ_{cv} critical state friction angle

φ_m mobilised friction angle

$$\sin\varphi_m = \frac{\sigma_1' - \sigma_3'}{\sigma_1' + \sigma_3' - 2 \cdot c \cdot \cot\varphi} \quad \textbf{(2.6)}$$

$$\sin\varphi_{cv} = \frac{\sin\varphi - \sin\psi}{1 - \sin\varphi \cdot \sin\psi} \quad \textbf{(2.7)}$$

The equations (2.5), (2.6) and (2.7) are adapted from the stress-dilatancy theory by Rowe [4]. For small mobilised friction angles plastic compaction is overpredicted. Therefore, negative values of ψ_m are cut-off in PLAXIS. For φ = *0* the mobilised dilatancy angle is set equal to zero. [2]

At small stress ratios $\varphi_m < \varphi_{cv}$ the material behavior is contractant, while at high stress ratios, when the mobilized friction angle exceeds the critical state friction angle, dilatancy occurs. [4]

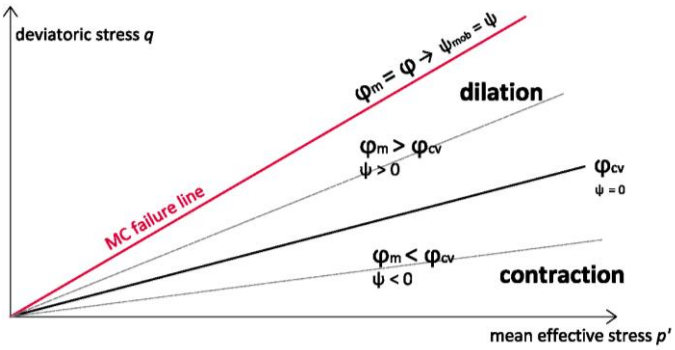

FIGURE 5: SHEAR HARDENING FLOW RULE - MOBILIZATION OF FRICTION

2.2.2 VOLUMETRIC YIELD SURFACE

The volumetric yield surface f_c is an ellipse in the *q*-*p'* plane. Its size is governed by the isotropic pre-consolidation pressure p_c on the *p*-axis. p_c is based on *OCR* (over-consolidation ratio) or *POP* (pre-overburden pressure). A more detailed description of the determination of initial stresses is given in chapter 3.4. On the *q*-axis the ellipse has a length of $\alpha * p_c$. α is an auxiliary parameter related to K_0^{nc}. [2]

The cap yield surface is defined by equation (2.8). [2]

$$f^c = \frac{\tilde{q}^2}{\alpha^2} + p'^2 - p_c^2 \tag{2.8}$$

With

Volumetric stress $$p' = \frac{\sigma_1' + \sigma_2' + \sigma_3'}{3} \tag{2.9}$$

Deviatoric stress $$\tilde{q} = \sigma_1' + (\delta - 1) \cdot \sigma_2' - \delta \sigma_3' \tag{2.10}$$

$$\delta = \frac{3 + \sin\varphi}{3 - \sin\varphi} \tag{2.11}$$

For volumetric yielding an associated flow rule is used. The plastic potential is defined as $g^c = f^c$ [3].

The pre-consolidation stress p_c is related to volumetric cap strain ε_v^{pc} by the hardening law [2]:

$$\epsilon_v^{pc} = \frac{\beta}{1 - m} \cdot \left(\frac{p_c}{p^{ref}}\right)^{1-m} \tag{2.12}$$

The volumetric cap strains are plastic volumetric strains in isotropic compression. β is not an input value, but related to E_{oed}^{ref}. [2]

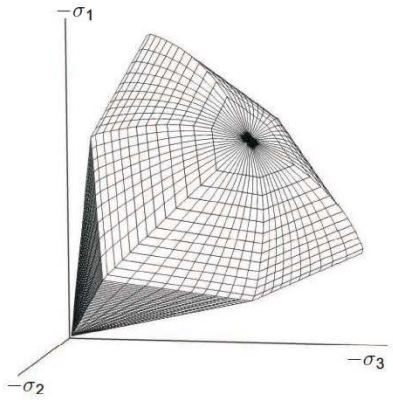

FIGURE 6: YIELD CONTOUR OF THE HARDENING SOIL MODEL IN THREE-DIMENSIONAL PRINCIPAL STRESS SPACE FOR COHESIONLESS SOIL [2]

2.3 HARDENING SOIL-SMALL MODEL

The Hardening Soil-small model is based on the Hardening Soil model and additionally considers strain dependency of stiffness at very small strains. The strain range at which soil behaviour can be considered truly elastic is very small. For the analysis of geotechnical structures small-strain stiffness and its non-linear strain-stiffness relationship should be taken into account. In addition to the Hardening Soil model two parameters are introduced: [2]

- Initial or very small-strain shear modulus G_0 at very small strains, e.g. $\gamma < 10^{-6}$
- Shear strain level $\gamma_{0,7}$ at which the secant shear modulus G_s is reduced to app. 70 % of G_0

The degradation of stiffness with increasing strain plotted at logarithmic scale follows an S-shaped curve. The stress-strain curve is derived from soil dynamics, where generally small strains are dominant. The most common model is the Hardin-Drnevich model, which describes the stress-strain relation by a simple hyperbolic law. The HS-small model in PLAXIS uses the shear strain $\gamma_{0.7}$ at which the secant shear modulus G_s is reduced to 72.2 % of its initial value. [2]

With respect to the stress-strain relationship in the HS-small model the tangent shear modulus is given as: [2]

$$G_t = \frac{G_0}{\left(1 + 0.385 \cdot \frac{\gamma}{\gamma_{0.7}}\right)^2} \quad \textbf{(2.13)}$$

If the tangent shear modulus G_t is lower than the un-/reloading stiffness G_{ur}, the model switches to hardening plasticity of the HS model as shown in Figure 7.

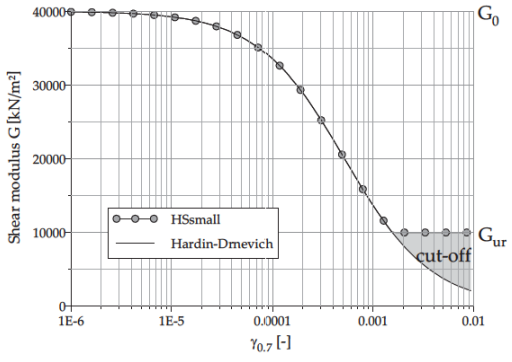

FIGURE 7: SMALL-STRAIN STIFFNESS REDUCTION CURVE IN THE HARDENING SOIL-SMALL MODEL [5]

The parameters G_0 is influenced by the actual stress state in the soil and the void ratio e. Assuming that the changes in void ratio are small within the computation, the material parameters are not updated for changes of e. In literature determination of small-strain shear stiffness G_0 is often related to void ratio e. The maximum ratio of G_0/G_{ur} in HS-small is limited to 10. [2] Benz [5] relates $\gamma_{0.7}$ to G_0 and soil strength. A realistic order of magnitude is: [6]

$$G_0^{ref} = (2.5\ to\ 10) \cdot G_{ur}^{ref} \tag{2.14}$$

With $G_{ur}^{ref} = \frac{E_{ur}^{ref}}{2 \cdot (1+\nu_{ur})}$

$$\gamma_{0,7} = (1\ to\ 2) \cdot 10^{-4} \tag{2.15}$$

In the HS-small model stress dependency of the shear modulus is taken into account by: [2]

$$G_0 = G_0^{ref} \cdot \left(\frac{c \cdot cos\,\varphi - \sigma_3' \cdot sin\,\varphi}{c \cdot cos\,\varphi + p_{ref}' \cdot sin\,\varphi} \right)^m \tag{2.16}$$

The threshold shear strain $\gamma_{0.7}$ is independent of the mean stress.

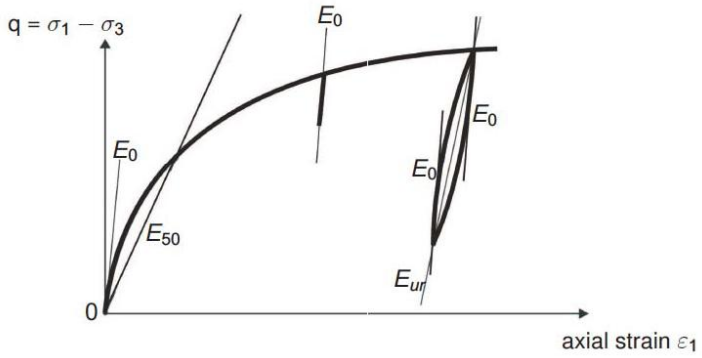

FIGURE 8: STIFFNESS PARAMETERS OF THE HARDENING SOIL MODEL WITH SMALL STRAIN STIFFNESS IN A TRIAXIAL TEST [2]

Another difference compared to the Hardening Soil model is that the mobilised dilatancy angle in compression is calculated differently. Negative values of ψ_m, computed by Rowe's theory, are not cut-off, but the mobilised dilatancy is then calculated by

$$\sin \psi_m = \frac{1}{10} \cdot \left(M \cdot e^{\frac{1}{15} \cdot \ln\left(\frac{\eta}{M} \frac{q}{q_a}\right)} + \eta \right) \tag{2.17}$$

With

M	stress ratio at failure
$\eta=q/p$	actual stress ratio

This is a simplification of the void ratio dependent formulation by Li and Dafalias (2000) [2].

3 NUMERICAL MODEL

3.1 TUNNEL GEOMETRY

The exploratory tunnel *Mitterpichling* is part of the investigation program for the Koralm tunnel. It is constructed as the top heading of the later to be built south tube of the final project using the New Austrian Tunnelling Method (NATM) [6].

The tunnel cross-section is non-circular with an average area of 48 m² [6] and an equivalent diameter of

$$d = \sqrt{\frac{4 \cdot A}{\pi}} = 7.818m \tag{3.1}$$

The final tunnel cross section has a diameter of 10.0 m.

The dimensions of the numerical model in PLAXIS 3D 2011 are chosen according to recommendations of the Committee on Numerical Methods in Geotechnics of the German Geotechnical Society "*Numerik in der Geotechnik*" [7] to avoid the influence of boundary conditions:

Height → 60.0 m
Width → 70.0 m
Length → 142.0 m

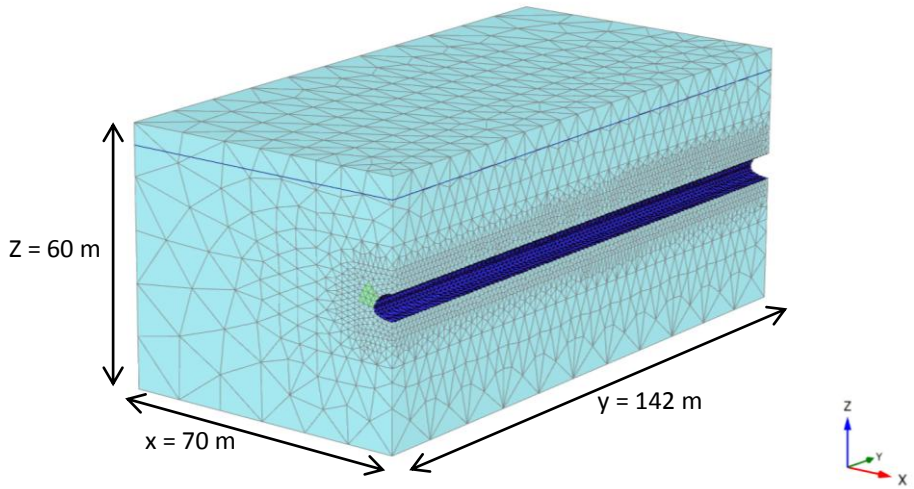

FIGURE 9: NUMERICAL MODEL

The deformations due to tunnel installation are negligible at the boundaries of the model, indicating that the size of the model is sufficient.
The excavation length for the calculation is 1.5 m. It is modelled as one slice. At the beginning and the end of the model 8 slices with 2.5 m (total 20.0 meters at each site) are modelled to bridge boundary conditions. For drained calculations this tunnel section is installed in one single phase ("wished-in-place"). In calculations considering groundwater conditions step-by-step excavation is modelled for the whole tunnel length.

For the input of the tunnel cross section in PLAXIS 3D 2011 some adaptions have to be made. In the 2D version of the program circular arcs are modelled as curved lines. In the 3D version they are approximated by a linear polyline. The approximation is governed by input of the discretization angle. The discretization angle has to be chosen carefully because it influences the mesh quality around the tunnel. Particular attention has to be paid to the coincidence of geometry points (end of segments) and discretization points. Otherwise the lining may be divided into very small segments. Short plate elements combined with a coarser local element size factor for the surrounding soil result in slender soil elements with low mesh quality around the tunnel.

Between discretization points the curve is approximated by a straight line. The green lines show the position of nodes of the plate elements for one segment. The nodes in the middle of the element are not on the curved line. Sharp bends in the lining cause jumps of the internal normal and shear forces.

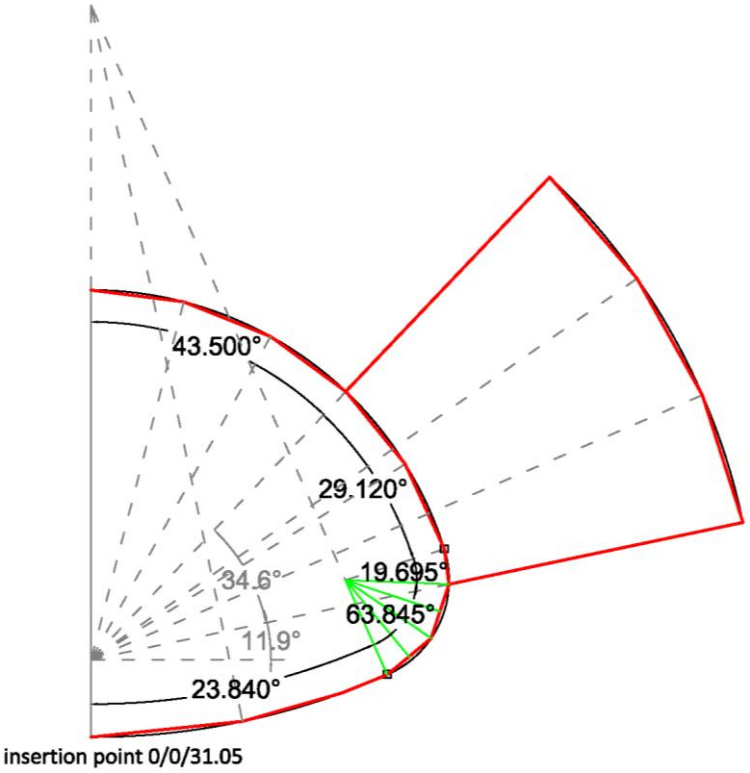

FIGURE 10: CROSS-SECTION OF THE TUNNEL

TABLE 1: INPUT PARAMETERS TUNNEL CROSS-SECTION

	Section 1	Section 2	Section 3	Section 4	Section 5	Section A
Central angle	23.840°	63.845°	19.685°	29.120°	43.500°	34.600°
radius	9.9 m	1.4 m	1.4 m	5.0 m	5.0 m	9.0 m
discretization	11.920°	15.961°	19.695°	14.560°	14.500°	11.530°

3.2 GROUND CONDITIONS

For numerical calculations the tunnel section between station 1016 and 1187.5 of the exploratory tunnel *Mitterpichling Ost* is chosen. It can be considered as more or less homogeneous with dominant rock type silt- and claystone, slightly consolidated. The ground was previously loaded by a 25 m thick soil layer resulting in 500 kN/m² pre-overburden pressure. The groundwater table is about 5 m beneath the surface. The overburden in this section increases from 22.5 meters to 27.5 meters. Therefore, the considered average overburden is about 25 meters above the tunnel crown. The tunnel is supported by a 20 cm thick layer of shotcrete and anchors. No pipe roof is needed to secure the tunnel face. In the considered section tunnelling was carried out conventionally using blasting and excavators. The length of advance is between 1.3 and 1.7 m. [8]

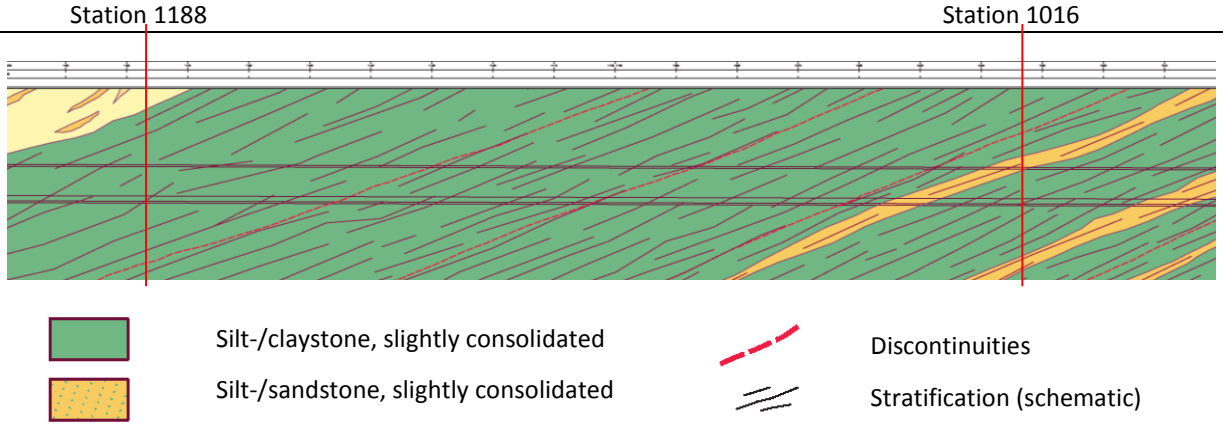

FIGURE 11: GEOLOGICAL PROFIL FROM STATION 1100 TO 1200 [8]

3.3 SOIL PARAMETERS

No material parameters were available for the considered tunnel section. Hence, data from the adjoining construction lot *Paierdorf* for the same geological unit are adapted.

TABLE 2: MATERIAL PARAMETERS GATHERED FROM GEOLOGICAL REPORT FROM EXPLORATION TUNNEL PAIERDORF [7]

γ [kN/m³]	E [MN/m²]	ν [-]	c [kN/m²]	φ [°]	K_0 [-]	Depth z [m]	m [-]
21.5	270	0.2	35	27	0.54	70	0.8

In the first step the stiffness in 70 meter depth is adjusted for the Mohr-Coulomb model to the level of the tunnel axis *z= 30.0 m*.

$$E_{MC} = \left(\frac{z}{70}\right)^{m} \cdot E_{70} = \left(\frac{30}{70}\right)^{0,8} \cdot 270 \cong 135\ MN/m^2 \tag{3.2}$$

In a second step reference stiffness parameters for the advanced Hardening Soil and HS-small models are back calculated from the stiffness in 70 meter depth according to [2]

$$E_{oed} = E_{oed}^{ref} \cdot \left(\frac{c\cdot\cos\varphi - \sigma_1' \cdot \sin\varphi}{c\cdot\cos\varphi + p_{ref}' \cdot \sin\varphi}\right)^{m} \tag{3.3}$$

$$E_{50} = E_{50}^{ref} \cdot \left(\frac{c\cdot\cos\varphi - \sigma_3' \cdot \sin\varphi}{c\cdot\cos\varphi + p_{ref}' \cdot \sin\varphi}\right)^{m} \tag{3.4}$$

$$E_{ur} = E_{ur}^{ref} \cdot \left(\frac{c\cdot\cos\varphi - \sigma_3' \cdot \sin\varphi}{c\cdot\cos\varphi + p_{ref}' \cdot \sin\varphi}\right)^{m} \tag{3.5}$$

$$E_{oed}^{ref} = E_{50}^{ref} = {}^{1}/_{3}\, E_{ur}^{ref} \tag{3.6}$$

The parameters used in FE-calculations are listed in Table 3 and Table 4.

For calculation model 2), 4), 7) and 8) the E-modulus from the neighbouring lot is set as E_{oed}, while for the calculation model 3), 5), 9) and 10) it is taken as E_{ur}.

For the Hardening Soil and HS-small model a pre-overburden of 500 kN/m² is considered. For over-consolidated soils the coefficient of lateral earth pressure at rest is higher than for normally consolidated soils. Its value is increased to 0.7.

To be able to compare the results of drained and undrained analysis after consolidation, groundwater conditions have to be considered for drained analysis. The additional loading on the tunnel due to water pressure leads to failure. Pore water pressure *u* shifts the Mohr's circle of stress to the left nearer to failure. The effective stresses are reduced, which govern the Mohr-Coulomb failure criterion. The tunnel face collapses into the cavity. The stiffness/strength of the soil is not sufficient to withstand loading in case of drained analysis, because no positive excess pore pressures are generated during excavation. Consequently no drained analysis considering groundwater conditions are carried out.

In drained analyses no groundwater is considered. In undrained analysis the groundwater table 5.0 m below the ground surface is taken into account. In the Hardening Soil models 4), 5) and HS-small model 8) and 10) stiffness parameters are recalculated considering the initial stress state due to pore water pressure. For the Mohr Coulomb model 6) the E-modulus remains 135 kN/m², but groundwater level is implemented in the model. The permeability of the soil is assumed as $k_x = k_y = k_z = 10^{-8}$ *m/s*, which is a realistic estimate for silt and clay. The undrained analysis is performed with effective parameters for stiffness and strength (undrained A).

For the analysis of geotechnical structures the strain-dependency of stiffness should be considered. The Hardening Soil-small model takes the higher initial stiffness of the soil at very small strains into account. In addition to the parameters of the Hardening Soil model the initial small-strain shear modulus G_0 and the shear strain level $\gamma_{0.7}$ are used. They are estimated as

$$G_0 = 4 \cdot G_{ur} \tag{3.7}$$

$$\gamma_{0,7} = 2.0 \cdot 10^{-4} \tag{3.8}$$

The other stiffness parameters are the same as for the corresponding Hardening Soil model.

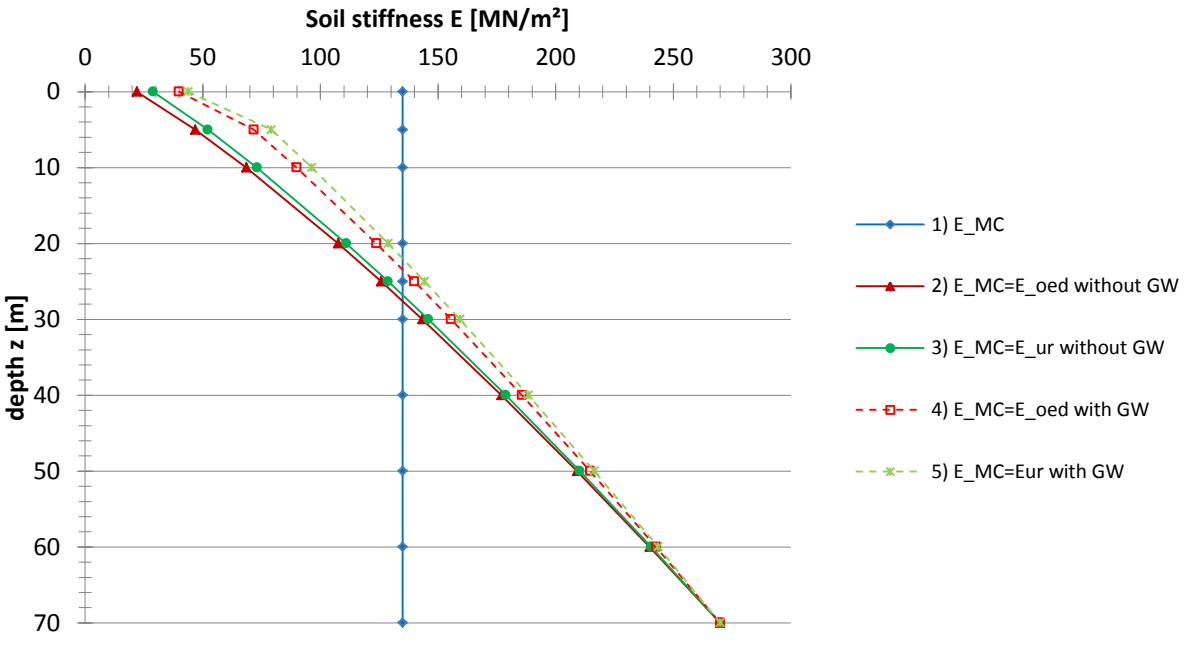

FIGURE 12: STIFFNESS PARAMETERS

3.3.1 PARAMETERS FOR DRAINED CALCULATION

TABLE 3: SOIL PARAMETERS WITHOUT CONSIDERATION OF GROUNDWATER

MODEL	$E_{oed,ref}$ [MN/m²]	$E_{50,ref}$ [MN/m²]	$E_{ur,ref}$ [MN/m²]	c [kN/m²]	φ [°]	m [-]	K_0 [-]	POP [kN/m²]	$K_{0,nc}$ [-]	ν_{ur} [-]	$G_{0,ref}$ [MN/m²]	$\gamma_{0,7}$ [-]
1)MC, E135	E=135 MN/m²			35	27	-	0.54	-	-	-	-	-
2)HS, $E_{MC}=E_{oed}$	45	45	135	35	27	0.8	0.7	500	0.54	0.2	-	-
3)HS, $E_{MC}=E_{ur}$	20	20	60	35	27	0.8	0.7	500	0.54	0.2	-	-
7)HSS, $E_{MC}=E_{oed}$	45	45	135	35	27	0.8	0.7	500	0.54	0.2	225	$2* 10^{-4}$
9)HSS, $E_{MC}=E_{ur}$	20	20	60	35	27	0.8	0.7	500	0.54	0.2	100	$2* 10^{-4}$

3.3.2 PARAMETERS FOR UNDRAINED CALCULATION

TABLE 4: SOIL PARAMETERS WITH CONSIDERATION OF GROUNDWATER

MODEL	$E_{oed,ref}$ [MN/m²]	$E_{50,ref}$ [MN/m²]	$E_{ur,ref}$ [MN/m²]	c [kN/m²]	φ [°]	m [-]	K_0 [-]	POP [kN/m²]	$K_{0,nc}$ [-]	ν_{ur} [-]	$G_{0,ref}$ [MN/m²]	$\gamma_{0,7}$ [-]
4)HS, $E_{MC}=E_{oed}$	69.3	69.3	207.8	35	27	0,8	0.7	500	0.54	0.2	-	-
5)HS, $E_{MC}=E_{ur}$	30	30	90	35	27	0.8	0.7	500	0.54	0.2	-	-
6)MC, E135	E=135 MN/m²			35	27	-	0.54	-	-	-	-	-
8)HSS, $E_{MC}=E_{oed}$	69.3	69.3	207.8	35	27	0.8	0.7	500	0.54	0.2	346.3	$2* 10^{-4}$
10)HSS, $E_{MC}=E_{ur}$	30	30	90	35	27	0.8	0.7	500	0.54	0.2	150	$2* 10^{-4}$

3.4 INITIAL STRESS STATE

The initial stress state prior to tunnel construction is controlled by the specific weight of the soil γ [kN/m³], groundwater conditions and many other factors like plate tectonics, weathering and erosion, previous overburden etc. Because of the high number of influencing factors the initial stress distribution is often very difficult to evaluate. In numerical calculations, however, reasonable assumptions regarding the initial stress state are required. [1]

In PLAXIS two different methods, *Gravity loading* and *K_0-procedure* are available to generate the initial stresses. In this thesis only the *K_0-procedure* is used and explained here.

The *K_0-procedure* is used to compute initial stresses for situations with a horizontal ground surface and homogeneous or horizontally layered ground. Effective vertical stresses σ_v' depend on the effective weight of the soil γ' and depth h. Effective horizontal stresses σ_h' are calculated multiplying the vertical stresses with the coefficient of lateral earth pressure at rest K_0. [2]

Pore water pressure u is taken into account beneath the ground water table.

$$\sigma_v' = \sigma_v - u = \gamma \cdot h - u = (\gamma - \gamma_w) \cdot h \quad \textbf{(3.9)}$$

$$\sigma_h' = K_0 \cdot \sigma_v' \quad \textbf{(3.10)}$$

The *K_0-procedure* imposes an initial stress state as a starting point for the numerical analysis. Hence, no deformations are calculated. [2]

The history of loading can be considered in PLAXIS by the input of an over-consolidation ratio (*OCR*) or a pre-overburden pressure (*POP*) for advanced soil models (HS, HSS, SS, SSC, MCC).

3.4.1 CONSTANT K_0

For a constant K_0 the horizontal initial stresses are calculated according to:

$$\sigma'_{yy,0} = \gamma' \cdot z \left[\frac{kN}{m^2}\right] \quad (3.11)$$

$$\sigma'_{xx,0} = K_0 \cdot \sigma'_{yy,0} \left[\frac{kN}{m^2}\right] \quad (3.12)$$

Therefore, the horizontal initial stresses at the surface are zero.

3.4.2 VARIABLE K_0 DUE TO LOADING HISTORY (POP)

The coefficient of lateral earth pressure in over-consolidated soils is larger than in normally consolidated soil. This effect is automatically taken into account by a variable K_0. For the generation of the initial stresses by the *K_0 procedure* in advanced soil models the value of K_0 is influenced by K_0^{nc}, ν_{ur}, *OCR* and *POP* and is calculated automatically resulting in a stress-dependent K_0-value [2]:

$$K_{0,x} = K_0^{nc} \cdot OCR - \frac{\nu_{ur}}{1-\nu_{ur}} \cdot (OCR - 1) + \frac{K_0^{nc} \cdot POP - \frac{\nu_{ur}}{1-\nu_{ur}} \cdot POP}{|\sigma^0_{yy}|} \quad (3.13)$$

K_0^{nc} Coefficient of lateral earth pressure at rest for normally consolidated soils
OCR over-consolidation ratio
POP pre-overburden pressure

For an automatically determined K_0 and *POP* > 0 initial horizontal stresses are calculated by:

$$\sigma_{xx,0} = K_0^{nc} \cdot \sigma_p - \frac{\nu_{ur}}{1-\nu_{ur}} \cdot POP \left[\frac{kN}{m^2}\right] \quad (3.14)$$

$$\sigma_p = \sigma'^0_{yy} + POP \quad (3.15)$$

This results in $\sigma_{xx,0}$ = 145.0 kN/m² at the surface and a linear increase of the horizontal stresses with depth.

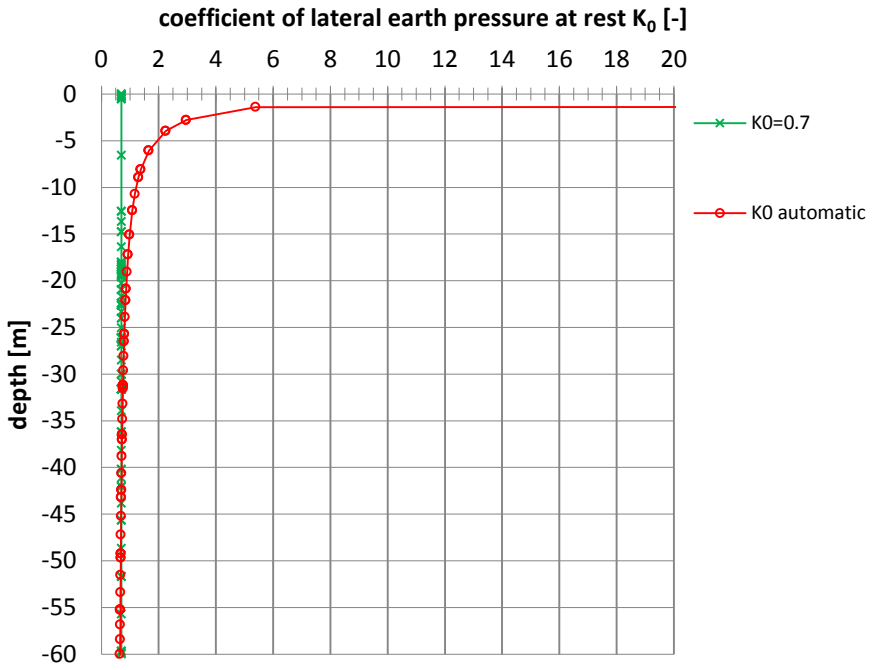

FIGURE 13: COEFFICIENT OF LATERAL EARTH PRESSURE AT REST K_0 WITH POP = 500 KN/M²

For this project a *POP = 500 kN/m²* and a constant $K_{0,x} = K_{0,y} = 0.7$ is considered. The calculated values of $K_{0,x}$ and $K_{0,y}$ can be overwritten by the user in PLAXIS 2D 2010. In PLAXIS 3D 2011 the missing user interface for the simultaneous input of POP and $K_{0,x}$, $K_{0,y}$ causes some problems. The automatically calculated default value results in a different horizontal initial stresses and consequently in different settlements. The problem can be solved by manually delaying the *K_0-calculation* and altering the temporary calculation file *data.plxmat* assigning a constant value 0.7 for $K_{0,x} = K_{0,y}$.

3.4.3 THE INFLUENCE OF POP ON INITIAL YIELD SURFACES

The position of the volumetric yield surface f_c on the *p*-axis is based on previous stress history. To determine the initial position of the cap-type yield surface PLAXIS needs an equivalent isotropic pre-consolidation stress p_p^{eq}, which is computed using the pre-consolidation stress σ_p. The pre-consolidation stress σ_p is based on *OCR* (over-consolidation ratio) or *POP* (pre-overburden pressure). [2]

$$OCR = {\sigma_p}/{\sigma'^0_{yy}} \tag{3.16}$$

$$POP = \left|\sigma_p - \sigma'^0_{yy}\right| \tag{3.17}$$

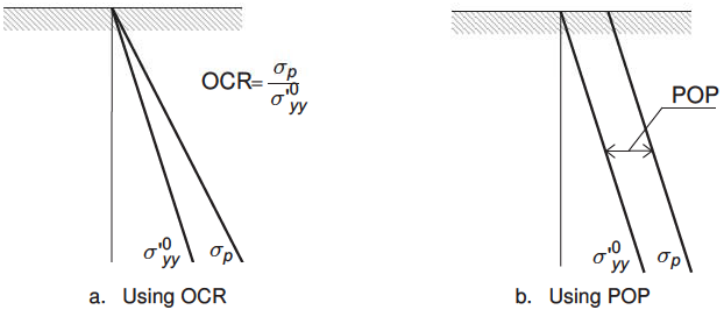

FIGURE 14: VERTICAL PRE-CONSOLIDATION STRESS σ_p IN RELATION TO VERTICAL IN-SITU STRESS σ [10]

For the Hardening Soil and HS-small model the equivalent isotropic pre-consolidation stress is defined as: [2]

$$p_p^{eq} = \sqrt{(p')^2 + \frac{q^2}{\alpha}} \tag{3.18}$$

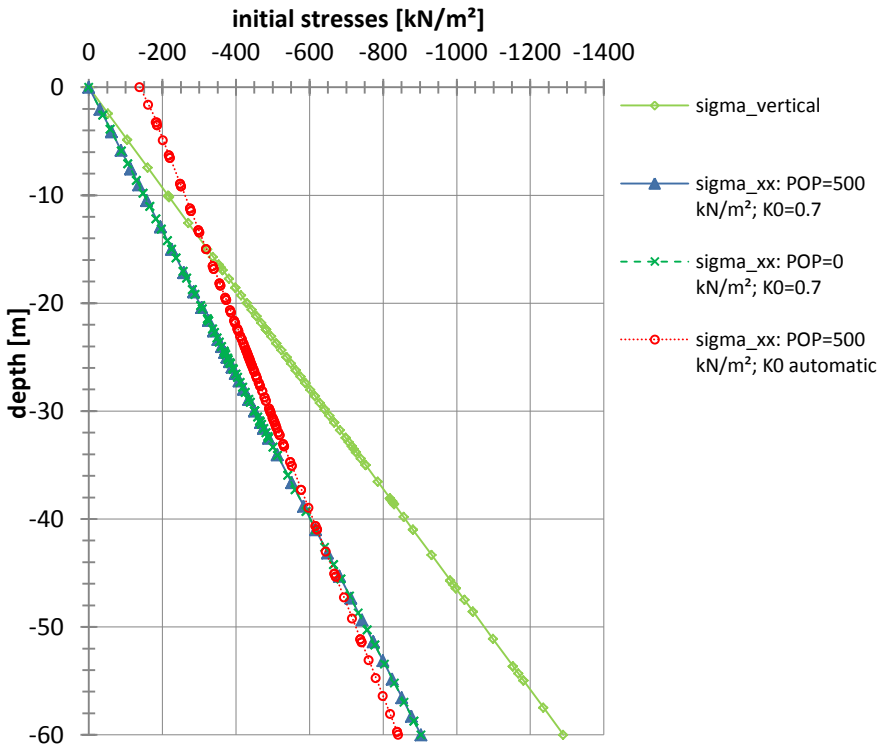

FIGURE 15: INITIAL VERTICAL AND HORIZONTAL STRESSES

The pre-overburden pressure influences the position of the cap-type yield surface, which governs volumetric hardening. The initial stress state of normally consolidated soils lies at the intersection of the deviatoric and the volumetric hardening yield surface. For over-consolidated soils the stress state is within the elastic region. The elastic region is confined by the two yield surfaces. Within this area soil behaviour is governed by the elastic un-/re- loading stiffness.

POP cannot be displayed in the output, but the equivalent value of overconsolidation ratio *OCR* is shown. In the output the isotropic over-consolidation ratio is displayed. It is the ratio between the isotropic pre-consolidation stress p_p and the equivalent isotropic stress p_{eq}.

$$OCR = \frac{p_p}{p_{eq}} \tag{3.19}$$

For *POP* = 0 kN/m² it is 1.0. For the *K_0-procedure* for the calculations with *POP* = 500 kN/m² it is also influenced by the coefficient of lateral earth pressure at rest K_0. As shown in Figure 16 for an automatically calculated K_0 *OCR* at the surface is smaller than for calculations with K_0 = const. Below *z* = -20.0 m both calculations result in a more or less equal *OCR*.

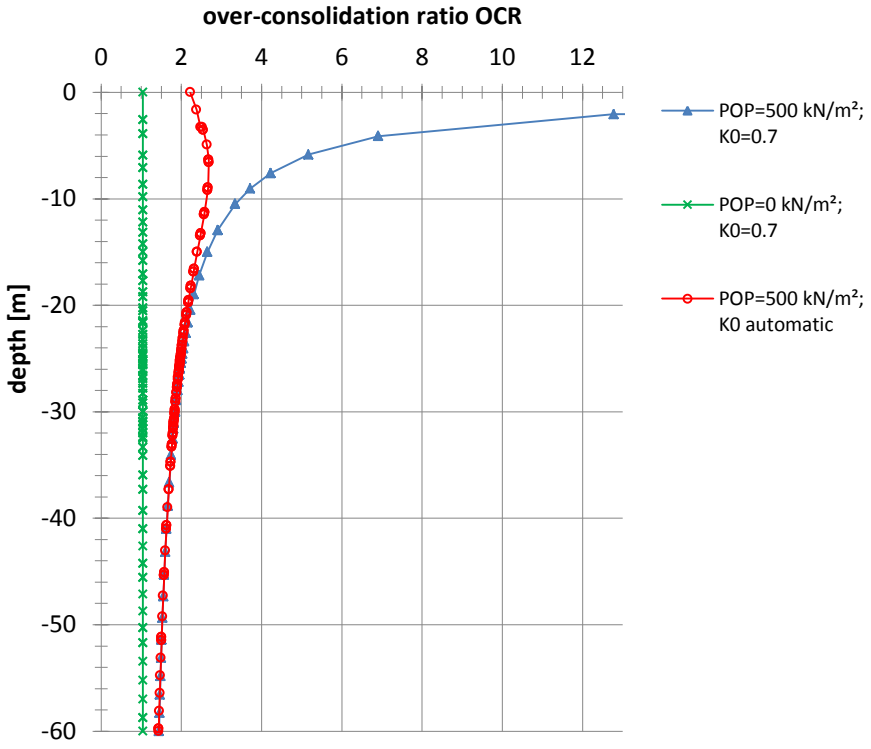

FIGURE 16: OVER-CONSOLIDATION RATIO (OCR)

3.5 SUPPORT MEANS

3.5.1 MATERIAL PARAMETERS OF THE LINING

The primary tunnel lining is made of sprayed concrete. The increase of stiffness with time is considered in a simplified manner by using two different parameter sets for *shotcrete young* and *old*. The reduced stiffness of *shotcrete young* is based on experience to account for distinct creep-properties of the soft shotcrete [9]. The material behaviour is assumed as linear-elastic. One calculation phase after excavation the tunnel lining is activated with the material parameter set *shotcrete young*. In all following phases the properties are changed to *shotcrete old*.

TABLE 5: MATERIAL PARAMETERS LINING

	γ [kN/m³]	E [MN/m²]	ν [-]
Shotcrete young	25	4000	0.2
Shotcrete old	25	15000	0.2

3.5.2 ANCHORS

The load-bearing behaviour of the systematic anchoring is modelled as an area with an increased cohesion of *c =125 kN/m²* [11] according to [9]

$$\Delta c_{RB} = \frac{1+\sin\varphi}{2\cdot\cos\varphi}\cdot p_{RB} \quad \textbf{(3.20)}$$

The shotcrete lining and anchors are the sole support means for the exploratory tunnel.

3.6 MESH GENERATION AND QUALITY

3.6.1 PLAXIS 3D 2011

To perform Finite element analysis the model has to be transformed into a Finite element mesh. In PLAXIS 3D 2011 the basic soil elements are 10-noded tetrahedral elements. Structural components are modelled with different types of elements. In the generated model in addition to soil elements only 6-noded plane plate elements are used. [2]

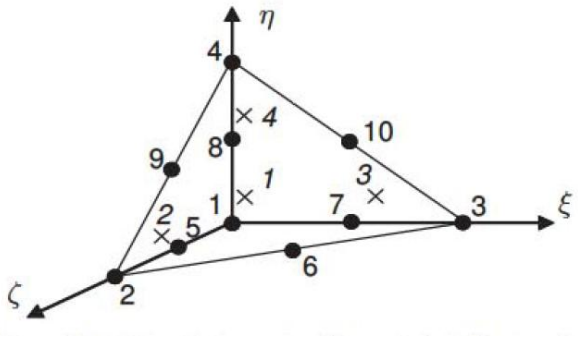

FIGURE 17: 10-NODED TETRAHEDRAL SOIL ELEMENTS (3D) [2]

As mentioned above the discretization angle for polylines and the modelled length per slice have a great impact on the shape of the generated elements and therefore the mesh quality. The mesh quality is a factor for the relation of inner to outer sphere of tetrahedral elements. For an ideal tetrahedron it is 1.0. Another parameter to determine the quality of the generated mesh is the target element size or average element size l_e [2].

$$l_e = \frac{r_e}{20} \cdot \sqrt{(x_{max} - x_{min})^2 + (y_{max} - y_{min})^2 + (z_{max} - z_{min})^2} \quad \textbf{(3.21)}$$

It can be influenced by the relative element size factor r_e and the local refinement of the mesh. It is important to find a good balance between coarseness of the mesh and consequently accuracy of results and calculation time. [2]

Furthermore polyline angle tolerance and surface angle tolerance influence the mesh quality. The default values can be changed in the expert settings of mesh generation [2]. The shape of soil elements around the tunnel is mostly determined by the discretization of the lining and respectively the size of the plate elements.

3.6.1.1 INPUT PARAMETERS

The following expert settings obtained by trial-and-error were used for the definition of the mesh:

Relative element size factor	→	1.5
Polyline angle tolerance	→	20°
Surface angle tolerance	→	5°
Finess Factors for local refinement of the mesh:		
Soil clusters above tunnel	→	0.5
Soil clusters around tunnel	→	0.1/0.3
Tunnel cluster	→	0.3
Anchor area	→	0.1
Plate elements (tunnel lining)	→	0.8

The polyline angle tolerance and surface angle tolerance define how accurately the mesh follows the lines of the project, respectively the surface. The smaller the input value, the finer the mesh. The *Finess factors* for local refinement of the mesh reduce the element size with respect to the target element size l_e. [2]

3.6.1.2 GENERATED MESH

The generated mesh consists of 112585 soil elements, 1559789 nodes and has an average element size of 2.302 m.

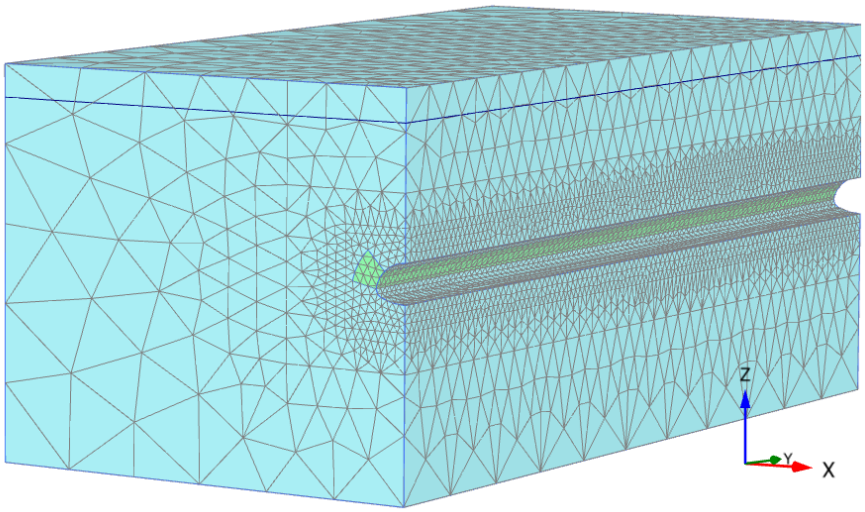

FIGURE 18: 3D FINITE ELEMENT MESH

The minimum mesh quality is 0.312. In Figure 19 all elements with a quality value < 0.45 are displayed. It is shown that the most critical area is the lower part of the intersection between tunnel lining and anchor area.

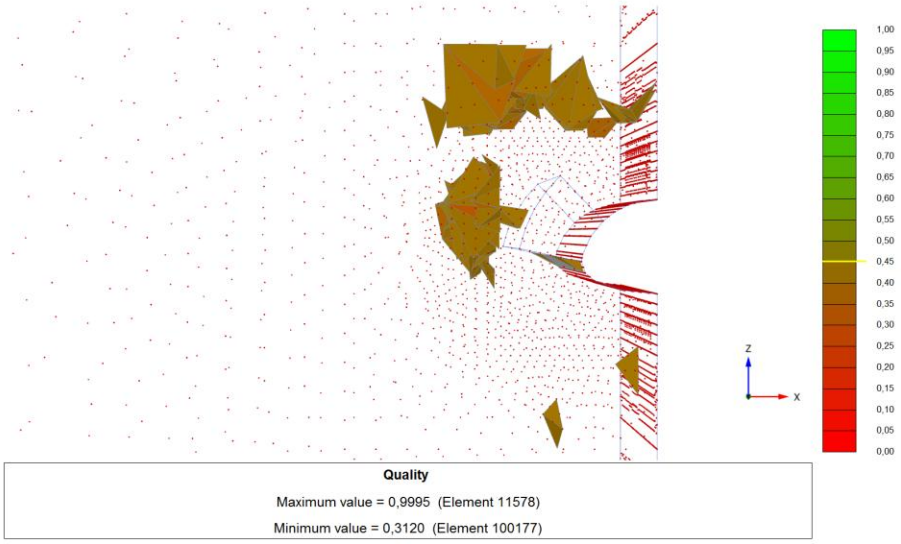

FIGURE 19: MESH QUALITY

3.6.2 PLAXIS 2D 2011

In PLAXIS 2D 2011 the basic soil elements are 15-noded or 6-noded triangular elements. 15-noded elements employ a 4^{th} order shape function, while 6-noded elements employ only a quadratic shape function. In these calculations 6-noded soil elements are used to achieve compatibility with the 3D calculations. Structural elements have to be compatible with soil elements. When 6-noded soil elements are used plates are modelled with 3-noded plate (line) elements with 3 degrees of freedom per node: two translational degrees of freedom (u_x, u_y) and one rotational degree of freedom in the x-y plane (ϕ_z). For a standard deformation analysis using a plain-strain model these elements provided efficient accuracy. [10]

FIGURE 20: 6-NODED SOIL ELEMENTS (2D) [5]

In 2D the average elements size is calculated from the outer geometry dimensions and the global coarseness factor n_c.

$$l_e = \sqrt{\frac{(x_{max} - x_{min}) \cdot (y_{max} - y_{min})}{n_c}} \quad \textbf{(3.22)}$$

The global coarseness is chosen as coarse (n_c = 50) to fit the average element size of the 3D calculation. Around the tunnel the mesh is refined locally by a factor of 0.5.

The generated mesh consists of 615 soil elements with an average element size of 2.613 m.

Near to the left model boundary an interface element is inserted in the model, which is not activated during calculation. Its presence is required for the used program function to work correctly (see chapter 7.2).

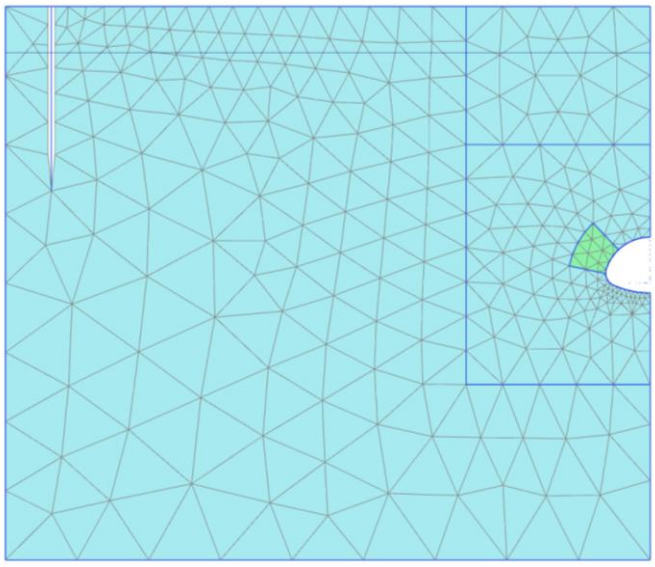

FIGURE 21: 2D FINITE ELEMENT MESH

3.7 CONSTRUCTION STAGES FOR 3D CALCULATION

For the 3D staged construction two different calculation scenarios are investigated:

1) "wished-in-place" calculation:
   - Excavation, installation of lining with material parameter set "*shotcrete old*" and activation of the increased cohesion for the anchor area for the entire model length in one phase (used to validate the 3D calculation program by comparison with the 2D WIP calculation)
2) Step-by-step excavation:
   Full-face advance for slice *i*:
   - Deactivation of the tunnel cluster (excavation) in slice *i*
   - Activation of the lining (material parameter set "*SC young*") in slice *i-1*

- Change of material of the anchor area from "*Silt*" to "*Silt + Anchor*" in slice *i-1*
- Change of the plate material set of the lining to "*SC old*" in slice *i-2*

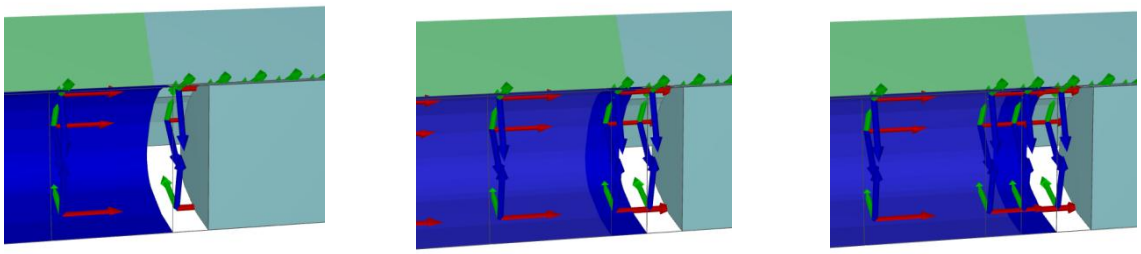

phase *i* - excavation | phase *i+1* – SC young + anchors | phase *i+2* – SC old

FIGURE 22: SEQUENTIAL EXCAVATION IN 3D

As mentioned in chapter 3.1, the excavation length is 1.5 m. To overcome the influence of boundary conditions at the beginning and the end of the tunnel a 20 m long interval with 2.5m-slices is modelled. For drained calculations it is excavated in one step, while for undrained calculation excavation is carried out in detail from the beginning to the end of the model to avoid the built-up of very high excess pore pressures as mentioned by Wohlfahrt. [8]

The evaluation of deformations and internal forces of the lining for the sequential excavation is carried out at y = 74.0/74.75/75.5 at the crown of the tunnel and at y = 71.0/74.23 at the surface representing the centre of the FE-model. The stations correspond to the beginning/centre/end of one excavation length.

3.8 CONSTRUCTION STAGES FOR 2D CALCULATION

For the 2D calculation two different scenarios are investigated:

1) "wished-in-place" calculation:
    1) Excavation of the tunnel, installation of the lining with material parameter set "*SC old*" and activation of the increased cohesion for the anchor area in one step (used to validate the 3D calculation program by comparison with 2D WIP calculation)
2) Sequential excavation:
    1) Stress-relaxation with ΣMStage< 1.0 in the tunnel cross-section (deactivation of the soil cluster in the tunnel)
    2) Activation of the lining (material parameter set "*SC young*") and change of material of the anchor area from "*Silt*" to "*Silt + Anchor*" with ΣMStage< 1.0
    3) Change of the plate material set of the lining to "*SC old*" (ΣMStage = 1.0)

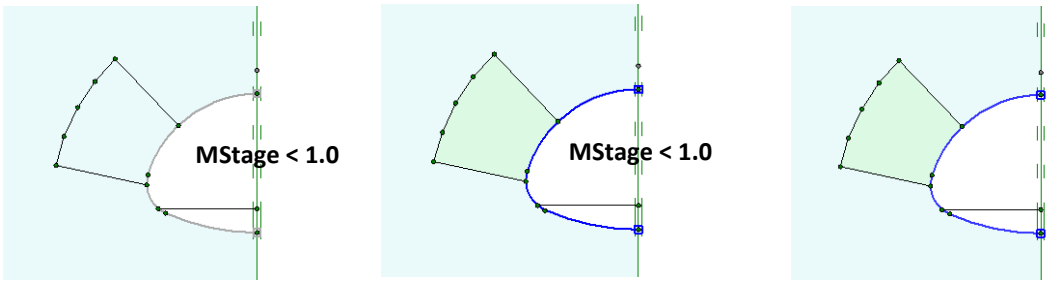

Pre-relaxation | Shotcrete young + anchors | Shotcrete old

FIGURE 23: SEQUENTIAL EXCAVATION IN 2D

4 "WISHED-IN-PLACE" CALCULATIONS IN 2D AND 3D

The major objective of the WIP calculations is to validate the 3D calculation program. A "wished-in-place" calculation represents a plain-strain problem. Therefore, 2D- and 3D-analysis are expected to give the same results.

WIP calculations are also used to investigate the influence of the initial stress state and small strain stiffness on settlements. Furthermore, the influence of pre-overburden pressure on the development of plasticity due to loading is evaluated by comparing calculation 2A) and 2C).

Undrained analyses with the Linear-Elastic (model 11) and the Mohr-Coulomb (model 6) model are carried out to evaluate the distribution of excess pore pressures in longitudinal direction of the tunnel.

4.1 PERFORMED CALCULATIONS

WIP calculations are performed with PLAXIS 2D 2010 and PLAXIS 3D 2011 for all listed calculation models.

4.1.1 CALCULATIONS WITHOUT GROUNDWATER (DRAINED)

TABLE 6: SOIL PARAMETERS WITHOUT CONSIDERATION OF GROUNDWATER

MODEL	$E_{oed,ref}$ [MN/m²]	$E_{50,ref}$ [MN/m²]	$E_{ur,ref}$ [MN/m²]	c [kN/m²]	φ [°]	m [-]	K_0 [-]	POP [kN/m²]	$K_{0,nc}$ [-]	ν_{ur} [-]	$G_{0,ref}$ [MN/m²]	$\gamma_{0,7}$ [-]
1)MC, E135	E = 135 MN/m²			35	27	-	0.54	-	-	-	-	-
2)HS, $E_{MC}=E_{oed}$	45	45	135	35	27	0.8			0.54	0.2	-	-
A							0.7	500				
B							auto	500				
C							0.7	0				
3)HS, $E_{MC}=E_{ur}$	20	20	60	35	27	0.8	0.7	500	0.54	0.2	-	-
7)HSS, $E_{MC}=E_{oed}$	45	45	135	35	27	0.8	0.7	500	0.54	0.2	225	$2*10^{-4}$
A	*Tolerated error = 1.0 % (Standard setting)*											
B	*Tolerated error = 0.1 %*											
9)HSS, $E_{MC}=E_{ur}$	20	20	60	35	27	0.8	0.7	500	0.54	0.2	100	$2*10^{-4}$

4.1.2 CALCULATIONS WITH GROUNDWATER (UNDRAINED)

TABLE 7: SOIL PARAMETERS WITH CONSIDERATION OF GROUNDWATER

MODEL	$E_{oed,ref}$ [MN/m²]	$E_{50,ref}$ [MN/m²]	$E_{ur,ref}$ [MN/m²]	c [kN/m²]	φ [°]	m [-]	K_0 [-]	POP [kN/m²]	$K_{0,nc}$ [-]	ν_{ur} [-]	$G_{0,ref}$ [MN/m²]	$\gamma_{0,7}$ [-]
4)HS, $E_{MC}=E_{oed}$	69.3	69.3	207.8	35	27	0.8	0.7	500	0.54	0.2	-	-
5)HS, $E_{MC}=E_{ur}$	30	30	90	35	27	0.8	0.7	500	0.54	0.2	-	-
6)MC, E135	E = 135 MN/m²			35	27	-	0.54	-	-	-	-	-
8)HSS, $E_{MC}=E_{oed}$	69.3	69.3	207.8	35	27	0.8	0.7	500	0.54	0.2	346.3	$2*10^{-4}$
A	*Tolerated error = 1.0 % (Standard setting)*											
B	*Tolerated error = 0.1 %*											
10)HSS, $E_{MC}=E_{ur}$	30	30	90	35	27	0.8	0.7	500	0.54	0.2	150	$2*10^{-4}$
11) LE	E = 135 MN/m² ; ν' = 0.2											

4.2 SETTLEMENTS

In 3D the deformations are evaluated at the centre of the model (y=71.0 m). The results of 3D FE-analysis are expressed as percentage of the settlements obtained from 2D calculations.

TABLE 8: WIP, SETTLEMENTS: 1) MC, DRAINED

	Surface settlements		Crown settlements	
PLAXIS 2D 2010	-8.2 mm		-21.3 mm	
PLAXIS 3D 2011	-8.1 mm	*98%*	-21.2 mm	*99%*

TABLE 9: WIP, SETTLEMENTS: 2) HS, $E_{MC} = E_{OED}$, DRAINED

	[mm]	Surface settlements		Crown settlements	
POP500	*PLAXIS 2D 2010*	-4.6 mm		-10.9 mm	
K_0=0.7	*PLAXIS 3D 2011*	-4.6 mm	*99%*	-10.8 mm	*99%*
POP500	*PLAXIS 2D 2010*	-3.3 mm		-9.2 mm	
K_0 automatic	*PLAXIS 3D 2011*	-3.3 mm	*101%*	-9.1 mm	*100%*
POP0	*PLAXIS 2D 2010*	-7.0 mm		-13.4 mm	
K_0=0.7	*PLAXIS 3D 2011*	-7.0 mm	*100%*	-13.3 mm	*100%*

TABLE 10: WIP, SETTLEMENTS: 3) HS, $E_{MC} = E_{UR}$, DRAINED

	Surface settlements		Crown settlements	
PLAXIS 2D 2010	-9.1 mm		-21.7 mm	
PLAXIS 3D 2011	-9.0 mm	*98%*	-21.5 mm	*99%*

TABLE 11: WIP, SETTLEMENTS: 4) HS, $E_{MC} = E_{OED}$, UNDRAINED

	Surface settlements		Crown settlements	
PLAXIS 2D 2010	-3.0 mm		-7.4 mm	
PLAXIS 3D 2011	-2.7 mm	*90%*	-6.7 mm	*90%*

TABLE 12: WIP, SETTLEMENTS: 5) HS, $E_{MC} = E_{UR}$, UNDRAINED

	Surface settlements		Crown settlements	
PLAXIS 2D 2010	-5.8 mm		-14.1 mm	
PLAXIS 3D 2011	-5.5 mm	*95%*	-13.6 mm	*96%*

TABLE 13: WIP, SETTLEMENTS: 6) MC, UNDRAINED

	Surface settlements		Crown settlements	
PLAXIS 2D 2010	-5.9 mm		-13.9 mm	
PLAXIS 3D 2011	-5.6 mm	*96%*	-13.5 mm	*97%*

TABLE 14: WIP, SETTLEMENTS: 7) HSS, $E_{MC} = E_{OED}$, DRAINED

	Surface settlements		Crown settlements	
PLAXIS 2D 2010	-1.7 mm		-4.3 mm	
PLAXIS 3D 2011 tol.error 0.01	-1.7 mm	*98%*	-4.2 mm	*99%*
PLAXIS 3D 2011 tol.error 0.001	-1.7 mm	*99%*	-4.3 mm	*99%*

TABLE 15: WIP, SETTLEMENTS: 8) HSS, $E_{MC} = E_{OED}$, UNDRAINED

	Surface settlements		Crown settlements	
PLAXIS 2D 2010	-1.4 mm		-3.4 mm	
PLAXIS 3D 2011 tol. error 0.01	-1.2 mm	*85%*	-3.1 mm	*90%*
PLAXIS 3D 2011 tol. error 0.001	-1.2 mm	*86%*	-3.1 mm	*91%*

TABLE 16: WIP, SETTLEMENTS: 9) HSS, $E_{MC} = E_{UR}$, DRAINED

	Surface settlements		Crown settlements	
PLAXIS 2D 2010	-3.5 mm		-9.1 mm	
PLAXIS 3D 2011 tol.error 0.001	-3.5 mm	*99%*	-9.0 mm	*99%*

TABLE 17: WIP, SETTLEMENTS: 10) HSS, $E_{MC} = E_{UR}$, UNDRAINED

	Surface settlements		Crown settlements	
PLAXIS 2D 2010	-2.6 mm		-6.3 mm	
PLAXIS 3D 2011 tol.error 0.001	-2.3 mm	*91%*	-6.0 mm	*94%*

The settlements obtained from 2D and 3D computation are in good agreement. Differences in undrained analysis are generally larger than in drained analysis when using the Hardening Soil and HS-small model. Except for calculation model 8) all results are within a 10 %-range.

4.2.1 INFLUENCE OF THE INITIAL STRESS STATE

Settlements obtained from calculations with *POP* = 0 kN/m² are expected to be larger than for calculations with POP *= 500 kN/m²* and K_0 = 0.7. Smallest settlements should result from calculation with *POP = 500 kN/m²* and an automatically calculated K_0. The pre-overburden pressure is used to calculate the initial pre-consolidation pressure, which determines the position of the initial cap yield surface. Previous loading leads to an expansion of the volumetric hardening yield surface and a larger elastic region. Within the elastic region soil behaviour is governed by the un- and reloading stiffness, which is three-times the secant stiffness in triaxial loading E_{50}. The higher stiffness restrains the development of deformations. The automatically calculated K_0 takes the higher coefficient of lateral earth pressure at rest for over-consolidated soils into account. It results in higher horizontal initial stresses, especially at the tunnel surface. Large horizontal stresses restrict the development of vertical deformations. The influence of the *automatically calculated* K_0 on vertical settlements compared to K_0 *= 0.7 = const*. at the surface exceed the influence at the crown by approximately 10 %.

4.2.2 INFLUENCE OF SMALL-STRAIN STIFFNESS

The influence of small strain stiffness on the development of settlements is investigated by comparing the corresponding calculation with the Hardening Soil and HS-small model.

TABLE 18: WIP: HARDENING SOIL VS. HS-SMALL

		Hardening Soil	Hardening Soil-small
drained	$E_{MC} = E_{oed}$	2)	7)
	$E_{MC} = E_{ur}$	3)	9)
undrained	$E_{MC} = E_{oed}$	4)	8)
	$E_{MC} = E_{ur}$	5)	10)

Due to increased stiffness at small strains settlement computed with the HS-small model are expected to be smaller than settlements obtained from calculations with the corresponding Hardening Soil model. The difference in magnitude depends on the applied shear modulus. For $G_0 = G_{ur}$ deformations calculated with the HS and HS-small model are approximately the same.

The small-strain shear modulus G_0 is 4-times higher than the un-/reloading shear stiffness G_{ur}. With increasing strains the initial stiffness decreases until it reaches G_{ur} (E_{ur} respectively). At G/G_{ur} the model switches to the hardening plasticity of the Hardening Soil model.

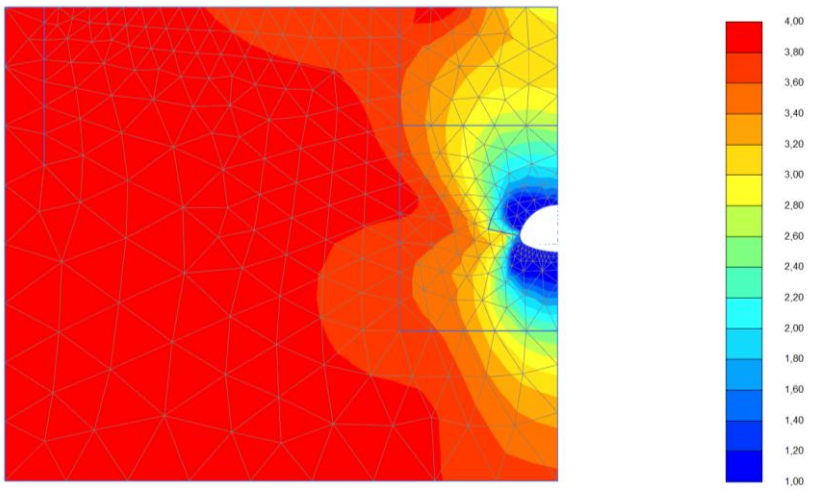

FIGURE 24: RATIO G/ G_{UR} FOR DRAINED "WISHED-IN-PLACE" COMPUTATIONS USING THE HS-SMALL MODEL (PLAXIS 2D 2010)

Tunnel excavation causes relatively large strains in the area close to the tunnel opening. The influence of tunnel construction decreases with growing distance. The shear modulus *G* of the soil around the tunnel reaches G_{ur} and increases up to the surface. Therefore, surface settlements are expected to be influenced more by small-strain stiffness than crown settlements.

TABLE 19: RATIO OF "WISHED-IN-PLACE" SETTLEMENTS: HARDENING SOIL VS. HS-SMALL (E_{MC}=E_{OED})

		surface	*crown*
Drained 2) and 7)	*2D*	2.7	2.5
	3D	2.7	2.5
Undrained 4) and 8)	*2D*	2.1	2.2
	3D	2.3	2.3

TABLE 20: RATIO OF "WISHED-IN-PLACE" SETTLEMENTS: HARDENING SOIL VS. HS-SMALL (E_{MC}=E_{UR})

		surface	*crown*
Drained 3) and 9)	*2D*	2.6	2.2
	3D	2.6	2.2
Undrained 5) and 10)	*2D*	2.1	2.1
	3D	2.4	2.3

When comparing "wished-in-place" deformations computed with the Hardening Soil model ($E_{MC} = E_{oed}$) and the corresponding HS-small model a factor of approximately 2.6 for drained calculations and 2.2 for undrained calculation is obtained. Under drained conditions surface settlements obtained from HS calculation 2) exceed the HS-small calculation 7) by a factor of 2.7 and crown settlements by 2.5. The influence of small-strain stiffness is, therefore, higher for surface settlements. The ratio of drained analysis with the parameter set E_{MC}=E_{ur} between HS 3) and HS-small model 9) is 2.6 for surface and 2.2 for crown settlements. The lower stiffness results in a smaller influence of small-strain stiffness. Under undrained conditions volumetric changes are restricted by incompressibility of pore water. The ratio of surface and crown settlements obtained from HS and HSS calculations are the same. Furthermore, in undrained analysis the ratio is not influenced by different soil parameter sets [4) and 5), 8) and 10)].

4.3 INFLUENCE OF PRE-OVERBURDEN PRESSURE ON THE DEVELOPMENT OF PLASTIC POINTS

The pre-overburden pressure has a strong influence on the development of plasticity in the WIP calculations. The position of the cap type yield surface is determined by the initial pre-consolidation pressure σ_{p0}, whose

calculation is based on *POP*. For *POP > 0* the elastic region, where no yield surface is active, is increased. When considering *POP = 500 kN/m²* less plasticity is expected.

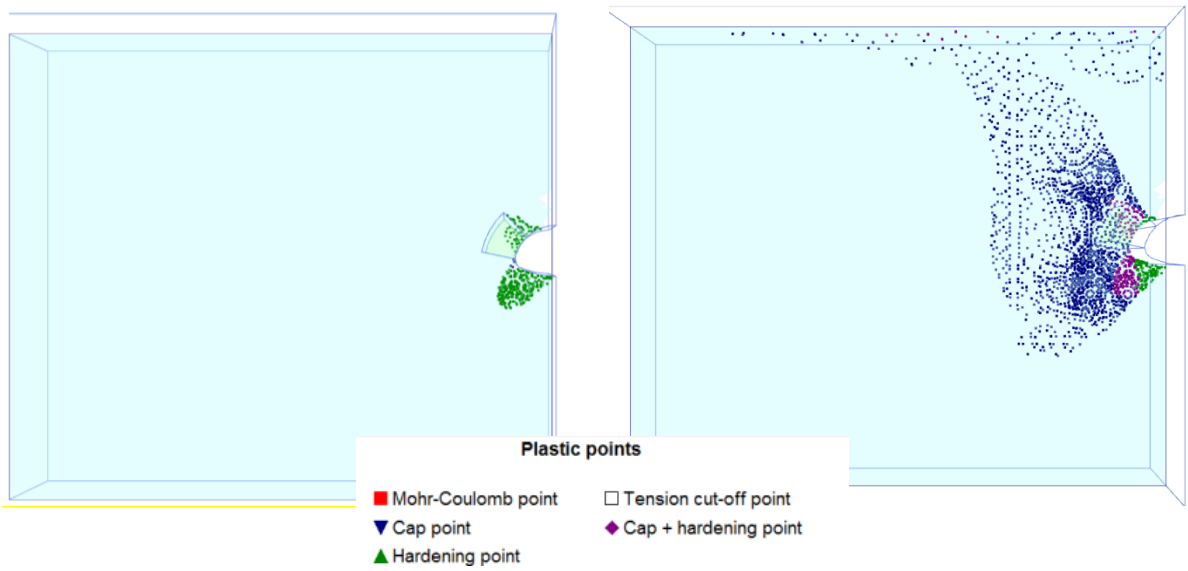

FIGURE 25: LEFT- PLASTIC POINTS FOR CALCULATION 2) WITH K_0=0.7 AND POP=500 KN/M²; RIGHT - PLASTIC POINTS FOR CALCULATION 2B) WITH K_0=0.7 AND POP=0 KN/M²

For calculation 2A) only in the area close to the tunnel the shear hardening yield surface is mobilized. If no pre-overburden pressure is applied (calculation 2B) the volumetric and shear hardening yield surface are mobilized. The influence of plasticity expands up to the surface.

4.4 DISTRIBUTION OF EXCESS PORE PRESSURES IN UNDRAINED ANALYSIS

The generated excess pore pressures in an undrained WIP calculation are expected to have a uniform distribution in longitudinal direction of the tunnel. Because the performed 3D computations yielded large variations of excess pore pressures along the tunnel axis, further investigations were carried out. Undrained analyses with the Linear-Elastic (model 11) and the Mohr-Coulomb (model 6) model are used to evaluate the distribution of excess pore pressures in longitudinal direction of the tunnel. The nodal values of excess pore pressure are compared for different y - values in 3 nodes:

- point A – tunnel shoulder
- point B – tunnel springline
- point C – tunnel invert

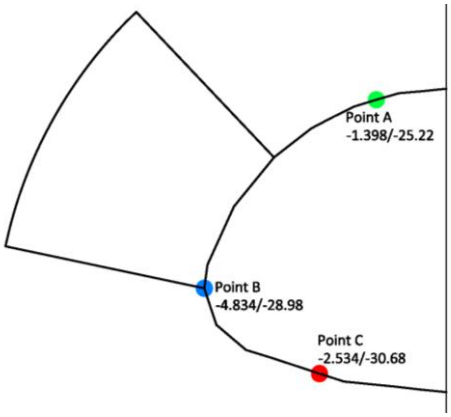

FIGURE 26: POSITION OF NODES

4.4.1 LINEAR-ELASTIC MODEL

To evaluate the source of inconsistencies a calculation with the Linear-Elastic model is performed. Influences of lining installation and water conditions in the tunnel are investigated.

TABLE 21: VERSIONS FOR "WISHED-IN-PLACE" CALCULATION USING LINEAR-ELASTIC MODEL

	Tunnel lining	Water conditions for the tunnel cluster
Calculation 1	yes	dry
Calculation 2	no	dry
Calculation 3	no	Phreatic level

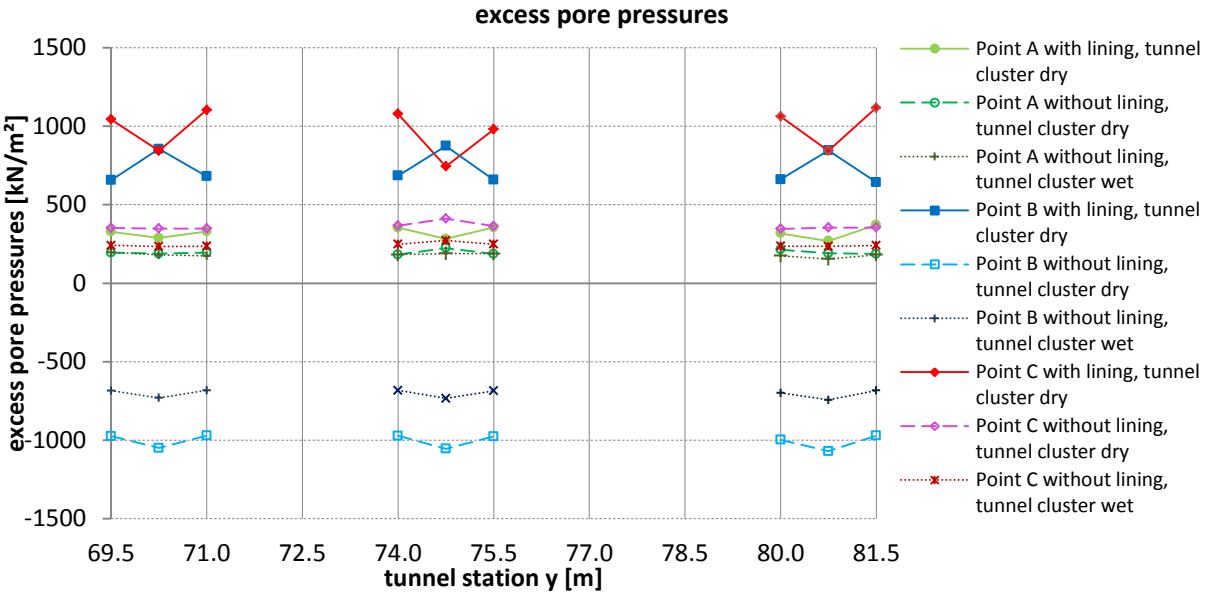

FIGURE 27: LE, WIP: DISTRIBUTION EXCESS PORE PRESSURES OVER TUNNEL LENGTH

In Figure 27 the nodal values of excess pore pressures for calculation 1 - 3 with the Linear-Elastic model are compared for 3 excavation lengths. At the junction between tunnel, anchor area and the ground the largest differences occur. Linear-elastic soil behaviour is assumed to evaluate the influence of lining installation. When using the Mohr-Coulomb model the ground collapses as consequence of tunnel excavation without support. Large variations of excess pore pressures along the tunnel axis within the 1.5m-slices are obtained from calculation 1. Without lining installation (calculation 2 and 3) the generated pore pressures show only small differences over the tunnel axis. The variations of excess pore pressures within the excavation length are likely to be caused by the plate elements. Furthermore, the influence of water conditions in the tunnel cluster is investigated. In calculation 3 water conditions in the excavated area are not set to dry. Compared to the results of calculation 2 the excess pore pressures are reduced, but the variation along the tunnel axis remains more or less the same.

Note that, pore water pressure in PLAXIS is displayed as negative values and suction is positive.

4.4.2 MOHR-COULOMB MODEL

The nodal values of excess pore pressure are also compared for an undrained Mohr-Coulomb analysis for 4 excavation lengths between station 63.5 and 91.5 m in the middle of the FE-model.

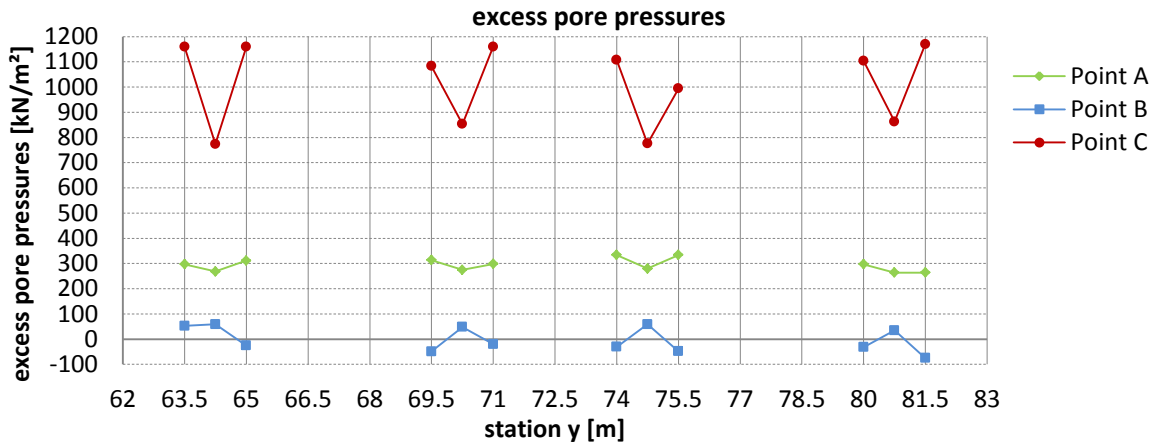

FIGURE 28: MC, UNDRAINED, WIP: DISTRIBUTION EXCESS PORE PRESSURES OVER TUNNEL LENGTH

Maximum deviation occurs in Point B at the junction from soil to anchor area at the tunnel spring line. In this area the variations along the tunnel axis are about 20 % larger than for the 11) Linear-Elastic model. Within one excavation length the differences are approximately 10 % larger. It is concluded that plasticity and lining installation have an influence on the distribution of excess pore pressures in PLAXIS 3D.

Further 2D and 3D calculations are compared. The results of 3D calculations are evaluated in the middle of the model at y = 71.0 m.

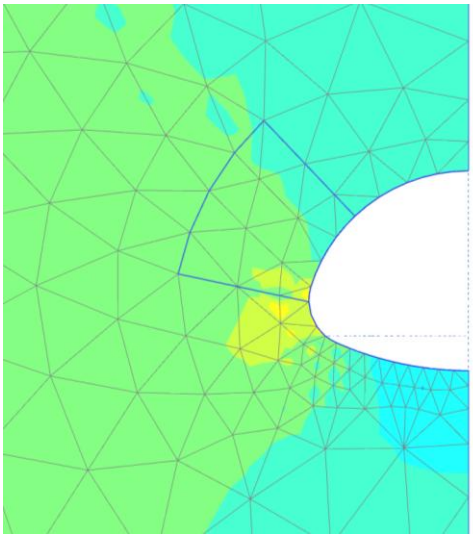

FIGURE 29: 2D 2010: MC, UNDRAINED, WIP: EXCESS PORE PRESSURE

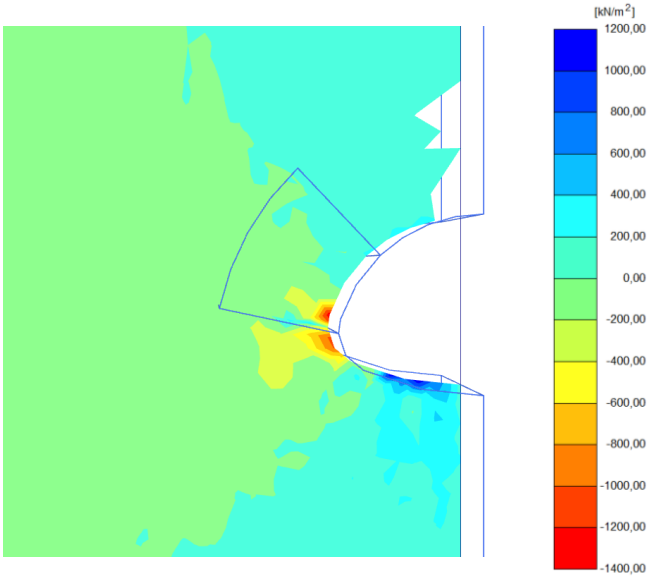

FIGURE 30: 3D 2011 (Y=71M): MC, UNDRAINED, WIP: EXCESS PORE PRESSURE

TABLE 22: MC, UNDRAINED, WIP: EXCESS PORE PRESSURES

	Plaxis 2D 2010		Plaxis 3D 2011	
minimum	-580.7	*kN/m²*	-3317	*kN/m²*
maximum	414.6	*kN/m²*	1320	*kN/m²*

2D and 3D calculation provide a similar image of the distribution of excess pore pressures, but the magnitude of the extreme values at the tunnel invert and springline shows significant differences for the Mohr-Coulomb model. The extreme values occur at the beginning and the end of the model, where 2.5 m slices are modelled.

The discretization in longitudinal direction influences the generation of excess pore pressures. A detailed modelling of short slices in y- direction is believed to prevent the built-up of very high excess pore pressures.

In the x-z- plane in the middle of the model (y = 71.0 m) the extreme values are reduced to 1160 kN/m² and -1351 kN/m², but they still exceed the results obtained from 2D undrained analysis. Positive excess pore pressures are displayed in shadings of blue. Negative excess pore pressures are plotted in yellow and red. Negative excess pore pressures are generated at the tunnel springline. At the tunnel invert and crown due to unloading of the ground positive excess pore pressures are generated.

4.4.3 HARDENING SOIL AND HS-SMALL MODEL

In undrained analysis with the Hardening Soil model and HS-small model negative excess pore pressures are generated at the tunnel springline and positive excess pore pressures at the tunnel crown and invert.

The influence of different soil stiffness parameters and the consideration of small-strain stiffness are investigated. In the figures below the results of 2D WIP calculations are compared.

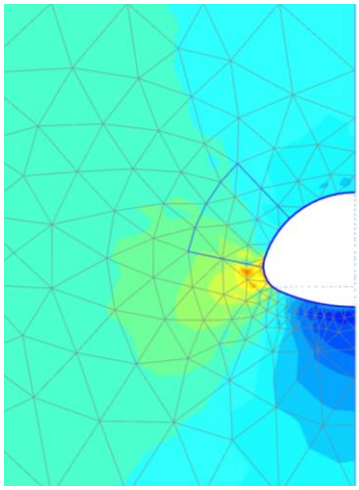

FIGURE 31: 2D 2010: 4) HS, UNDRAINED, WIP: EXCESS PORE PRESSURE

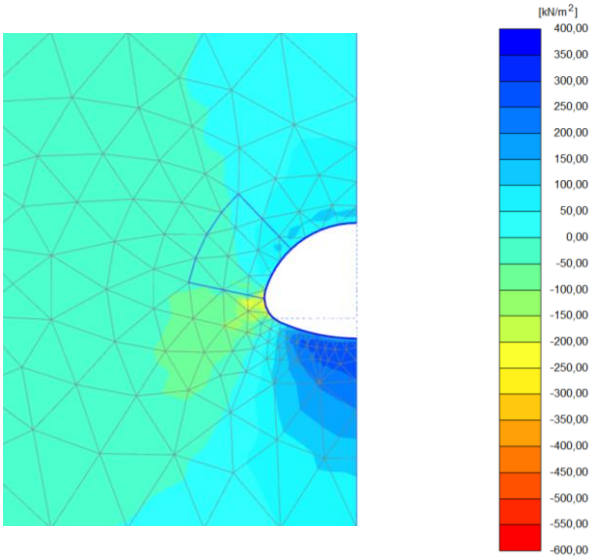

FIGURE 32: 2D 2010: 8) HSS UNDRAINED, WIP: EXCESS PORE PRESSURE

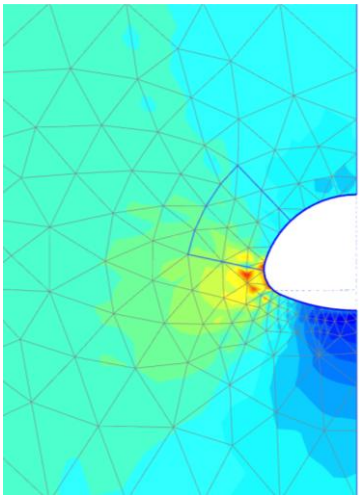

FIGURE 33: 2D 2010: 5) HS, UNDRAINED, WIP: EXCESS PORE PRESSURE

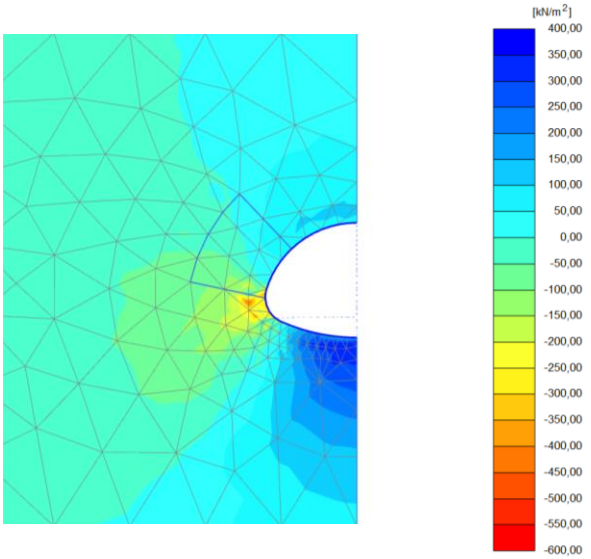

FIGURE 34: 2D 2010: 10) HSS UNDRAINED, WIP: EXCESS PORE PRESSURE

In the calculation models 4) and 8) higher reference stiffness values are used compared to 5) and 10). Generally less excess pore pressures in the area close to the tunnel are generated in stiffer ground independently of the used constitutive model. The consideration of small-strain stiffness results in smaller excess pore pressures at the tunnel invert and springline. At the tunnel crown slightly larger excess pore pressures are generated.

Generally calculations with PLAXIS 3D 2011 highly over predict excess pore pressures. The maximum values are about 4-times higher than in 2D FE-analysis. The extreme values are limited to certain nodes at the beginning and end of the model. They have no informative value for the magnitude of overall excess pore pressures. Due to the large variations along the tunnel axis excess pore pressures generated in 3D are not reliable. Results of undrained analysis have to be evaluated carefully.

5 DRAINED 3D CALCULATIONS

Drained analyses are performed without consideration of groundwater conditions due to insufficient ground stability as explained in chapter 3.3. To overcome boundary conditions a 20 m "wished-in-place" section is inserted at the beginning and the end of the model.

5.1 PERFORMED CALCULATIONS

TABLE 23: SOIL PARAMETERS WITHOUT CONSIDERATION OF GROUNDWATER

MODEL	$E_{oed,ref}$ [MN/m²]	$E_{50,ref}$ [MN/m²]	$E_{ur,ref}$ [MN/m²]	c [kN/m²]	φ [°]	m [-]	K_0 [-]	POP [kN/m²]	$K_{0,nc}$ [-]	ν_{ur} [-]	$G_{0,ref}$ [MN/m²]	$\gamma_{0,7}$ [-]
1)MC, E135	E=135 MN/m²			35	27	-	0.54	-	-	-	-	-
2)HS, $E_{MC}=E_{oed}$	45	45	135	35	27	0.8	0.7	500	0.54	0.2	-	-
A							0.7	500				
B							auto	500				
C							0.7	0				
3)HS, $E_{MC}=E_{ur}$	20	20	60	35	27	0.8	0.7	500	0.54	0.2	-	-
7)HSS, $E_{MC}=E_{oed}$	45	45	135	35	27	0.8	0.7	500	0.54	0.2	225	$2*10^{-4}$
A	*Tolerated error = 1.0 % (Standard setting)*											
B	*Tolerated error = 0.1 %*											
9)HSS, $E_{MC}=E_{ur}$	20	20	60	35	27	0.8	0.7	500	0.54	0.2	100	$2*10^{-4}$

5.2 INFLUENCE OF TOLERATED ERROR IN HS-SMALL CALCULATIONS

When using the Hardening-Soil model with small strain stiffness for computation of sequential tunnel excavation the out-of-balance force at the tunnel face has to be checked. At the tunnel face the total stresses in longitudinal direction σ_{yy} have to be around zero to be in equilibrium.

In any non-linear analysis with a finite number of calculation steps no exact solution is reached. It has to be ensured that the error remains in acceptable bounds. In PLAXIS the error limits of the solution algorithm are linked to the input value *Tolerated error*. In most cases the default value of 1.0 % is adequate. During iteration an automatic error check is performed. The used error indicators are based on global equilibrium error and local error. Both values have to be below predetermined limits. The global error is related to the sum of out-of-balance nodal forces. The local error refers to the error at each stress point. If the local error exceeds the *Tolerated error* the stress point is defined as inaccurate plastic point. The number of inaccurate points is limited. The global error has to be lower than the *Tolerated error*. [2]

$$Global\ error = \frac{\sum \|Out\ of\ balance\ nodal\ forces\|}{\sum \|Active\ loads\|} \leq Tolerated\ error \quad (5.1)$$

To increase the accuracy of the equilibrium stress field the *Tolerated error* can be reduced. In the case of modelling sequential excavation, this may be necessary. 3D FE-analysis of tunnelling requires large model dimensions to achieve steady state conditions. In relation to model dimensions the excavation of one slice has little influence on the total system. Therefore the sum of out-of-balance nodal forces can be small without fulfilling local equilibrium at the tunnel face. The *Tolerated error* was reduced manually to 0.1 % for HS-small calculations to increase the accuracy of the equilibrium stress field. For "wished-in-place" calculations the zone of influence is significantly larger compared to model dimensions and the default value can be used.

The *Tolerated error* also influences the accuracy of computed surface settlement. To obtain reliable results a relatively tight value is required, while e.g. structural forces are less affected by error checking. [1]

For drained calculations above the ground water table effective stresses equal total stresses. In Figure 35 longitudinal effective stresses σ_{yy}' [kN/m²] in phase 70 at the tunnel face are displayed and compared with results of corresponding HS computations. When using the default value of 0.01 for the *Tolerated error,* negative longitudinal stresses are generated at the tunnel face. With the reduced value of 0.001, σ_{yy}' is approximately zero and corresponds to the results of the Hardening Soil model. When using a *Tolerated error* of 1 % PLAXIS the excavation phase is performed in one single calculation step as for elastic behaviour. The number of steps increases significantly for a reduced *Tolerated error*. Therefore, only the results for calculation B with a tolerated error of 0.1 % are evaluated further on.

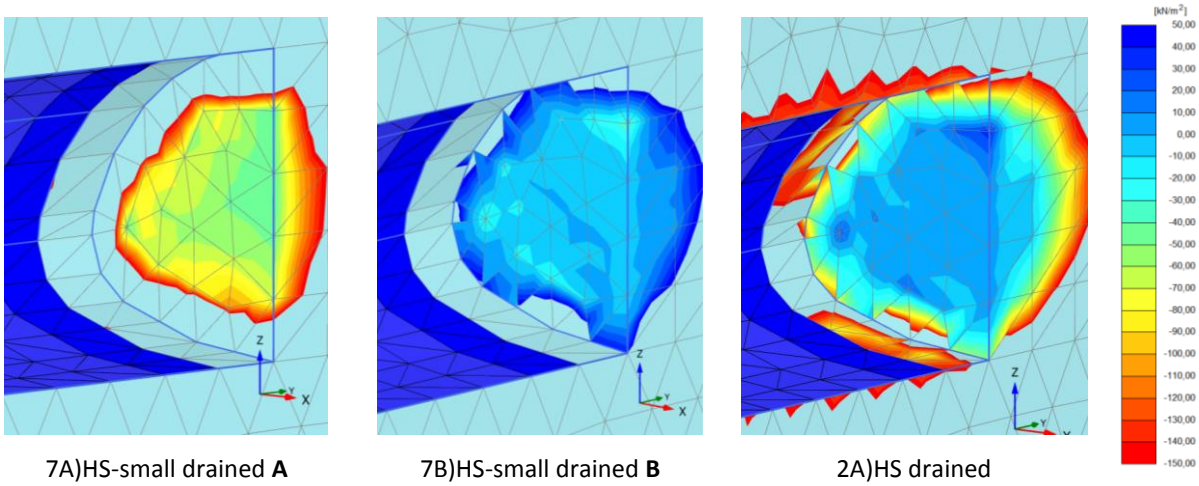

7A)HS-small drained **A** 7B)HS-small drained **B** 2A)HS drained

FIGURE 35: LONGITUDINAL EFFECTIVE STRESSES AT THE TUNNEL FACE FOR HS-SMALL UNDER DRAINED CONDITIONS

5.3 SURFACE SETTLEMENTS

Surface settlements are evaluated after completed tunnel construction in two nodes in the middle of the FE-model above the tunnel centre-line.

- Node 1: 0.0/71.0/0.0
- Node 2: 0.0/74.23/0.0

The vertical settlements obtained from the three-dimensional numerical calculations are summarized in Table 24. In the middle of the FE-model steady state surface settlements are obtained. The largest deformations are predicted by calculation 3) and 9) with the lowest stiffness parameters $E_{MC} = E_{ur}$. Settlements calculated with the Hardening Soil model exceed the results of the corresponding HS-small model. The initial stress state has a significant influence on surface settlements.

TABLE 24: SURFACE SETTLEMENTS FROM DRAINED FE-ANALYSIS

	Eoed,ref	***E50,ref***	***Eur,ref***	***station***	
	[MN/m²]	*[MN/m²]*	*[MN/m²]*	*71.00 m*	*74.23 m*
1) MC	*E=135 MN/m²*			-15 mm	-15 mm
2A) HS E45	*45*	*45*	*135*	-11 mm	-11 mm
2B) HS E45				-7 mm	-7 mm
2C) HS E45				-16 mm	-16 mm
3) HS E20	*20*	*20*	*60*	-23 mm	-23 mm
7) HSS E45	*45*	*45*	*135*	-5 mm	-5 mm
9) HSS E20	*20*	*20*	*60*	-11 mm	-11 mm

5.3.1 TRANSVERSAL SETTLEMENT TROUGH

The corresponding transversal settlement troughs in Station y = 71.0 m are displayed in Figure 36. They are compared to field measurements at station MQ 1015, 1040, 1067 and 1146.

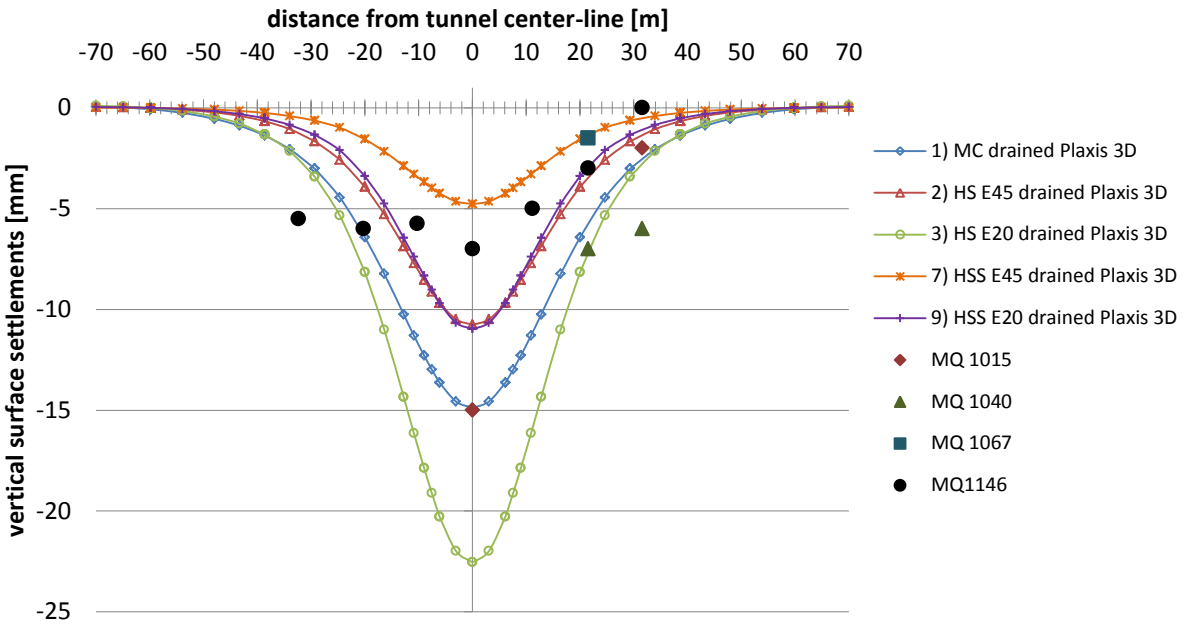

FIGURE 36: COMPARISON OF THE TRANSVERSAL SURFACE SETTLEMENT TROUGH AT STATION 1015, 1040, 1067 AND 1146 WITH THE RESULTS OF THE NUMERICAL DRAINED CALCULATIONS IN STATION 71

The magnitude of settlements depends on the assumed soil stiffness parameters. The shallowest settlement trough is obtained for calculation 7), the deepest for calculation 3). The consideration of small-strain stiffness results in a significantly shallower transversal settlement profile compared to the standard Hardening Soil model. Surface settlements obtained from calculations using standard Hardening Soil model with $E_{MC} = E_{oed}$ exceed the corresponding deformations computed with HS-small model by a factor of 2.2. Crown settlements are 1.6-times larger. When using lower stiffness values ($E_{MC} = E_{ur}$) the ratio becomes smaller. Surface settlements calculated with the standard Hardening Soil model are approximately twice the settlements calculated with the corresponding HS-small model. Crown settlements are about 1.3-times larger. Model 2) Hardening Soil drained $E_{MC} = E_{oed}$ and 9) HS-small drained $E_{MC} = E_{ur}$ calculate a very similar surface settlement profiles. The HS-small model results in a slightly narrower profile. The influence of the initial stress state is investigated for calculation model 2). The deepest and widest settlement trough is generated in the case of no pre-overburden pressure and constant K_0. For $POP = 500\ kN/m^2$ the model with K_0 varying with depth (calculation 2B) leads to a shallower settlement trough compared to a constant value of K_0 (calculation 2A).

From field measurements a complete settlement profile is only available in station 1146. The measured trough is not symmetrical as expected for homogeneous ground conditions. Between station 1145 and 1155 the tunnel passes under a mixed water channel, a street and a water pipe. [8] The existing installations could be a possible reason for the unsymmetrical settlement profile. At the building “Seebacher” located near station 1040 max. 2 mm settlement of the structure was measured. [8]

5.3.2 LONGITUDINAL SETTLEMENT PROFILE

In Figure 37 the longitudinal settlement profile for station 71.0 m over the position of the advancing tunnel face is displayed. It is compared to field measurements in station 1015 and 1146.

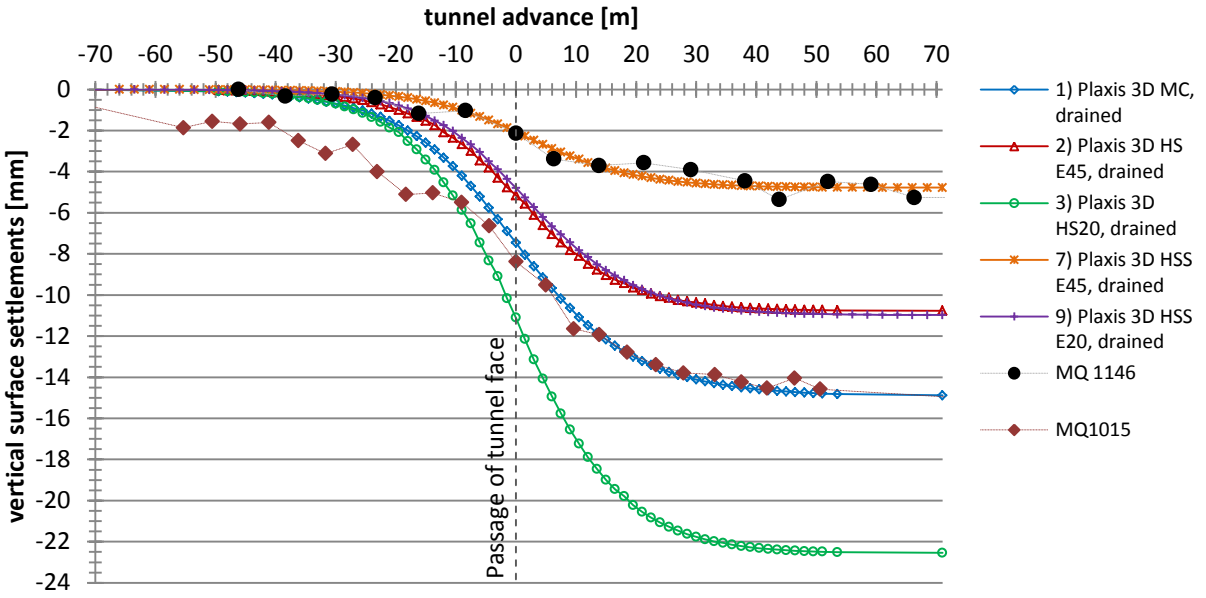

FIGURE 37: COMPARISON OF THE DEVELOPMENT OF SURFACE SETTLEMENTS AT STATION 1015 AND 1146 WITH THE RESULTS OF THE NUMERICAL DRAINED CALCULATIONS IN STATION 71

Steady state conditions are reached when the tunnel face advances about 50 m beyond the considered observation section. The order of magnitude is the same as for the transversal settlement trough. About 50 % of the steady state settlements occur prior to the passage of the tunnel face in the calculations using the MC and the HS model. The HS-small model predicts a pre-displacement of about 44 % of steady state settlements.

The shapes of the settlement curves predicted by FE-analysis and obtained from field measurements are in good agreement. Field measurements in observation point MQ 1146 are best matched by calculation 7), the measurements in station MQ 1015 by calculation 1). Except calculation 3) all models predict a surface settlement profile within the measured range.

5.4 LINING FORCES AND DEFORMATIONS

5.4.1 CROWN SETTLEMENT

Crown settlements are evaluated after completed tunnel construction at the beginning, end and centre of one excavation length in the middle of the FE-model.

The vertical settlements obtained from the three-dimensional numerical calculations are summarized in Table 25.

TABLE 25: CROWN SETTLEMENTS FROM DRAINED FE-ANALYSIS

	Eoed,ref	***E50,ref***	***Eur,ref***	***station***		
	[MN/m²]	*[MN/m²]*	*[MN/m²]*	*74.00 m*	*74.75 m*	*75.50 m*
1) MC	*E=135 MN/m²*			-36 mm	-39 mm	-36 mm
2A) HS E45	*45*	*45*	*135*	-27 mm	-32 mm	-27 mm
2B) HS E45				-26 mm	-31 mm	-26 mm
2C) HS E45				-29 mm	-33 mm	-27 mm
3) HS E20	*20*	*20*	*60*	-56 mm	-67 mm	-56 mm
7) HSS E45	*45*	*45*	*135*	-17 mm	-21 mm	-17 mm
9) HSS E20	*20*	*20*	*60*	-41 mm	-52 mm	-41 mm

The crown settlements range from -17 to -56 mm. The largest settlements are obtained from calculations with $E_{MC} = E_{ur}$. When considering small-strain stiffness smaller deformations are calculated compared to the corresponding standard HS model. The initial stress state (K_0 and *POP*) has little influence on the crown settlements. Furthermore, a sagging of the tunnel crown in 3D FE-analysis is observed. Due to the support of the tunnel face ahead and the shotcrete lining behind deformations in the unsupported length are largest in the centre. With lining installation settlements are restricted and the sagging of the tunnel crown is preserved.

In Figure 38 the crown settlement profile in longitudinal direction obtained from drained FE-analysis is displayed.

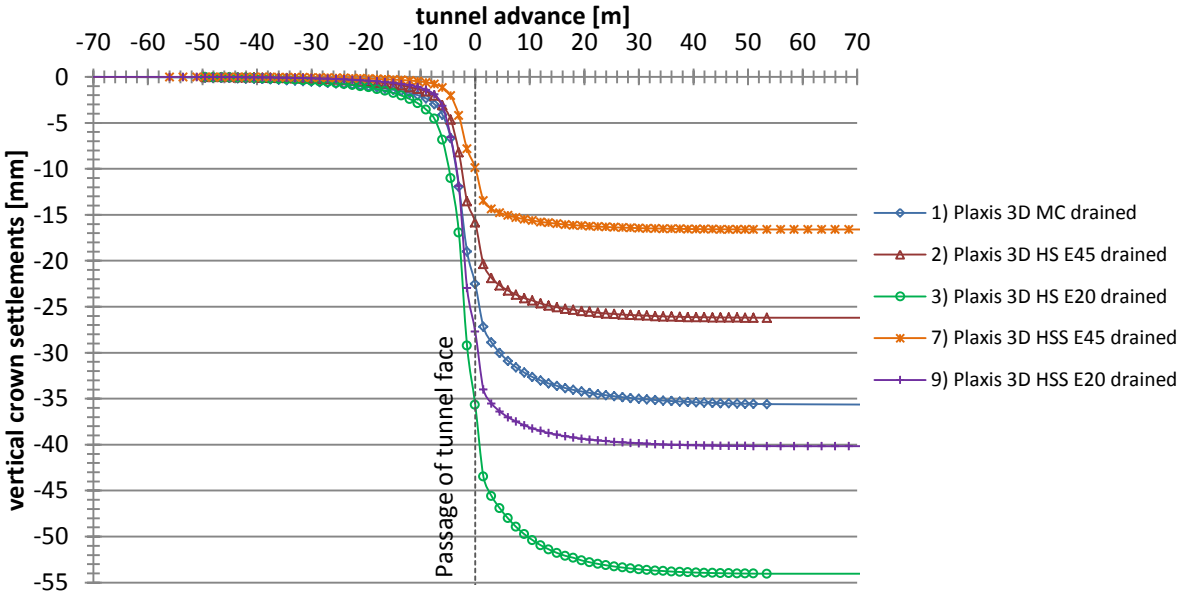

FIGURE 38: DEVELOPMENT OF CROWN SETTLEMENT IN LONGITUDINAL DIRECTION FOR DRAINED FE-ANALYSIS

FE calculations predict a pre-displacement of 60 – 69 % of steady state settlements. The deformation increase caused by the passage of the tunnel face is more distinctive in HS-small calculations than in the corresponding HS calculations. Steady state conditions are reached faster compared to surface settlements. 35 m after the passage of the tunnel face settlements can be considered constant.

At the tunnel crown the longitudinal development of the settlements is compared to measurements at station 1044 and 1176. Prior to the passage of the face no measurement data are available. Hence, the relation between the settlements at the passage of the face and steady state settlements are compared.

In Table 26 the difference between predicted crown settlements at the time of the passage of the tunnel face and steady state crown settlements is shown. The pre-displacements are expressed as percentage of steady state deformations.

TABLE 26: DIFFERENCE BETWEEN CROWN SETTLEMENTS AT THE PASSAGE OF THE TUNNEL FACE AND STEADY STATE CROWN SETTLEMENTS

	Passage of the tunnel face		***Steady state***	***Difference***
1) MC drained	-22.5 mm	*63%*	-35.6 mm	-13.1 mm
2) HS E45 drained	-15.8 mm	*60%*	-26.2 mm	-10.4 mm
3) HS E20 drained	-35.7 mm	*66%*	-54.0 mm	-18.4 mm
7) HSS E45 drained	-9.9 mm	*60%*	-16.6 mm	-6.7 mm
9) HSS E20 drained	-27.7 mm	*69%*	-40.2 mm	-12.5 mm
MQ 1044	0.0 mm		-19.5 mm	-19.5 mm
MQ 1176	0.0 mm		-9.0 mm	-9.0 mm

At station 1044 the maximum measured settlement -19.5 mm, in station 1176 it is -9.0 mm. The results of drained numerical calculation vary depending on the model and the parameter set between -6.7 and -18.4 mm, lying in the range of the measurements.

In Figure 39 the development of crown settlements after the passage of the tunnel face is displayed.

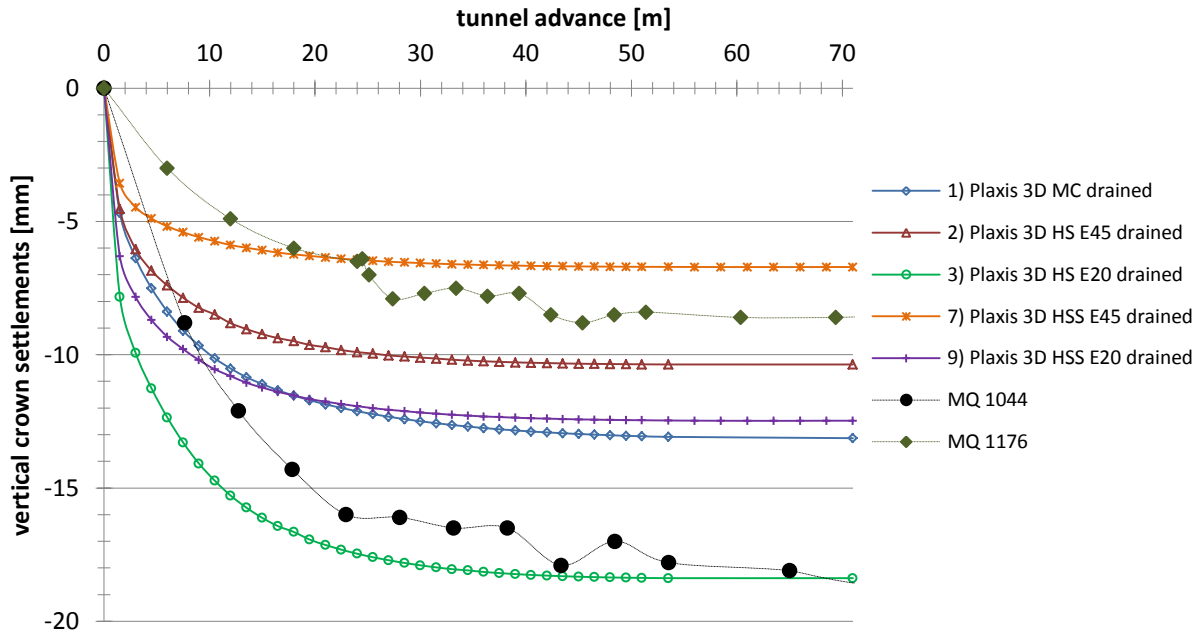

FIGURE 39: COMPARISON OF THE DEVELOPMENT OF CROWN SETTLEMENTS AT STATION 1015 AND 1146 WITH THE RESULTS OF THE NUMERICAL DRAINED CALCULATIONS IN STATION 71

Numerical calculations predict a large increase in settlements caused by the passage of the tunnel face. Field measurements show a smaller gradient immediately after excavation. Differences may result from a marginal delayed installation of the observation system. Steady state conditions from field measurements are reached about 55 m after the passage of the tunnel face.

5.4.2 LINING FORCES

The axial forces and bending moments in the lining are displayed in the figures below. Table 27 summarises the minimum and maximum values. Internal lining forces obtained from calculations with PLAXIS 3D 2011 have to be evaluated carefully. Due to the discretization of the curved tunnel circumference with straight lines and tetrahedral elements no smooth distribution of internal forces is obtained.

TABLE 27: INTERNAL LINING FORCES (DRAINED ANALYSIS)

		1)MC	2)HS $E_{MC}=E_{oed}$	3)HS $E_{MC}=E_{ur}$	7)HSS $E_{MC}=E_{oed}$	9)HS $E_{MC}=E_{ur}$
M	*min*	-54	-31	-43	-18	-30
[kNm/m]	*max*	59	37	65	19	39
N	*min*	356	481	481	410	484
[kN/m]	*max*	793	817	851	624	741

The minimum axial forces occur at the tunnel crown, the maximum values at the tunnel springline. Compared to the Hardening Soil and HS-small model, the Mohr Coulomb model predicts the smallest values at the crown. The consideration of small-strain stiffness leads to a reduction of maximum axial forces by 10 – 20 %. The bending moments are reduced by 30 – 50 %. The influence is greater for the higher soil stiffness $E_{MC} = E_{oed}$. Generally internal lining forces are smaller for tunnels constructed in relatively stiffer ground as a higher proportion of loading is carried by the ground.

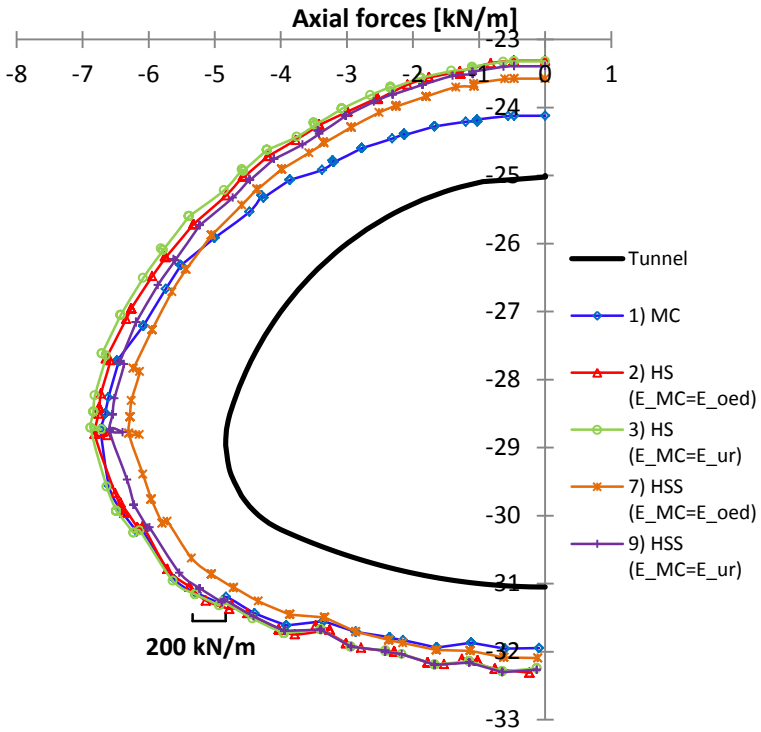

FIGURE 40: AXIAL FORCES (DRAINED ANALYSIS)

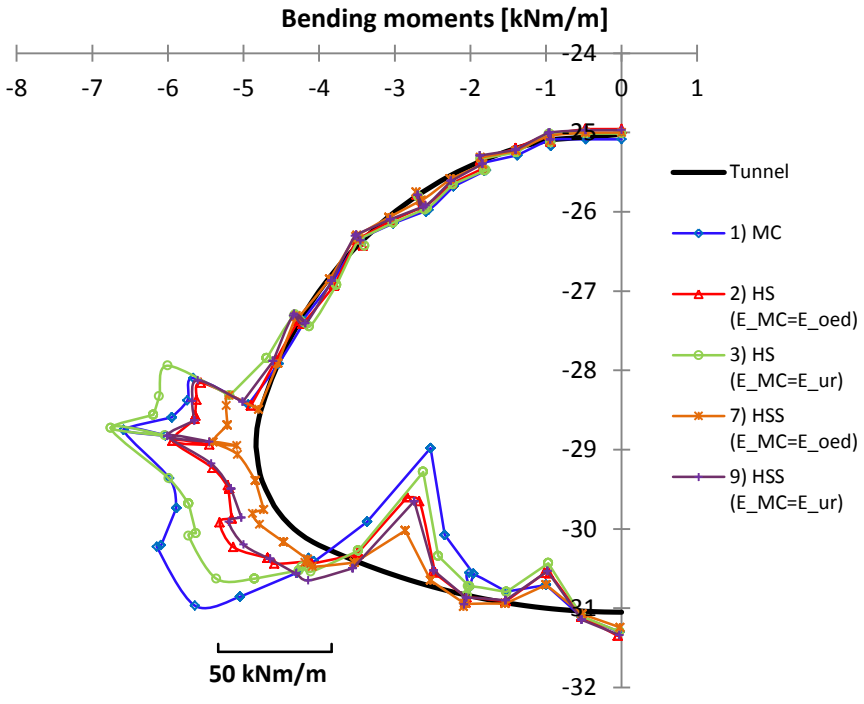

FIGURE 41: BENDING MOMENTS (DRAINED ANALYSIS)

6 UNDRAINED 3D CALCULATIONS

6.1 MODELLING UNDRAINED BEHAVIOUR IN PLAXIS

An undrained analysis is required when the permeability of the soil is low, the rate of loading is high and short term behaviour has to be assessed [12].

According to Terzaghi's principle the pore water pressure contributes to the total stress level in the soil body.

$$\underline{\sigma_{tot}} = \underline{\sigma'} + \underline{\sigma_w} \tag{6.1}$$

Water cannot sustain any shear stresses. Therefore, the total shear stresses equal the effective shear stresses. The pressure of fluid applies in all direction at a certain point. The pore pressure generated from phreatic levels (input data) is called steady state pore pressure and excess pore pressures are generated by loading/unloading during plastic calculation or during consolidation analysis. [13]

For completely saturated soil beneath the phreatic level undrained analysis is performed under the assumption that no volume change occurs. According to Hooke's law a fully incompressible behaviour is obtained for $v_u = 0.5$ and a bulk modulus $K_w = \infty$. This would lead to singularities in the stiffness matrix. Hence, PLAXIS uses a default value of $v_u = 0.495$. In order to obtain reliable results from numerical calculations the bulk modulus of water has to be very high compared to the bulk modulus of soil skeleton. This is ensured by using realistic values of $\nu' \leq 0.35$ for the soil body. [2]

In PLAXIS three different drainage types for undrained analysis are possible.

1) *Undrained (A):* Undrained effective stress analysis with effective strength parameters
2) *Undrained (B):* Undrained effective stress analysis with undrained strength parameters
3) *Undrained (C):* Undrained total stress analysis with undrained parameters

In the following calculation method A was chosen for undrained analysis.

Method A uses effective strength parameters to calculate the undrained shear strength c_u. The use of this method is recommended, because soil behaviour is always governed by effective stresses. The undrained shear strength depends on the magnitude of stresses, the stress path and the volumetric behaviour of the soil. Most material models are not able to provide the correct effective stress path in undrained loading. The linear elastic-perfectly plastic Mohr-Coulomb model over predicts undrained shear strength. It considers a fully undrained isotropic elastic behaviour with constant effective volumetric stress *p'*. The effective stress path is a straight line up to failure. The advanced material models are able to account for the reduction of *p'* as a result of shear induced excess pore pressures, yielding a more realistic value of c_u. [2]

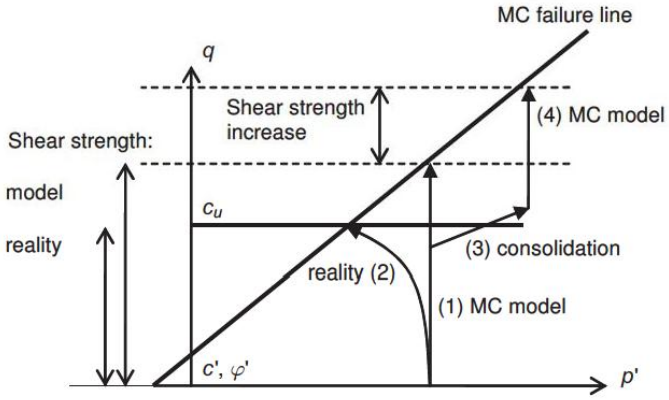

FIGURE 42: EFFECTIVE STRESS PATHS FOR UNDRAINED ANALYSIS WITH THE MOHR-COULOMB MODEL [2]

For the undrained effective stress analysis (method A and B) the effective parameters are transferred into undrained parameters E_u und ν_u according to

$$E_u = 2 \cdot G \cdot (1 + \nu_u) \tag{6.2}$$

With $G = \frac{E'}{2 \cdot (1+\nu')}$

and $\nu_u = 0{,}495$ (Default settings)

$\nu_u = \frac{3 \cdot \nu' + B \cdot (1-2*\nu')}{3 - B \cdot (1-2*\nu')}$ (Manual settings: input *B*)

The calculation of pore pressures according to Skempton (1954) is valid for fully saturated soil with no inflow or outflow of pore water and isotropic linear elastic material behaviour (validity of Hooke's law) [6].

$$\Delta p_w = B \cdot [\Delta\sigma_3 + A \cdot (\Delta\sigma_1 - \Delta\sigma_3)] \tag{6.3}$$

With $B = \frac{1}{1+\frac{n \cdot K'}{K_w}}$ (depending on the saturation of the soil)

$A = \frac{1}{3}$ for triaxial compression; $\frac{2}{3}$ for triaxial extension; $\frac{1}{2}$ for plain strain conditions

Assuming a fully saturated soil and incompressibility of the pore water, *B* is 1.0. Due to numerical reasons the pore water is assumed to be slightly compressible in PLAXIS. For the HS model *B* depends on the soil stiffness, but the differences are negligible. Hence, in PLAXIS the parameter *B* is approximately 1.0. [14]

The parameter A depends on the stress path and cannot be determined a priori for complex elastic-plastic constitutive models. For a non-dilatant Mohr-Coulomb model the value is 1/3. For the Hardening Soil model *A* depends on the relation E_{oed} to E_{50} and changes with loading. [14]

6.2 PERFORMED CALCULATIONS

The groundwater table lies 5.0 m below the surface. The steady state pore pressures are generated using the phreatic level. This results in a maximum water pressure at the model bottom. With tunnel construction stress distribution of the ground is changed and excess pore pressures are generated.

Undrained analyses are performed with consideration of groundwater conditions. To avoid the built-up of very high excess pore pressures sequential excavation is modelled over the complete model length.

Note that, pore water pressure in PLAXIS is displayed as negative values and suction is positive.

TABLE 28: SOIL PARAMETERS WITH CONSIDERATION OF GROUNDWATER

MODEL	$E_{oed,ref}$ [MN/m²]	$E_{50,ref}$ [MN/m²]	$E_{ur,ref}$ [MN/m²]	c [kN/m²]	φ [°]	m [-]	K_0 [-]	POP [kN/m²]	$K_{0,nc}$ [-]	ν_{ur} [-]	$G_{0,ref}$ [MN/m²]	$\gamma_{0,7}$ [-]
4)HS, $E_{MC}=E_{oed}$	69.3	69.3	207.8	35	27	0,8	0.7	500	0.54	0.2	-	-
C1	*Consolidation phase after completed tunnel construction (100 days)*											
C2	*Tunnel construction during consolidation*											
5)HS, $E_{MC}=E_{ur}$	30	30	90	35	27	0.8	0.7	500	0.54	0.2	-	-
C1	*Consolidation phase after completed tunnel construction (100 days)*											
6)MC, E135	E=135 *MN/m²*			35	27	-	0.54	-	-	-	-	-
C1	*Consolidation phase after completed tunnel construction (100 days)*											
C2	*Tunnel construction during consolidation*											
C3	*Consolidation phase after every plastic, staged construction phase*											
8)HSS, $E_{MC}=E_{oed}$	69.3	69.3	207.8	35	27	0.8	0.7	500	0.54	0.2	346.3	$2*10^{-4}$
A	*Tolerated error = 1.0 % (Standard settings)*											
B	*Tolerated error = 0.1 %*											
	C1	*Consolidation phase after completed tunnel construction (30 days)*										
10)HSS, $E_{MC}=E_{ur}$	30	30	90	35	27	0.8	0.7	500	0.54	0.2	150	$2*10^{-4}$

6.3 INFLUENCE OF TOLERATED ERROR IN HS-SMALL CALCULATIONS

As for drained analysis the equilibrium stress field in longitudinal direction at the tunnel face is checked. For tunnelling under undrained conditions below the phreatic level the water pressure at the tunnel face has to be considered. The total longitudinal stresses have to be in equilibrium. Negative stresses σ_{yy} are generated independent of the constitutive model and the *Tolerated error* used.

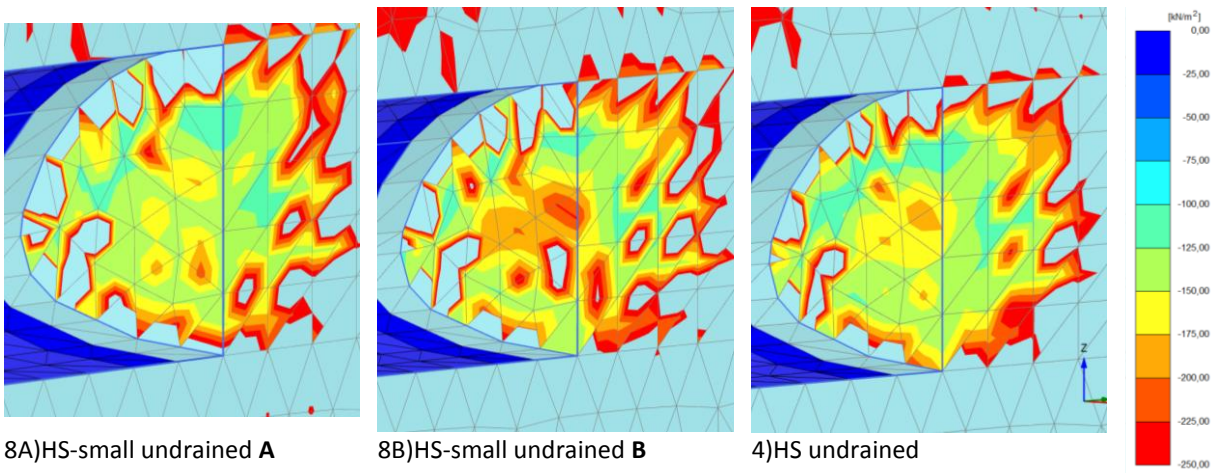

8A)HS-small undrained **A** 8B)HS-small undrained **B** 4)HS undrained

FIGURE 43: LONGITUDINAL TOTAL STRESSES AT THE TUNNEL FACE UNDER UNDRAINED CONDITIONS

6.4 SURFACE SETTLEMENTS

Surface settlements are evaluated after completed tunnel construction in two nodes in the middle of the FE-model above the tunnel centre-line.

- Node 1: 0.0/71.0/0.0
- Node 2: 0.0/74.23/0.0

The vertical settlements obtained from the three-dimensional numerical calculations are summarized in Table 29.

TABLE 29: SURFACE SETTLEMENTS FROM UNDRAINED FE-ANALYSIS

	Eoed,ref	***E50,ref***	***Eur,ref***	***position***	
	[MN/m²]	*[MN/m²]*	*[MN/m²]*	*71.00 m*	*74.23 m*
4) HS E69	*69*	*69*	*208*	-8 mm	-8 mm
5) HS E30	*30*	*30*	*90*	-16 mm	-16 mm
6) MC	*E=135 MN/m²*			-12 mm	-12 mm
8) HSS E69	*69*	*69*	*208*	-4 mm	-4 mm
10) HSS E30	*30*	*30*	*90*	-11 mm	-11 mm

Settlements obtained from undrained analysis are generally smaller compared to the results of the corresponding drained analysis. The soil stiffness parameters have a significant influence on the magnitude of surface settlements. Settlements resulting from calculations 5) and 10) with $E_{MC} = E_{ur}$ exceed the deformations obtained from calculation 4) and 8) with $E_{MC} = E_{oed}$ by about 100 %.

6.4.1 TRANSVERSAL SETTLEMENT TROUGH

The corresponding transversal settlement troughs in Station y = 71.0 m are displayed in Figure 44. The numerical results are compared to field measurements at station MQ 1015, 1040, 1067 and 1146.

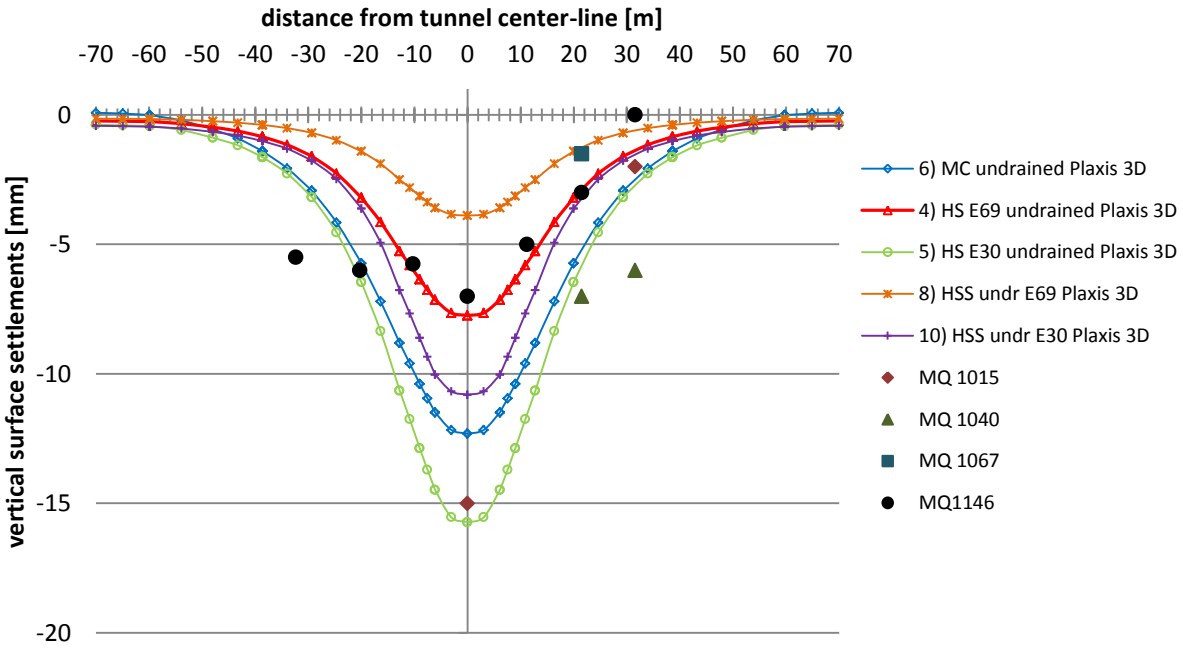

FIGURE 44: COMPARISON OF THE TRANSVERSAL SURFACE SETTLEMENT TROUGH AT STATION 1040, 1067 AND 1146 WITH THE RESULTS OF THE NUMERICAL UNDRAINED CALCULATIONS IN STATION 71

Settlements calculated in undrained analysis are generally smaller than the deformations obtained from comparable drained analysis. Unlike in drained analysis the softer HS-small model 10) results in a significantly deeper settlement trough than the stiffer HS model 4). Settlements obtained from calculations using the standard Hardening Soil model are 2.4-times larger than corresponding deformations computed with the HS-small model. The influence of small-strain stiffness is approximately the same for crown and surface settlements.

Except for the Mohr- Coulomb model (model 6) the vertical deformations are not completely decayed at the model boundary (x = -70.0 m). The largest settlements are calculated by the HS-small model (model 10) with 0.4 mm.

The best fit to field measurements is obtained by computation with the Hardening Soil model undrained (E_{MC} = E_{oed}).

6.4.2 Longitudinal Settlement profile

In Figure 45 the longitudinal settlement profile for station 71.0 m over the position of the advancing tunnel face is displayed. It is compared to field measurements in station 1015 and 1146.

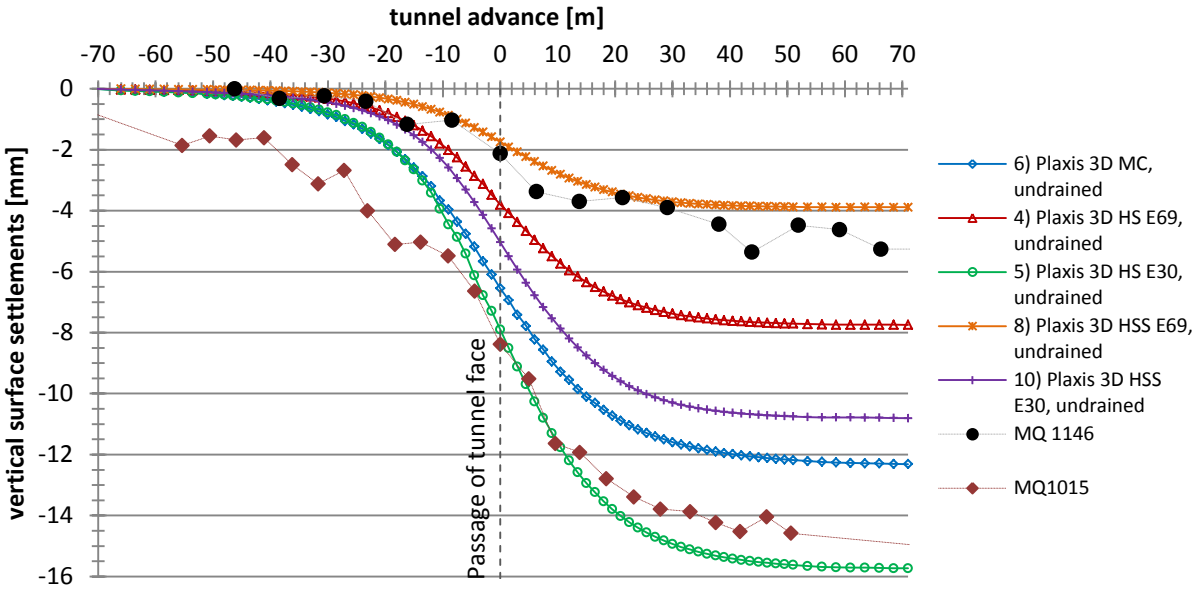

FIGURE 45: COMPARISON OF THE DEVELOPMENT OF SURFACE SETTLEMENTS AT STATION 1015 AND 1146 WITH THE RESULTS OF THE NUMERICAL UNDRAINED CALCULATIONS IN STATION 71

As for drained analysis steady state conditions are reached when the tunnel face advances about 50 m beyond the considered observation section. About 50 % of the steady state settlements occur prior to the passage of the tunnel face for calculations using the MC and HS model. The HS-small model predicts a pre-displacement of about 45 % of the steady state settlements.

The influence of groundwater conditions and undrained analysis on surface settlements is very small when using the Hardening Soil small model. Almost the same settlement profile is obtained from calculation 7) and 8), respectively 9) and 10).

Field measurements in observation point MQ 1146 are best matched by calculation 8), the measurements in station MQ 1015 by calculation 5). All undrained calculations are within the measured range.

6.5 Lining forces and deformations

6.5.1 Crown settlements

Crown settlements are evaluated after completed tunnel construction at the beginning, end and centre of one excavation length in the middle of the FE-model.

The vertical settlements obtained from the three-dimensional numerical calculations are summarized in Table 30.

TABLE 30: CROWN SETTLEMENTS FROM UNDRAINED FE-ANALYSIS

	Eoed,ref	*E50,ref*	*Eur,ref*	*station*		
	[MN/m²]	*[MN/m²]*	*[MN/m²]*	*74.00*	*74.75*	*75.50*
4) HS E69	*69*	*69*	*208*	-20 mm	-21 mm	-20 mm
5) HS E30	*30*	*30*	*90*	-40 mm	-42 mm	-39 mm
6) MC	*E=135 MN/m²*			-28 mm	-29 mm	-28 mm
8) HSS E69	*69*	*69*	*208*	-10 mm	-10 mm	-10 mm
10) HSS E30	*30*	*30*	*90*	-27 mm	-28 mm	-27 mm

Settlements obtained from undrained analysis are generally smaller than settlements resulting from drained calculations due to the incompressibility of pore water. Furthermore, it reduces the sagging of the tunnel crown. No significant difference between the deformations at the beginning/end and centre of the excavation length is obtained. The vertical crown settlements in undrained analysis range from -42 to -10 mm. The largest displacements are obtained from calculation 5). The consideration of higher soil stiffness parameters and small-strain stiffness leads to a reduction of deformations.

In Figure 46 the crown settlement profile in longitudinal direction obtained from undrained FE-analysis is displayed.

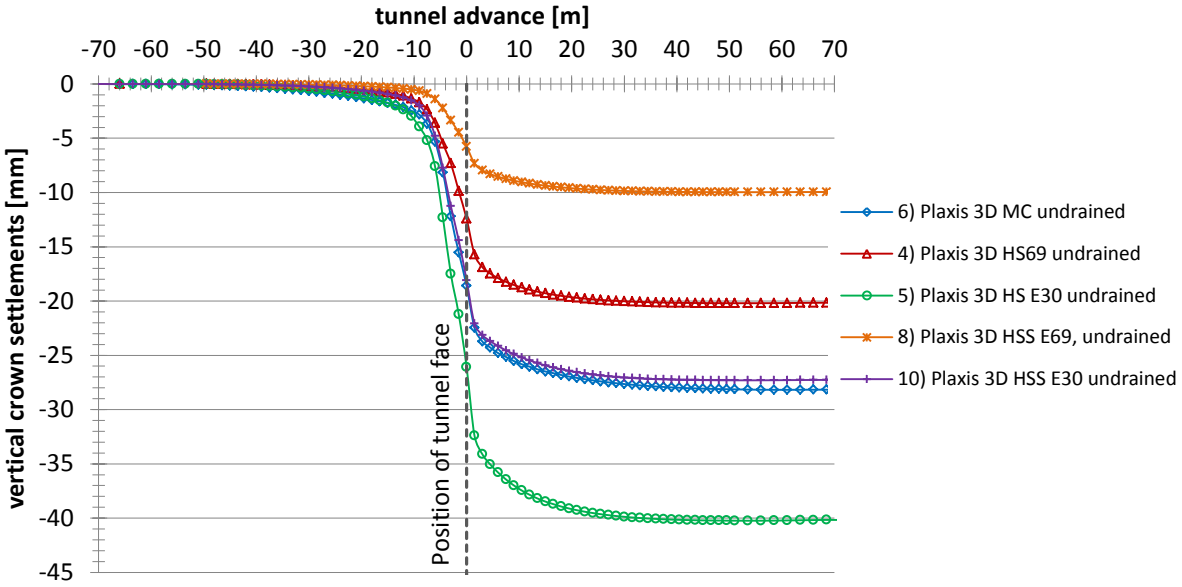

FIGURE 46: DEVELOPMENT OF CROWN SETTLEMENTS IN LONGITUDINAL DIRECTION FOR UNDRAINED FE-ANALYSIS

FE calculations predict a pre-displacement of 58 – 66 % of steady state settlements. The deformation increase caused by the passage of the tunnel face is more pronounced in HS-small calculations than in the corresponding HS calculations. Steady state conditions are reached approximately 30 m after the tunnel face has passed the observation point. Like in drained analysis steady state crown settlements are reached faster than steady state surface settlements.

At the tunnel crown the longitudinal development of the settlements is compared to measurements at station 1044 and 1176. Prior to the passage of the face no measurement data are available. Hence, the relation between the settlements at the passage of the face and steady state settlements are compared.

In Table 31 the difference between predicted crown settlements at the time of the passage of the tunnel face and steady state crown settlements is shown. The pre-displacements are expressed as percentage of steady state deformations.

TABLE 31: DIFFERENCE BETWEEN CROWN SETTLEMENTS AT THE PASSAGE OF THE TUNNEL FACE AND STEADY STATE CROWN SETTLEMENTS

	Passage of the tunnel face		*Steady state*	*difference*
6) MC undrained	-18.6 mm	66%	-28.2 mm	-9.6 mm
4) HS E69 undrained	-12.4 mm	62%	-20.2 mm	-7.7 mm
5) HS E30 undrained	-26.1 mm	65%	-40.2 mm	-14.1 mm
8) HSS E69 undrained	-5.8 mm	58%	-10.0 mm	-4.2 mm
10) HSS E30 undrained	-18.1 mm	66%	-27.3 mm	-9.2 mm
MQ 1044	0.0 mm		-19.5 mm	-19.5 mm
MQ 1176	0.0 mm		-9.0 mm	-9.0 mm

At station 1044 the maximum measured settlement is -19.5 mm, in station 1176 it is -9.0 mm. The results of undrained numerical calculation vary depending on the model and the parameter set between -4.2 and -14.1 mm, lying in the range of the measurements.

In Figure 47 the development of crown settlements after the passage of the tunnel face is displayed.

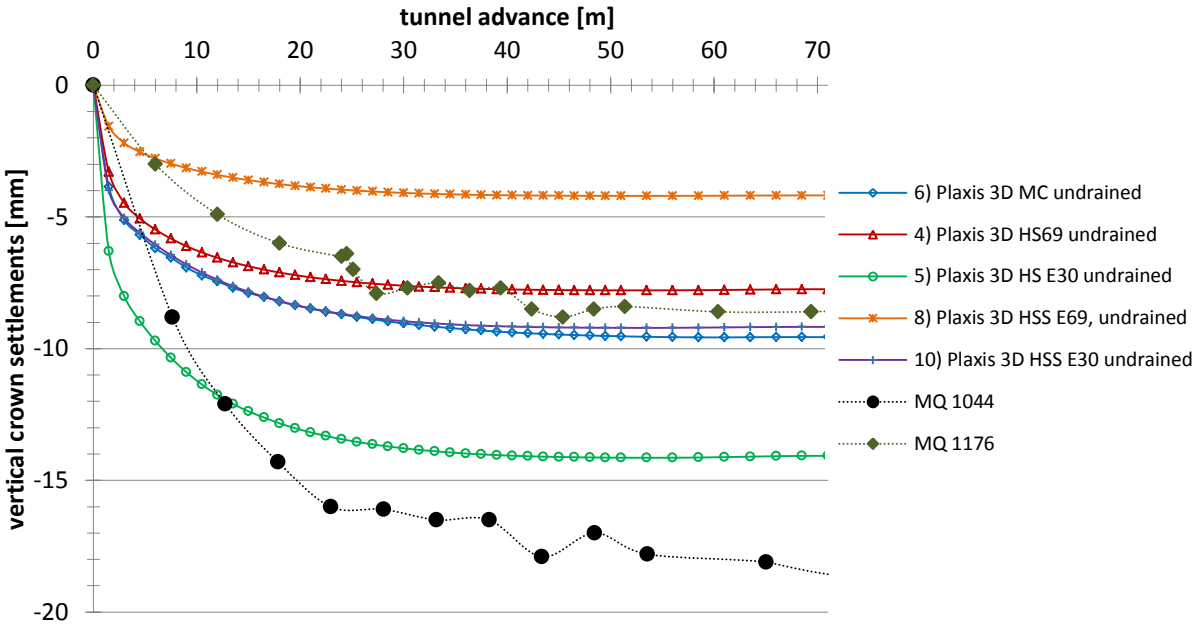

FIGURE 47: COMPARISON OF THE DEVELOPMENT OF CROWN SETTLEMENTS AT STATION 1015 AND 1146 WITH THE RESULTS OF THE NUMERICAL UNDRAINED CALCULATIONS IN STATION 71

Numerical calculations predict a large increase in settlements caused by the passage of the tunnel face. Field measurements show a smaller gradient immediately after excavation. Differences may result from a marginal delayed installation of the observation system. Field measurements in station 1176 are in the middle of the predictions from calculations 4), 6) and 10).

6.5.2 LINING FORCES

The axial forces and bending moments in the lining are displayed in the figures below. Table 32 summarizes the minimum and maximum values. Internal lining forces obtained from calculations with PLAXIS 3D 2011 have to be evaluated carefully. Due to the discretization of the curved tunnel circumference with straight lines and tetrahedral elements no smooth distribution in the 3D FE-calculations of internal forces is obtained. In undrained analysis additionally very high excess pore pressures are generated at the tunnel springline causing a jump in the axial forces. No reliable internal forces are obtained.

Due to the irregular distribution of internal forces the extreme values are not usable for the design of the lining. The peak values resulting from unreliable high excess pore pressures and bends in the modelled lining have to be eliminated.

TABLE 32: INTERNAL LINING FORCES (UNDRAINED ANALYSIS)

		6)MC	4)HS $E_{MC}=E_{oed}$	5)HS $E_{MC}=E_{ur}$	8)HSS $E_{MC}=E_{oed}$	10)HS $E_{MC}=E_{ur}$
M	*min*	-35	-24	-38	-13	-23
[kNm/m]	*max*	43	30	43	19	30
N	*min*	546	585	656	461	493
[kN/m]	*max*	955	982	1159	892	1263

In undrained analysis no general statement about the influence of different soil models can be made. The magnitude of internal lining forces depends on the used soil stiffness parameters and generated excess pore pressures.

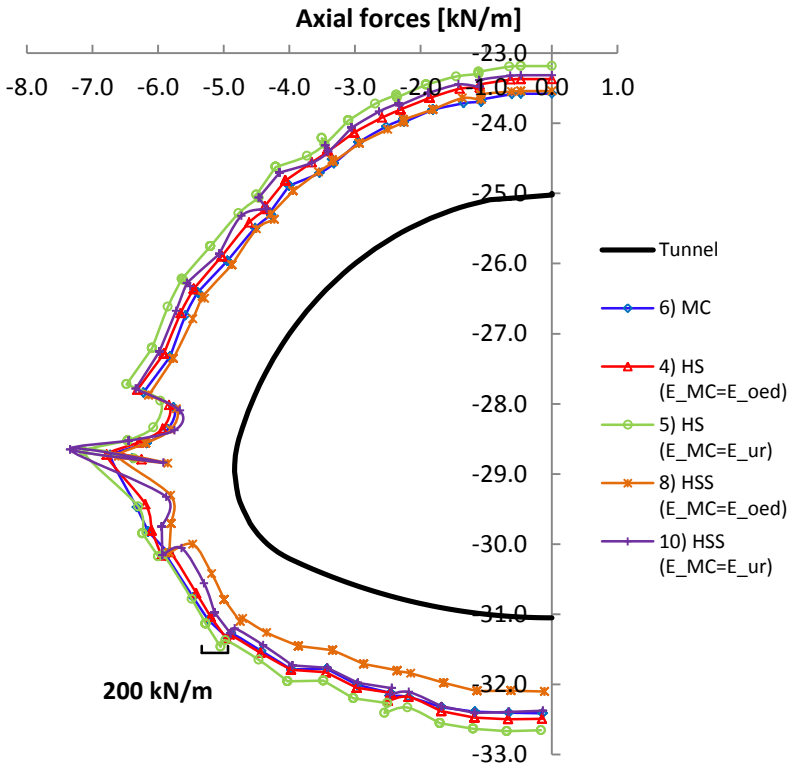

FIGURE 48: AXIAL FORCES (UNDRAINED ANALYSIS)

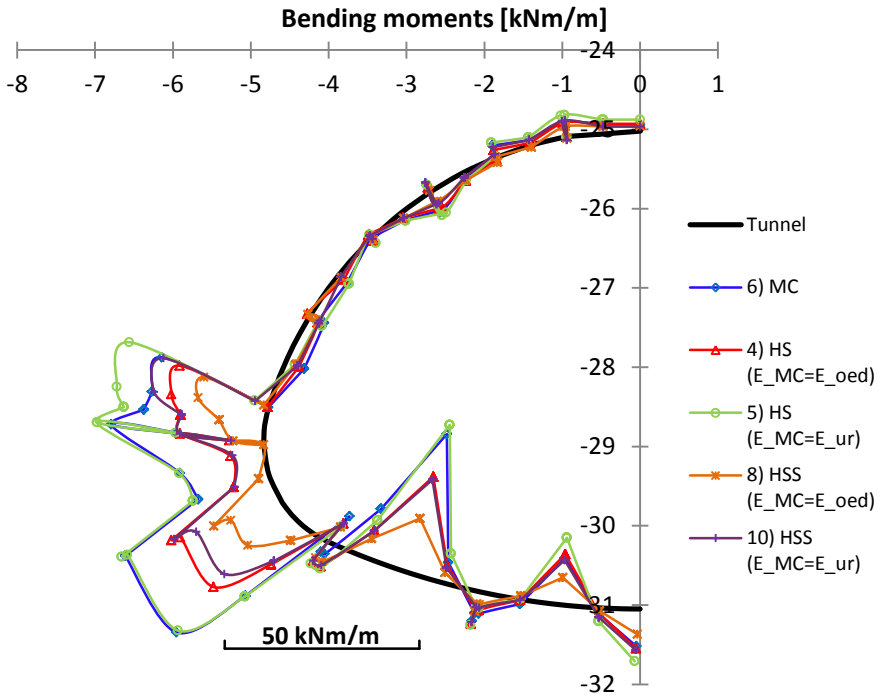

FIGURE 49: BENDING MOMENTS (UNDRAINED ANALYSIS)

6.6 INFLUENCE OF CONSOLIDATION

Consolidation is the process of dissipation of excess pore water pressures over time, causing the soil volume to decrease. The reduction of excess pore pressures results in a change of effective stresses causing settlements. Consolidation analysis is usually performed for saturated clay-type soil with low permeability. Long-term settlements may be considerably larger than settlements immediately after tunnel construction. [15]

Ground movements associated with the construction of a tunnel with sprayed concrete lining are caused by:

1) stress relief due to excavation: deformations of the ground at the tunnel face (longitudinal and radial)
2) lining deformations due to load redistribution
3) consolidation

Immediate settlements are related to 1) and 2) and are often called “ground loss settlements” [16]. Their distribution can be described by a normal probability function according to Peck [17] and Attewell & Woodman [18]. The deflection of the lining usually is small compared to other deformation components. The magnitude of immediate settlements for NATM tunnels can be related to the unsupported length.

Consolidation settlements are caused by the dissipation of excess pore pressure over a longer time period, depending on the permeability of the soil. They are largest at the surface and decrease with depth. They are an accumulation of settlements of all underlying soil layers. [16]

The development of post-construction settlements is influenced by:

1) distribution and magnitude of excess pore pressures
2) permeability and compressibility of the ground
3) drainage boundary conditions, especially the permeability of the tunnel lining relative to the permeability of the soil [15]

For open face tunnelling the ground is unloaded during construction and generally negative excess pore pressures (commonly suction) are generated. Particularly for tunnelling in over-consolidated soils with a

tendency for dilatant behaviour, negative excess pore pressures are induced. In normally consolidated clays, even for unloading during construction, zones of positive excess pore pressures can be generated at a short distance from the tunnel due to shearing. If the lining is of relative high permeability compared to the soil the tunnel is acting as a drain. This leads to a development of steady state seepage towards the tunnel and results in a widespread reduction of excess pore pressures. If the permeability of the lining is relatively low, in soft clay consolidation settlements are only caused by dissipation of local positive excess pore pressures. An additional settlement trough of similar width to the immediate trough develops. In stiff clays negative excess pore pressures are generated during tunnel construction causing swelling rather than consolidation. [15]

6.6.1 PERFORMED CALCULATIONS

To account for time-dependent dissipation of excess pore pressures in PLAXIS the calculation type has to be set to *consolidation*. Plastic calculation does not take time effects into account, except when the Soft Soil Creep model is used. [2]

The consolidation procedure is modelled in two different ways:

1) After the completed excavation of the tunnel in undrained plastic analysis a consolidation phase with a time step of 100 days is added. (C1)
2) For the undrained analysis the calculation mode was changed to consolidation and a time step of 1 day is applied per round length. Loading and consolidation are carried out simultaneously. (C2)

In general a consolidation calculation is performed without additional loading after an undrained plastic calculation phase (C3). It is also possible to apply loads in the consolidation phase, but when approaching failure the iteration procedure may not converge [2]. Due to the great number of calculation phases for simulating step-by-step excavation in tunnelling, tunnel installation is applied in a consolidation phase with a time step of 1 day to prevent further increase of the quantity of calculation phases. The number of calculation phases in PLAXIS 3D is limited to 100.

The flow boundary conditions are open, except for the symmetry axis and the model bottom. Internal model boundaries that are created by deactivating soil clusters (excavation) are always draining [2]. The permeability of plate elements in PLAXIS is very high. To create an impermeable screen an interface element has to be implemented at the tunnel boundary. Without an interface element to model impermeability of the tunnel lining, the tunnel acts as a drain during consolidation the tunnel. A high hydraulic gradient at the boundary of the tunnel draws the water inside the tunnel or into the soil, if positive excess pore pressures (suction) are generated.

To investigate the interaction of loading and consolidation an additional coupled consolidation analysis with the *6) MC, undrained* model was performed. A calculation with separate loading and consolidation was carried out until day 15 when the limit of 100 calculation phases was reached.

6.6.2 DISSIPATION OF EXCESS PORE PRESSURES

For the understanding of the general dissipation of excess pore pressures over time the nodal value at the bottom in the middle of the model (0/71/-60) in tunnel axis is shown as example and compared to 2D analysis. A consolidation phase of 100 days is inserted after step-by-step excavation. In 2D the *MStage*-values obtained by matching crown settlements in station 69.5 m are used (cf. chapter 7). In Figure 50 the dissipation of excess pore pressures in node 0/71.0/-60.0 is compared for 2D and 3D FE-analysis. The diagram shows the relevant area of p_{ex} < 150.0 kN/m² and *time* < 30 days.

In Table 33 the corresponding maximum excess pore pressures at the end of staged construction before consolidation are listed.

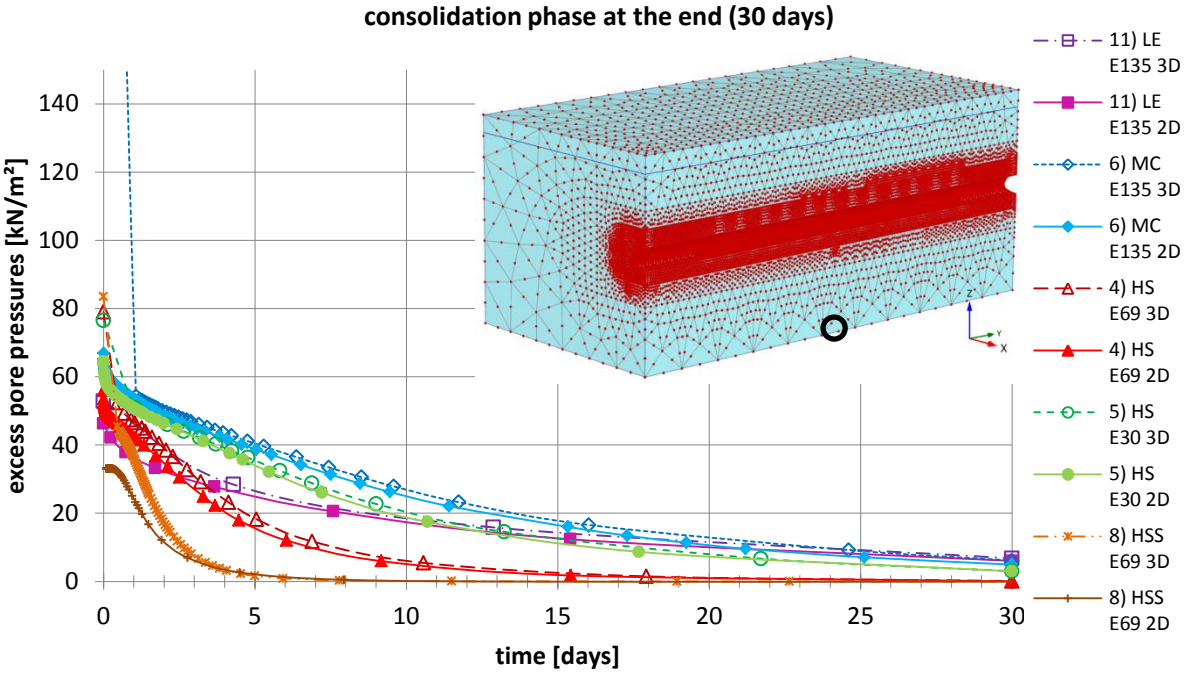

FIGURE 50: DEVELOPMENT OF EXCESS PORE PRESSURES OVER TIME FOR CONSOLIDATION AT THE END OF THE EXCAVATION (30 DAYS)

TABLE 33: RELATION OF EXCESS PORE PRESSURES GENERATED BY 2D AND 3D ANALYSIS

	2D	***3D***	
11) LE undrained E=135	46.3 kN/m²	52.8 kN/m²	*14%*
6) MC undrained E=135	65.1 kN/m²	408.2 kN/m²	*527%*
4) HS undrained (E_{MC}=E_{oed})	55.9 kN/m²	79.0 kN/m²	*41%*
5) HS undrained (E_{MC}=E_{ur})	64.0 kN/m²	76.5 kN/m²	*20%*
8) HSS undrained (E_{MC}=E_{oed})	33.0 kN/m²	83.5 kN/m²	153%

As mentioned in chapter 4.4 excess pore pressures generated in 3D computation exceed the results of 2D for "wished-in-place" calculation. The extreme values of excess pore pressures in the area around the tunnel are not realistic. A more reliable result is obtained from 2D analysis. The highest values result from undrained analysis using the Mohr-Coulomb model. When consolidation analysis is performed, the high excess pore pressures are dissipated within the first calculation step. The difference of p_{ex} generated at the model bottom between 2D and 3D analysis with the Hardening Soil model depends on soil stiffness.

6.6.3 SETTLEMENTS

Long-term settlements after consolidation can be compared to deformations obtained from drained analysis. Because in this case drained calculations had to be carried out without consideration of groundwater conditions, no connection between drained and consolidation analysis can be made. The results of different types of consolidation analysis are compared for calculation model 6) and 4).

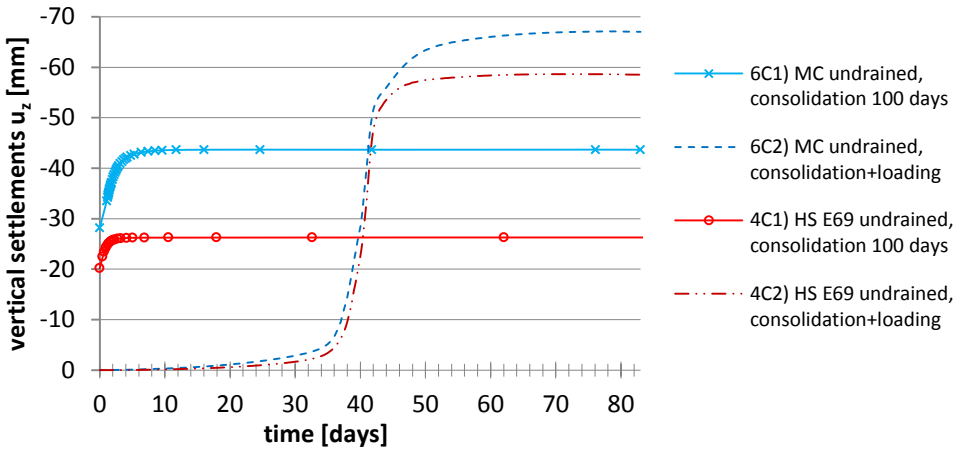

FIGURE 51: DEVELOPMENT OF CONSOLIDATION SETTLEMENTS AT THE TUNNEL CROWN IN STATION 71.0 M (PASSAGE OF TUNNEL FACE IN PHASE 41)

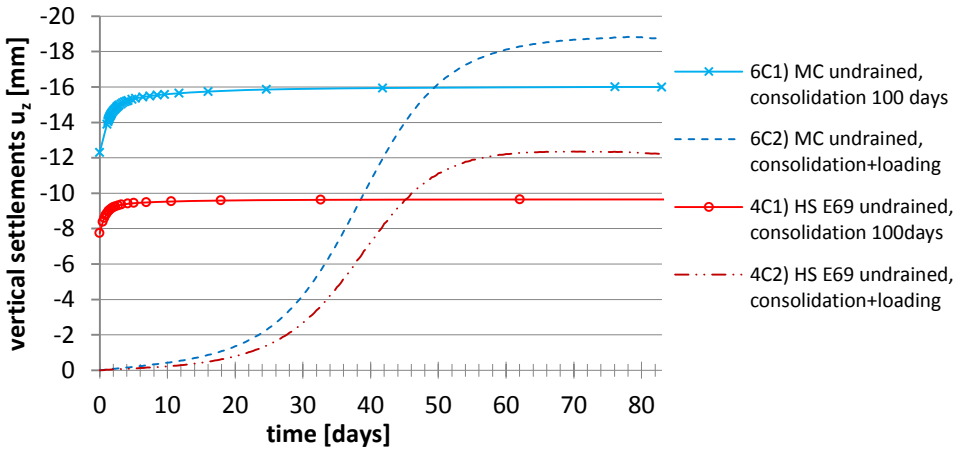

FIGURE 52: DEVELOPMENT OF CONSOLIDATION SETTLEMENTS AT THE SURFACE IN STATION 71.0 M (PASSAGE OF TUNNEL FACE IN PHASE 41)

The settlements obtained from a coupled consolidation analysis (loading in consolidation phase) exceed the long-term settlements calculated by a consolidation phase at the end of completed tunnel installation.

The increase of settlements due to consolidation expressed as percentage of the total undrained settlements for FE-analysis depends on the model used. Calculations with the MC model show an increase of 55 % at the tunnel crown and 30 % at the surface. For the Hardening Soil model settlements increase by approximately 30 % at the crown and by 25 % at the surface due to consolidation.

TABLE 34: COMPARISON OF SURFACE AND CROWN SETTLEMENTS FOR UNDRAINED ANALYSIS AND CONSOLIDATION

	surface (0/71.0/0)		***crown (0/71.0/-25.0)***	
6) MC				
undrained	-12.3 mm		-28.2 mm	
consolidation 100 days (C1)	-16.0 mm	*30%*	-43.7 mm	*55%*
Consolidation + loading(C2)	-18.7 mm	*17%*	-67.0 mm	*54%*
4) HS E69				
undrained	-7.7 mm		-20.2 mm	
consolidation 100 days (C1)	-9.7 mm	*25%*	-26.3 mm	*30%*
Consolidation + loading(C2)	-12.2 mm	*27%*	-58.5 mm	*123%*

When the loads are applied in the consolidation phase massive sagging of the tunnel crown can be observed as shown in Figure 53. Least differences of crown settlements between beginning/end and centre of one

excavation length are observed for undrained analysis due to restricted volumetric changes. The sagging of the tunnel crown for parallel loading and consolidation is caused by an unrealistic consolidation boundary condition at the tunnel crown. Due to positive excess pore pressures, water is drawn into the material, and consequently soil strength reduces rapidly. This cannot occur in reality. Avoiding this effect numerically requires a more advanced boundary condition.

The largest proportion of settlements develops prior to lining installation. The same phenomenon is observed if after every plastic calculation phase a consolidation phase is added. Consolidation settlements obtained from consolidation at the end of the excavation are plotted as dashed lines. Settlements due to loading and consolidation per step are plotted as dash-dotted lines.

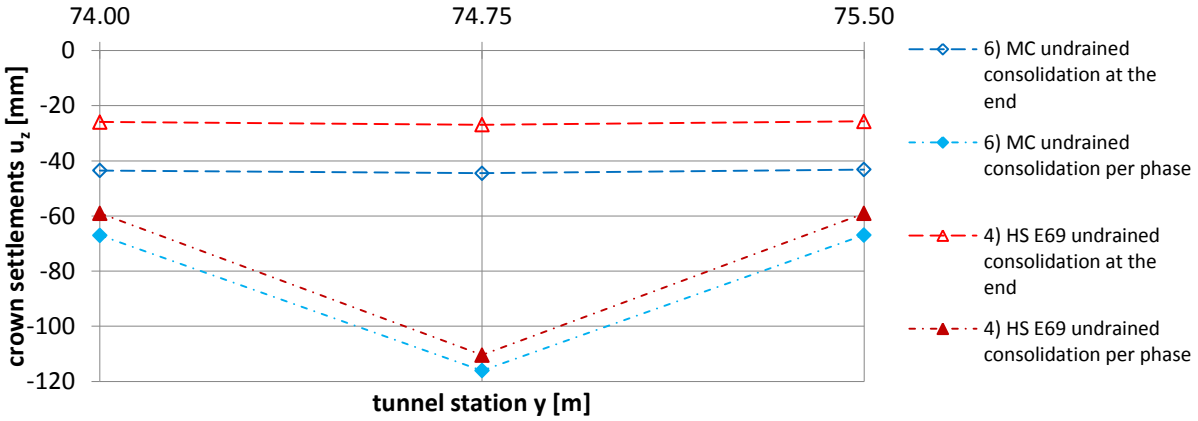

FIGURE 53: COMPARISON CROWN SETTLEMENTS FOR UNDRAINED ANALYSIS AFTER CONSOLIDATION

The transversal settlement trough in station 71.0 m obtained from different consolidation analysis is compared to 3D and 2D undrained analysis. The results are displayed in Figure 54. The 2D calculation is calibrated with crown settlements in station 69.5 m as explained in chapter 7.

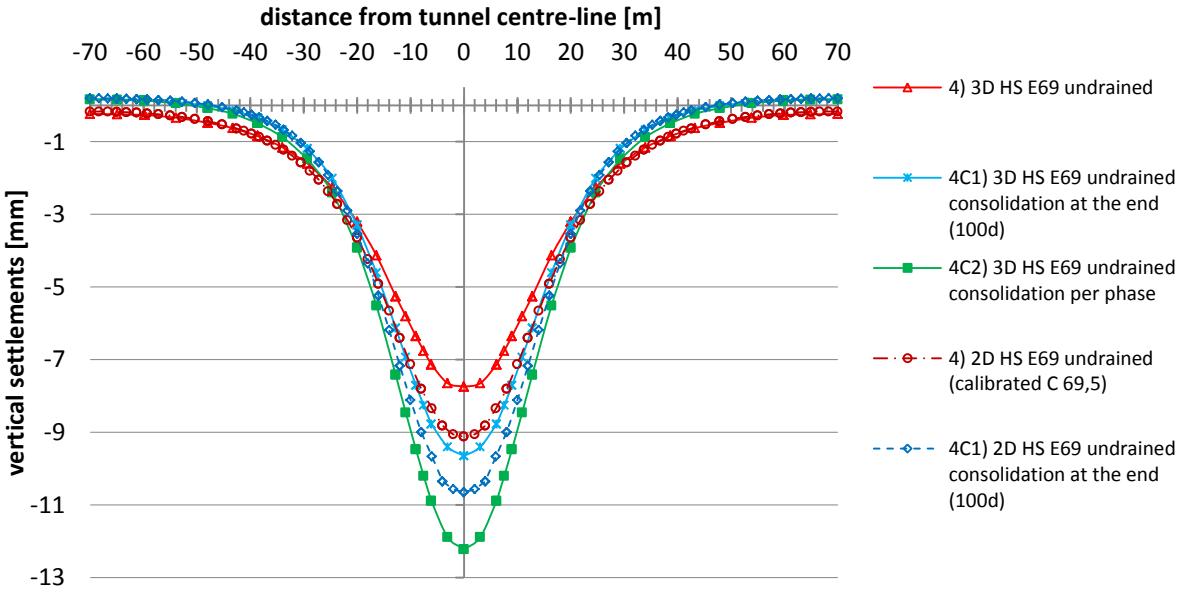

FIGURE 54: INFLUENCE OF CONSOLIDATION ON THE TRANSVERSAL SURFACE SETTLEMENT TROUGH

According to literature additional settlements due to consolidation tend to cause wider settlement profiles. For tunnelling in soft clays settlements increase 30 – 90 % of the total settlements over the long term. For

tunnelling in stiff clays negative excess pore pressures are generated during construction, resulting in no discernible post-construction surface settlements. [15]

Due to consolidation a deeper settlement profile is developed. A consolidation phase (100 days) at the end of tunnel excavation causes a 25 % increase of settlements. Simultaneous loading and consolidation result in 27 % larger settlements.

For the Mohr-Coulomb model a calculation with separate loading and consolidation is carried out until day 15 when the limit of 100 calculation phases is reached. Settlements caused by excavation of the tunnel can be separated from consolidation settlements. Results of parallel loading and consolidation should be treated with care due to the unrealistic consolidation boundary condition at the tunnel crown (water in draw). This causes a widespread reduction of pore pressures around the tunnel and significantly larger consolidation settlements.

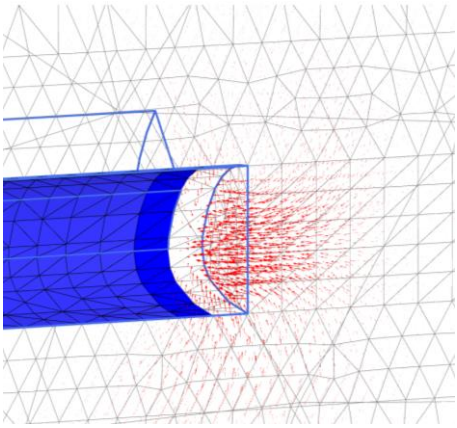

FIGURE 55: MC, UNDRAINED: MAGNITUDE OF SETTLEMENTS RESULTING FROM TUNNEL CONSTRUCTION

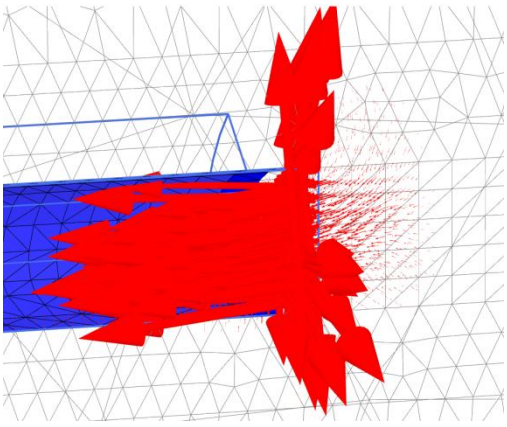

FIGURE 56: MC, UNDRAINED: MAGNITUDE OF SETTLEMENTS RESULTING FROM CONSOLIDATION

The crown settlements calculated from consolidation after loading exceed the deformations obtained from loading in the consolidation phase. Consolidation after loading leads to larger consolidation settlements because during loading higher excess pore pressures are generated.

In Figure 57 loading in the consolidation phase and consolidation after loading are compared.

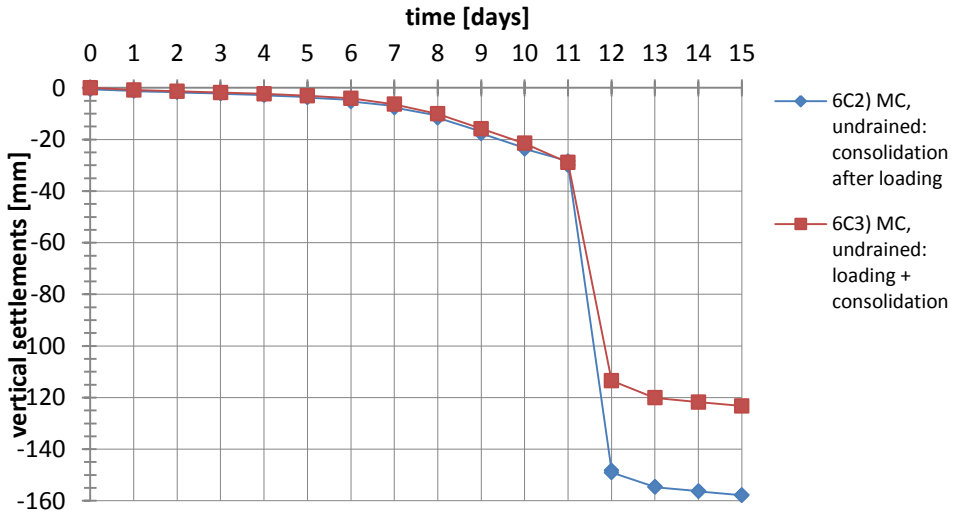

FIGURE 57: DEVELOPMENT OF CROWN SETTLEMENTS DUE TO COUPLED CONSOLIDATION ANALYSIS AT POINT (0/26.75/-25) WITH PASSAGE OF THE TUNNEL FACE ON DAY 11/12

TABLE 35: CROWN SETTLEMENTS DUE TO TUNNEL EXCAVATION AND CONSOLIDATION

	1) loading + consolidation				**2) consolidation after loading**		
Station	*26*	*26.75*	*27.5*	*Station*	*26*	*26.75*	*27.5*
loading (day 11)	-31.7 mm	-30.0 mm	-25.9 mm	*day 11*	-39.3 mm	-29.0 mm	-24.1 mm
consolidation (day 12)	-41.6 mm	-148.3 mm	-32.0 mm	*day 12*	-51.4 mm	-113.5 mm	-40.4 mm

If tunnel construction is modelled in the consolidation phases smaller settlements are calculated than for separate loading and consolidation. The difference results from the calculation phase in which the tunnel face passes the observation point.

7 CALIBRATION OF 2D CALCULATIONS

7.1 THREE-DIMENSIONAL EFFECTS IN TUNNELLING

Tunnelling causes a change in the three-dimensional stress-strain-situation in the ground, which has to be considered in 2D FE-analysis. Arching around the unsupported tunnel heading is important for ground stability during tunnel construction. By rotation of the principal stress directions an arch over-spanning the unsupported length is developed, distributing vertical ground loads to the lining and the undisturbed ground ahead of the tunnel face.

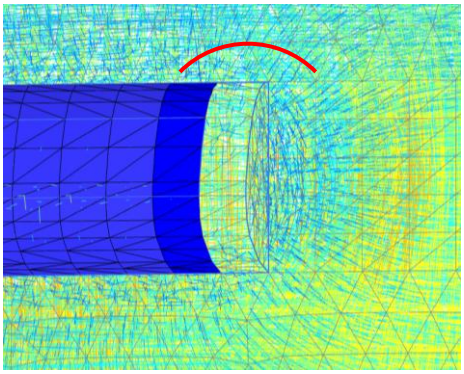

FIGURE 58: THREE-DIMENSIONAL ARCHING AROUND THE UNSUPPORTED TUNNEL HEADING

7.2 STRESS REDUCTION METHOD

Approximation methods are used in 2D FE-analysis to account for these three-dimensional effects of tunnelling. For 2D approximation of conventional tunnelling with sprayed concrete lining (NATM) the stress reduction approach or convergence confinement method, referred to as β-method, is the most common one. Due to delayed installation of the shotcrete lining a prior deformation of the surrounding soil towards the cavity takes place, resulting in a stress relaxation in the soil. This is simulated by switching off the ground elements inside the tunnel, referred to as tunnel cluster. The initial ground pressure p_0 on the tunnel is reduced to $(1-\beta)*p_0$ with $0 < \beta < 1$. β is called the load reduction factor or pre-relaxation factor. In a second calculation step the lining is installed and the remaining load $\beta*p_0$ is applied. [19]

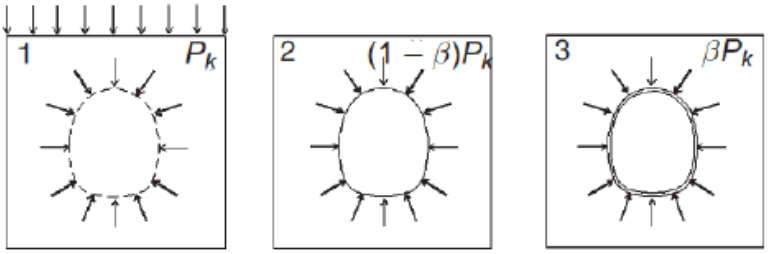

FIGURE 59: SCHEMA OF THE STRESS-REDUCTION METHOD [8]

To account for the proportion of loading acting on young and old shotcrete a second load reduction factor is introduced in this study. Immediately after installation the shotcrete provides a ductile support, able to respond to ground deformations. After hardening an increased stiffness can be considered for long-time behaviour. To account for time-dependency of shotcrete stiffness two different material parameter sets, "*shotcrete young*" and "*shotcrete old*", are determined. The installation of the lining is divided into two calculation phases. In the first phase the lining is activated with the material parameters "*shotcrete young*" and a load reduction factor $\beta < 1$. In the second phase the stiffness of the lining is increased to account for the properties of the aged shotcrete. Material parameters are changed to "*shotcrete old*".

In PLAXIS load reduction is expressed by the input value *ΣMstage* in plastic, staged construction. It gives the applied proportion of the loading and is *1* for the case that all loads are applied and the plastic calculation phase is completed. [10]

$$\Sigma MStage = 1 - \beta \tag{7.1}$$

In the case of two subsequent calculation phases with *MStage* less than 1 PLAXIS applies the second load reduction factor on the already reduced stress level. The load is increased by

$$(1 - MStage_1) \cdot MStage_2 \tag{7.2}$$

In the pre-relaxation phase the pressure on the tunnel is reduced to $MStage_1 * p_0$. The lining is activated with the parameter set "*shotcrete young*" and ground pressure is increased by $(1-MStage_1)*MStage_2*p_0$. In a third calculation step, the material of the lining is changed to "*shotcrete old*" and the remaining load is applied. The remaining load is

$$1 - [MStage_1 + (1 - MStage_1) \cdot MStage_2] \tag{7.3}$$

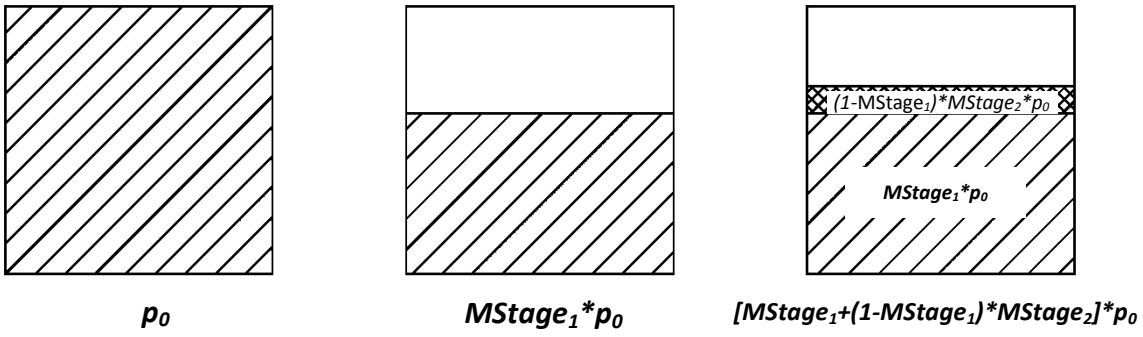

FIGURE 60: SCHEMA OF STRESS-REDUCTION METHOD USING TWO β –FACTORS

It should be noted, that the presence of an interface element anywhere in the model is required for this program function to work.

The value of the load reduction factor β depends on ground conditions and installation procedure (length of unsupported span, advance rate, workmanship,…). It is based on experience or can be obtained from 3D numerical computations. Schikora and Fink (1982) [19] suggest a value between 0.35 and 0.6 for tunnelling in drained conditions with an overburden of 2-4 diameters of the tunnel. Generally small β-factors correspond to a large unsupported length (large round length and/or late installation of the tunnel lining), resulting in relatively large ground deformations and small lining forces [1].

7.3 DETERMINATION OF THE LOAD REDUCTION FACTORS

The β-factors are determined from 3D FE-analysis. In 2D calculations *MStage* is varied to match deformations and lining forces obtained from 3D. Different calibration values and soil models result in different *MStage*-factors.

Load reduction factors are obtained by matching of:

a) Crown settlements
b) Surface settlements
c) Axial forces in the lining

The calculation phases in 2D for the step-by-step excavation with 2 load reduction factors are:

1) Stress-reduction with *MStage* < 1.0 in the tunnel cross-section (deactivation of soil clusters in the tunnel)
2) Activation of lining (material parameter set "*shotcrete young*") and change of material of the anchor area from "*Silt*" to "*Silt + Anchors*" with *MStage* < 1.0
3) Change of the material set of the lining to "*shotcrete old*" (*MStage* = 1.0)

For tunnel design prediction of internal forces in the lining is essential. Before the final lining is installed the primary shotcrete lining has to withstand the ground pressure and prevent large deformations. The change of forces on the lining between shotcrete young and old is achieved by a second load reduction factor in phase 2), otherwise no significant change of internal forces occurs.

For the determination of *MStage*-factors using lining normal forces the calculation phases in 2D are modified. In the pre-relaxation phase no lining is installed. Therefore, normal forces of 3D and 2D calculation cannot be compared. Instead only one pre-relaxation factor is determined, using either the primary stiffness of the shotcrete lining or the stiffness of the old shotcrete.

Sequential excavation with one load reduction factor:

1) Stress-reduction with *MStage* < 1.0 in the tunnel cross-section (deactivation of the soil cluster in the tunnel)
2) Activation of lining (material parameter set "*shotcrete young*") and change of material of the anchor area from "*Silt*" to "*Silt + Anchors*" (*MStage* = 1.0)
3) Change of the material set of the lining to "*shotcrete old*" (*MStage* = 1.0)

Between phase 2) and 3) no changes occur in the internal lining forces.

7.3.1 DETERMINATION OF β USING CROWN SETTLEMENTS

For determination of β by matching crown settlements in 2D and 3D two different values are considered, the settlement in the middle (station 70.25 m) and beginning (station 69.5 m) of one excavation length. *MStage*-values in 2D are varied until the settlements at the crown equal the corresponding value in 3D analysis. The settlements in the 2D calculation phase "*pre-relaxation*" are matched with settlements in phase 41 and "*shotcrete young + anchors*" with phase 42.

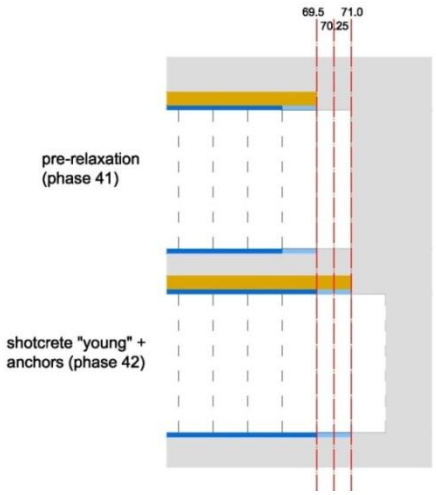

FIGURE 61: EXCAVATION PHASES FOR THE CALIBRATION OF THE 2D-MODEL USING CROWN SETTLEMENTS

The settlements calculated in phase "*shotcrete old*" should match the steady state settlements of the 3D computation. In Table 36 settlements from 3D and 2D calculation and the related *MStage*-values are listed.

TABLE 36: CROWN SETTLEMENTS IN 3D AND 2D WITH CORRESPONDING MSTAGE-VALUES

	pre-relaxation (Phase 41)			***SC young + anchors (Phase 42)***			***steady state/ SC old (Phase 83)***	
Station	*3D*	*2D*		*3D*	*2D*		*3D*	*2D*
	u_y *[mm]*	*Mstage*	u_y *[mm]*	u_y *[mm]*	*Mstage*	u_y *[mm]*	u_y *[mm]*	u_y *[mm]*
1) MC, drained								
70.25	-28.3	0.647	-28.3	-31.0	0.313	-31.0	-38.5	-37.2
69.5	-27.0	0.630	-27.0	-28.7	0.205	-28.8	-35.5	-36.1
2A) HS, $E_{MC}=E_{oed}$, drained, POP500, $K_0=0,7$								
70.25	-24.0	0.731	-24.0	-26.3	0.340	-26.4	-31.3	-29.9
69.5	-20.9	0.698	-20.9	-22.1	0.178	-22.1	-26.5	-26.3
2C) HS, $E_{MC}=E_{oed}$, drained, POP0, $K_0=0,7$								
70.25	-24.1	0.668	-24.2	-26.8	0.310	-26.8	-33.5	-31.4
69.5	-21.2	0.642	-21.3	-22.7	0.175	-22.7	-28.8	-28.1
3) HS, $E_{MC}=E_{ur}$, drained, POP500, $K_0=0,7$								
70.25	-52.6	0.725	-52.6	-56.6	0.350	-56.6	-65.9	-63.0
69.5	-42.5	0.676	-42.5	-44.6	0.183	-44.6	-53.1	-52.7
4A) HS, $E_{MC}=E_{oed}$, undrained, POP500, $K_0=0,7$								
70.25	-15.0	0.587	-15.0	-16.8	0.260	-16.8	-20.6	-20.6
69.5	-15.8	0.599	-15.7	-16.9	0.197	-16.8	-20.1	-20.9
4C) HS, $E_{MC}=E_{oed}$, undrained, POP500, $K_0=0,7$								
70.25	-20.6	0.547	-20.6	-23.8	0.304	-23.8	-30.0	-28.6
69.5	-22.3	0.558	-22.3	-24.2	0.189	-24.2	-29.7	-29.5
5) HS, $E_{MC}=E_{ur}$, undrained, POP500, $K_0=0,7$								
70.25	-31.4	0.572	-31.5	-34.7	0.292	-34.7	-41.4	-41.0
69.5	-32.4	0.579	-32.4	-34.2	0.165	-34.2	-40.2	-41.3
6) MC, undrained								
70.25	-21.8	0.552	-21.8	-23.8	0.262	-23.8	-28.8	-28.7
69.5	-22.7	0.565	-22.7	-23.7	0.145	-23.8	-28.2	-29.1
7) HSS, $E_{MC}=E_{oed}$, drained, POP500, $K_0=0,7$								
70.25	-16.5	0.797	-16.5	-18.3	0.313	-18.3	-20.9	-20.4
69.5	-13.3	0.774	-13.3	-14.2	0.160	-14.2	-16.4	-17.0
8) HSS, $E_{MC}=E_{oed}$, undrained, POP500, $K_0=0,7$								
70.25	-6.8	0.626	-6.8	-7.8	0.178	-7.8	-10.1	-10.6
69.5	-7.3	0.635	-7.3	-8.0	0.115	-8.0	-10.0	-10.9
9) HSS, $E_{MC}=E_{ur}$, drained, POP500, $K_0=0,7$								
70.25	-41.7	0.775	-41.7	-44.8	0.354	-44.8	-50.1	-49.0
69.5	-34.3	0.750	-34.3	-35.8	0.184	-35.8	-40.4	-40.9
10) HSS, $E_{MC}=E_{ur}$, undrained, POP500, $K_0=0,7$								
70.25	-20.905	0.628	-20.9	-23.0	0.227	-20.9	-27.6	-27.4
69.5	-22.073	0.626	-22.1	-23.1	0.117	-23.1	-27.3	-28.0

7.3.1.1 ADVANCE-SETTLEMENT CURVES FOR 3D AND 2D ANALYSIS

In the following figures the development of crown settlements in station 69.5 and 70.25 correlated to the position of the advancing tunnel face are displayed. The continuous lines show the result of 3D numerical calculations. The settlements obtained from the calibrated 2D model are displayed as small squares connected by a dashed line. A very good match of final 3D deformations is obtained by matching crown settlements of 2D FE-analysis.

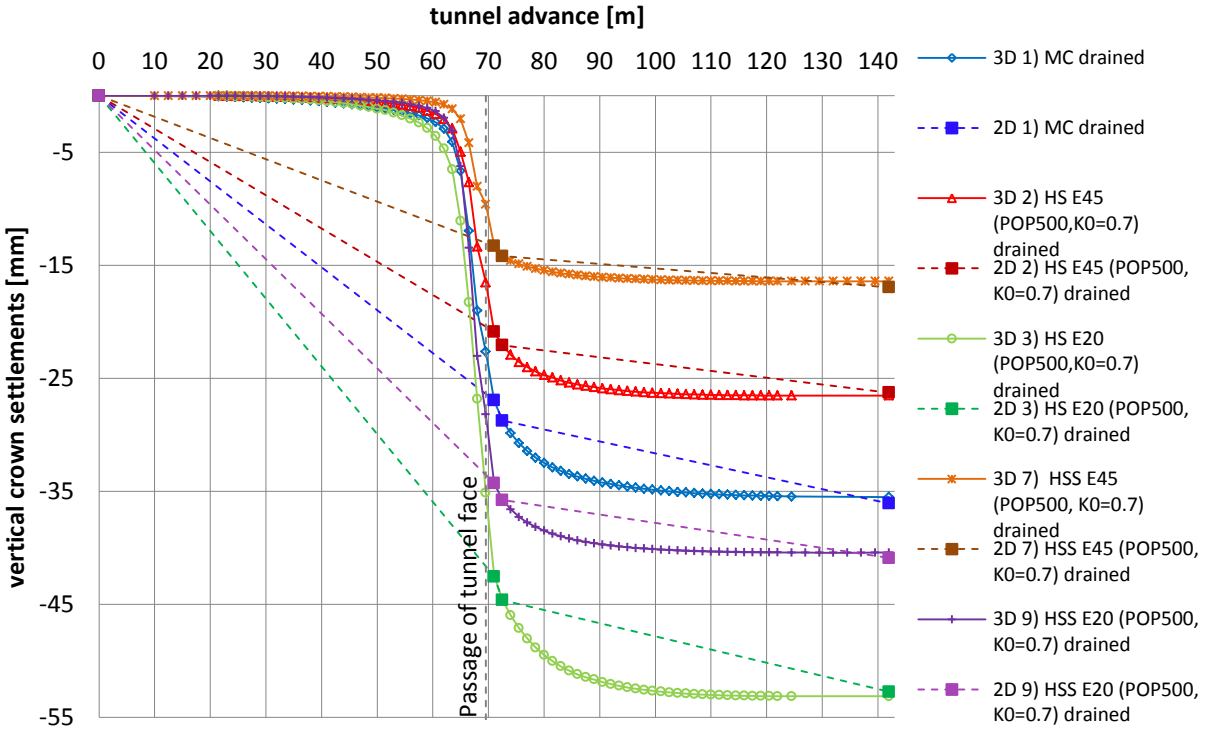

FIGURE 62: CROWN SETTLEMENTS AT STATION 69.5 FOR 3D AND 2D DRAINED ANALYSIS

Deformations u_z at station 0/69.5/-25 in drained conditions are predicted by 2D within a ±1.5 % range.

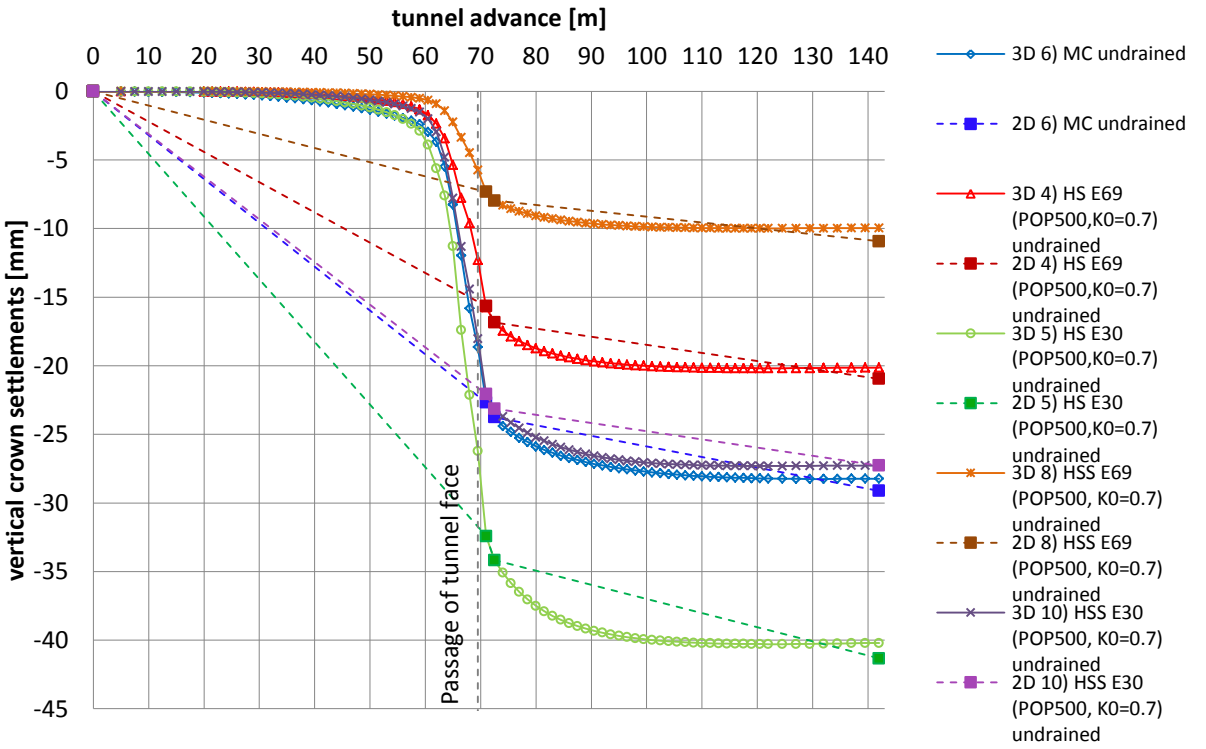

FIGURE 63: CROWN SETTLEMENTS AT STATION 69.5 FOR 3D AND 2D UNDRAINED ANALYSIS

Deformations u_z at station 0/69.5/-25 in undrained conditions are slightly under-predicted by 2D about -3 %. Only the HS-small model under-predicts settlements about -10 %.

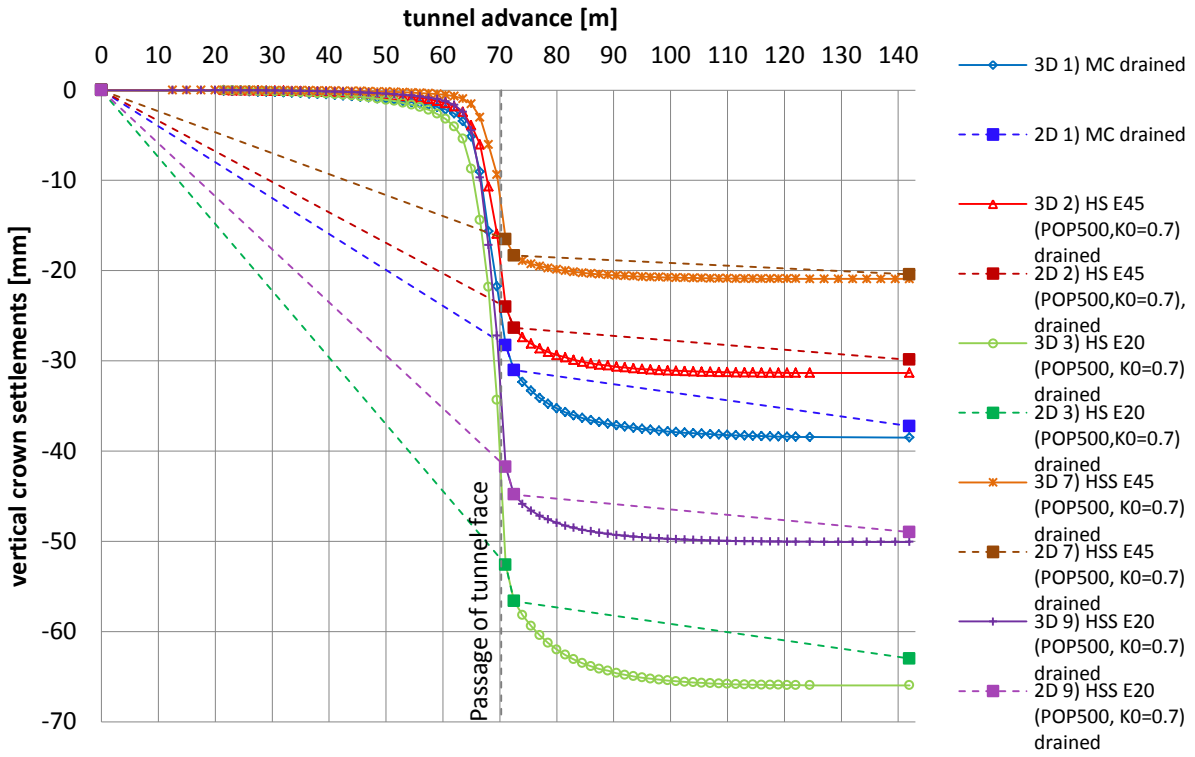

FIGURE 64: CROWN SETTLEMENTS AT STATION 70.25 FOR 3D AND 2D DRAINED ANALYSIS

Deformations u_z at station 0/70.25/-25 in drained conditions are slightly over-predicted by 2D about +4 %.

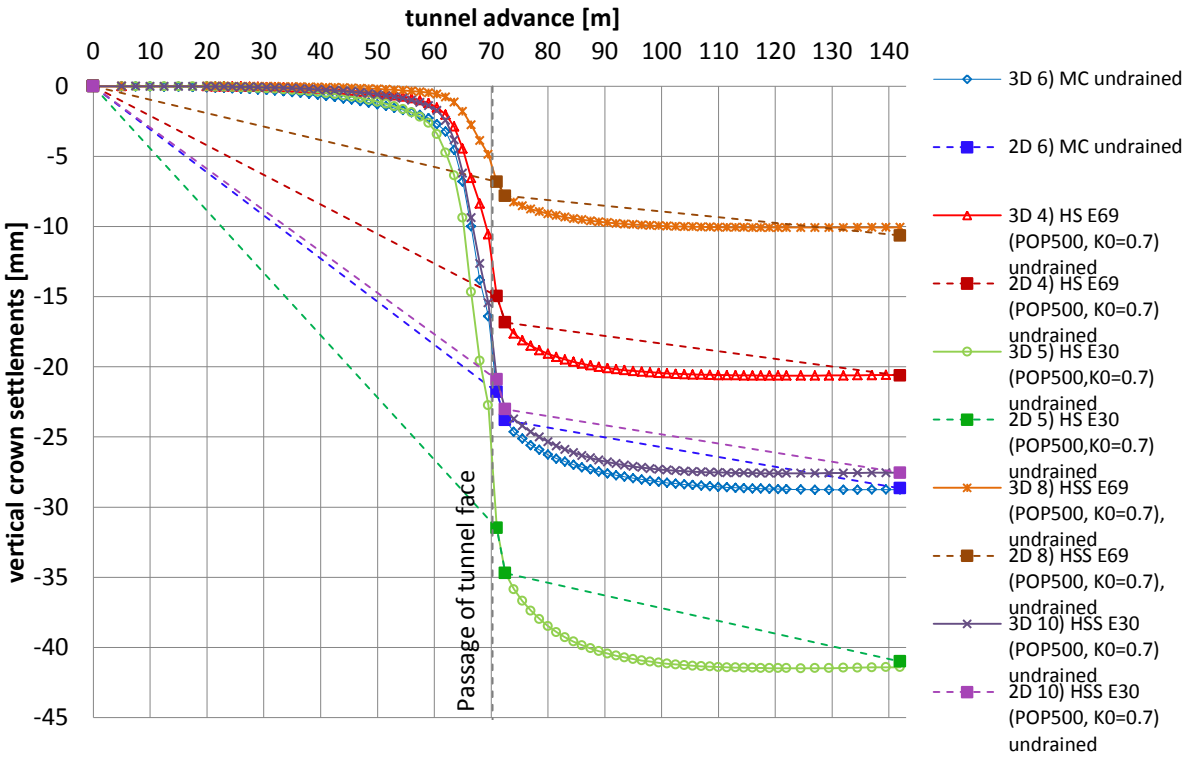

FIGURE 65: CROWN SETTLEMENTS AT STATION 70.25 FOR 3D AND 2D UNDRAINED ANALYSIS

Deformations u_z at station 0/70.25/-25 in undrained conditions are matched by 2D calculations within 1 %.

7.3.1.2 SURFACE SETTLEMENTS

Because steady state values of crown settlements are predicted within a ±5 % range, the related surface settlements of 2D calculation are expected to match the results of 3D analysis. In Table 37 the surface settlements in phase 83 are compared to the corresponding values in phase "*shotcrete old*" in 2D analysis.

TABLE 37: SURFACE SETTLEMENTS OF 2D CALCULATION CALIBRATED WITH CROWN SETTLEMENTS

[mm]	*3D (phase 83)*	*2D (calibrated at 70.25)*		*2D (calibrated at 69.5)*	
DRAINED					
1) Mohr-Coulomb	-14.9 mm	-16.0 mm	*8%*	-15.3 mm	*3 %*
2) Hardening Soil (E=45MN/m², POP=500 kN/m²)	-10.8 mm	-13.7 mm	*27%*	-12.1 mm	*12%*
2) Hardening Soil (E=45MN/m², POP=0 kN/m²)	-16.0 mm	-17.3 mm	*8%*	-15.5 mm	*-3%*
3) Hardening Soil (E=20 MN/m²)	-22,5 mm	-29.0 mm	*29%*	-24.1 mm	*7%*
7) HS-small (E=45MN/m²)	-4.8 mm	-8.3 mm	*73%*	-6.9 mm	*45%*
9) HS-small (E=20 MN/m²)	-11.0 mm	-19.3 mm	*76%*	-16.0 mm	*46%*
UNDRAINED					
6) Mohr-Coulomb	-12.2 mm	-12.8 mm	*5%*	-13.2 mm	*8%*
4) Hardening Soil (E=69 MN/m², POP=500 kN/m²)	-7.7 mm	-8.8 mm	*14%*	-9.0 mm	*17%*
4) Hardening Soil (E=69 MN/m²,POP=0 kN/m²)	-13.0 mm	-13.0 mm	*0%*	-13.5 mm	*4%*
5) Hardening Soil (E=30 MN/m²)	-15.7 mm	-17.8 mm	*13%*	-18.1 mm	*15%*
8) HS-small (E=69 MN/m²)	-3.9 mm	-4.6 mm	*18%*	-4.7 mm	*22%*
10) HS-small (E=30 MN/m²)	-10.8 mm	-13.1 mm	*21%*	-13.5 mm	*25%*

However, the surface settlements of the 2D model are slightly over predicted. The best results are obtained for calculation with the Mohr-Coulomb model and Hardening Soil model without pre-overburden pressure. For calibration in station 69.5 (end of excavation length) and undrained analysis generally a better consistency is achieved. The worst result is obtained for calculations with the HS-small model.

The better agreement for calibration in station 69.5 m can be related to the sagging of the crown in 3D FE-analysis. For 3D computation the supporting effect of the tunnel face and the lining result in a sagging of the tunnel crown over the unsupported length. This phenomenon is responsible for different settlement values at beginning/end and centre of one excavation length obtained from 3D calculation.

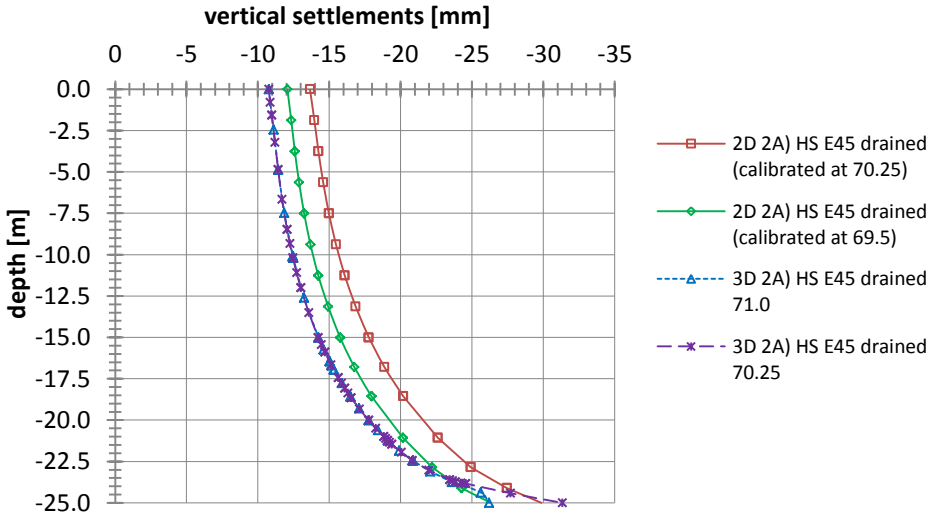

FIGURE 66: COMPARISON OF THE SETTLEMENT PROFILE ABOVE THE TUNNEL AXIS FROM THE TUNNEL CROWN TO THE SURFACE OBTAINED FROM 2D AND 3D CALCULATION WITH THE HARDENING SOIL MODEL (E=45 KN/M², DRAINED)

The influence of pre-overburden pressure on the results is explained by means of different OCR obtained from 2D and 3D at the surface. In Figure 67 the over-consolidation ratio OCR at the end of the calculation is displayed. The highest value is calculated by the 3D analysis. The lowest value is obtained from the 2D calculation calibrated in station 70.25m. Differences at the surface above the tunnel axis also develop in the distribution of relative shear stresses and horizontal effective stresses.

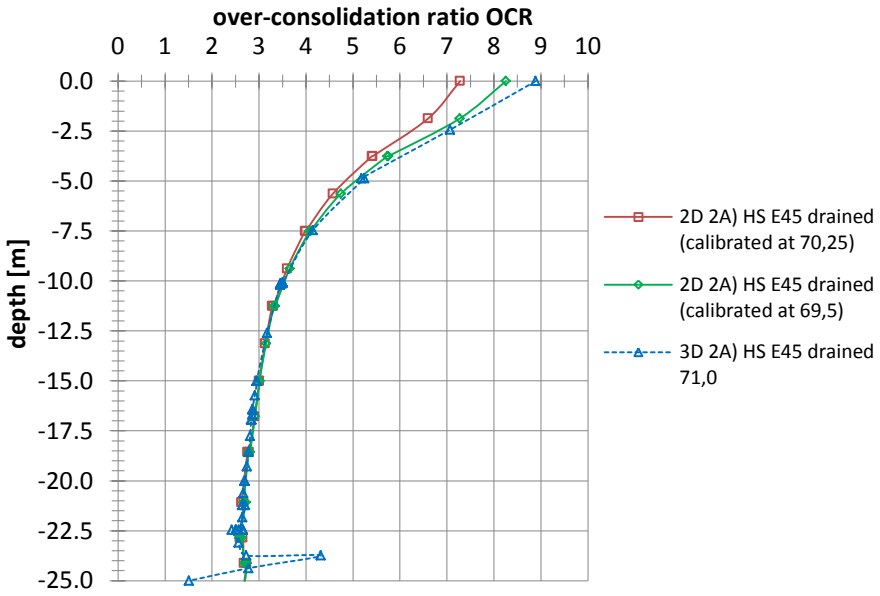

FIGURE 67: OVER-CONSOLIDATION RATIO ABOVE THE TUNNEL AXIS OBTAINED FROM 2D AND 3D CALCULATION WITH THE HARDENING SOIL MODEL (E=45 KN/M², DRAINED) CONSIDERING PRE-OVERBURDEN PRESSURE POP

It is concluded that it is preferable to match crown settlements at the end of the excavation length (station 69.5 m). When looking at the related surface settlements, the influence of pre-overburden pressure and small-strain stiffness has to be evaluated carefully.

7.3.1.3 AXIAL FORCES OF THE LINING

In the figures below the axial forces obtained from 2D analysis calibrated with crown settlements in station 69.5 m are compared to the internal forces in the middle of the plate element of the 3D computation. The approximation of the curved tunnel contour by straight lines leads to an inhomogeneous distribution of forces. Especially at element boundaries significant jumps are observed.

The axial forces are displayed over the developed tunnel perimeter length starting from the crown down to the invert. The maximum value lies in the region of the tunnel springline.

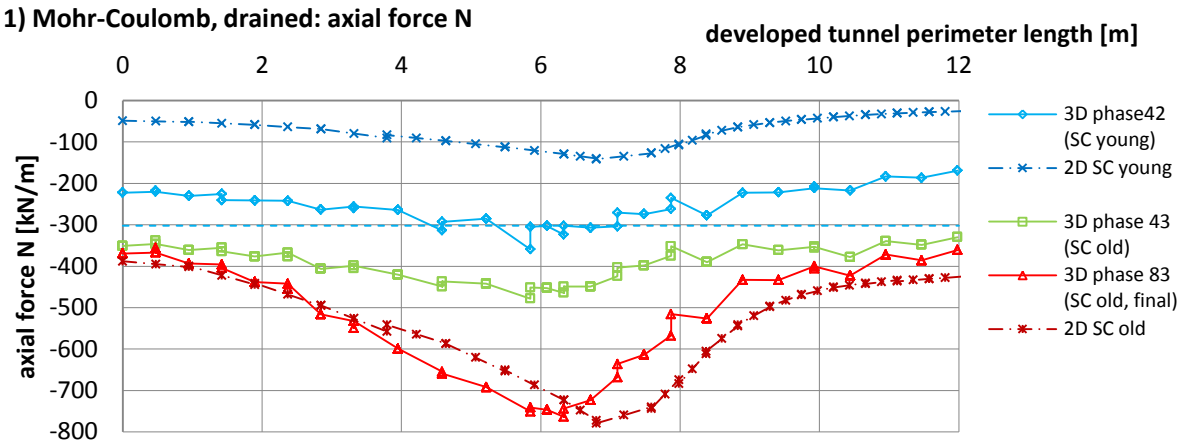

FIGURE 68: AXIAL FORCES FOR 3D AND 2D ANALYSIS WITH 1) MOHR-COULOMB, DRAINED; CALIBRATION USING CROWN SETTLEMENTS IN STATION 69.5 M

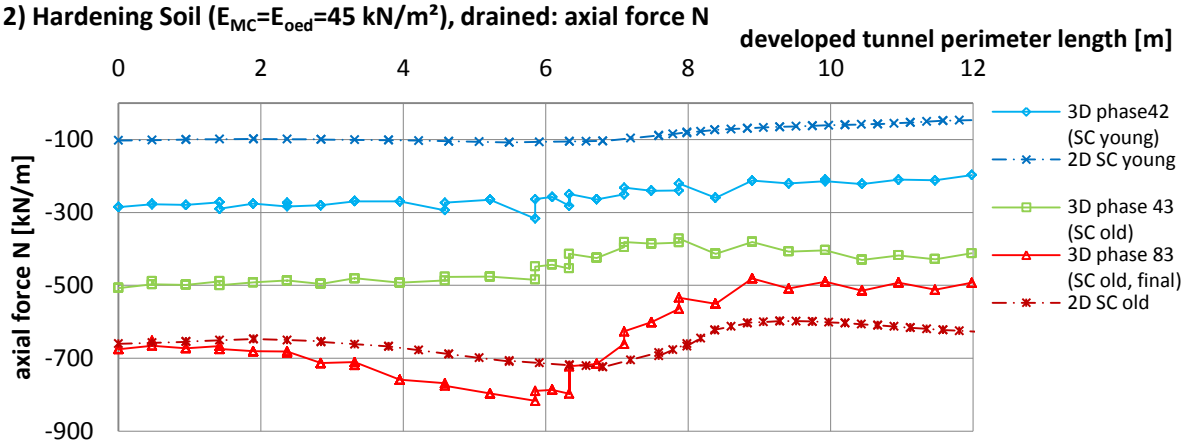

FIGURE 69: AXIAL FORCES FOR 3D AND 2D ANALYSIS WITH 2) HARDENING SOIL ($E_{MC}=E_{OED}$), DRAINED; CALIBRATION USING CROWN SETTLEMENTS IN STATION 69.5 M

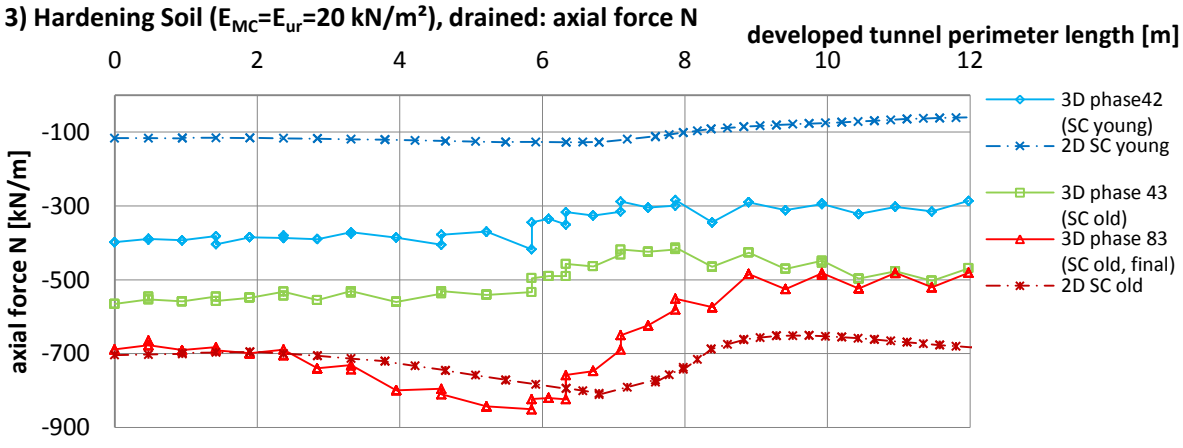

FIGURE 70: AXIAL FORCES FOR 3D AND 2D ANALYSIS WITH 3) HARDENING SOIL ($E_{MC}=E_{UR}$), DRAINED; CALIBRATION USING CROWN SETTLEMENTS IN STATION 69.5 M

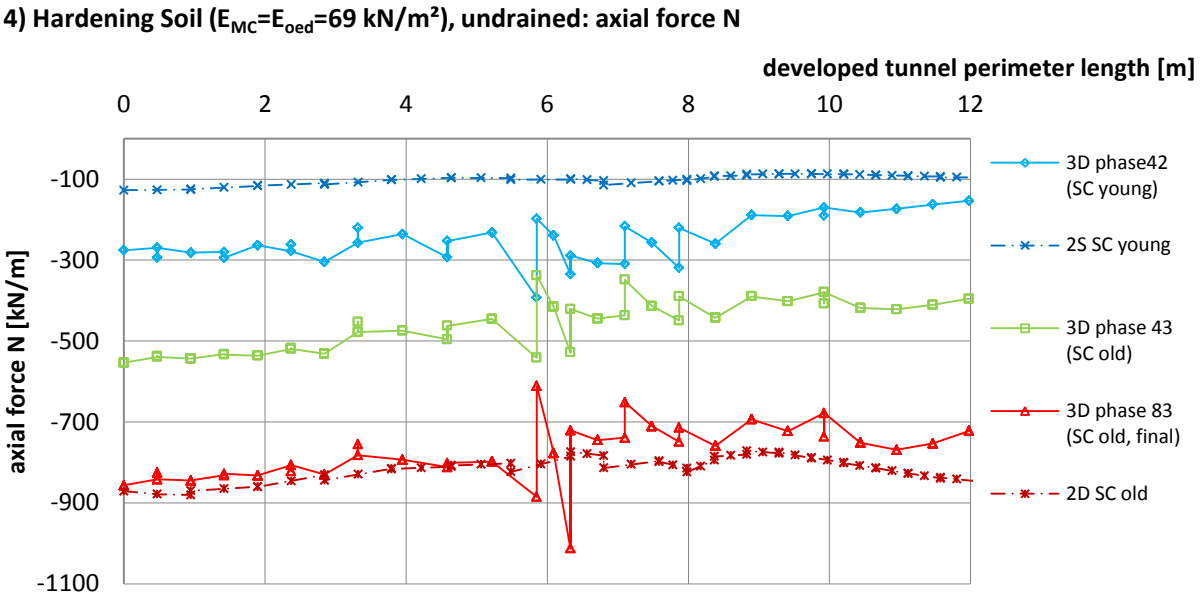

FIGURE 71: AXIAL FORCES FOR 3D AND 2D ANALYSIS WITH 4) HARDENING SOIL ($E_{MC}=E_{OED}$), UNDRAINED; CALIBRATION USING CROWN SETTLEMENTS IN STATION 69.5 M

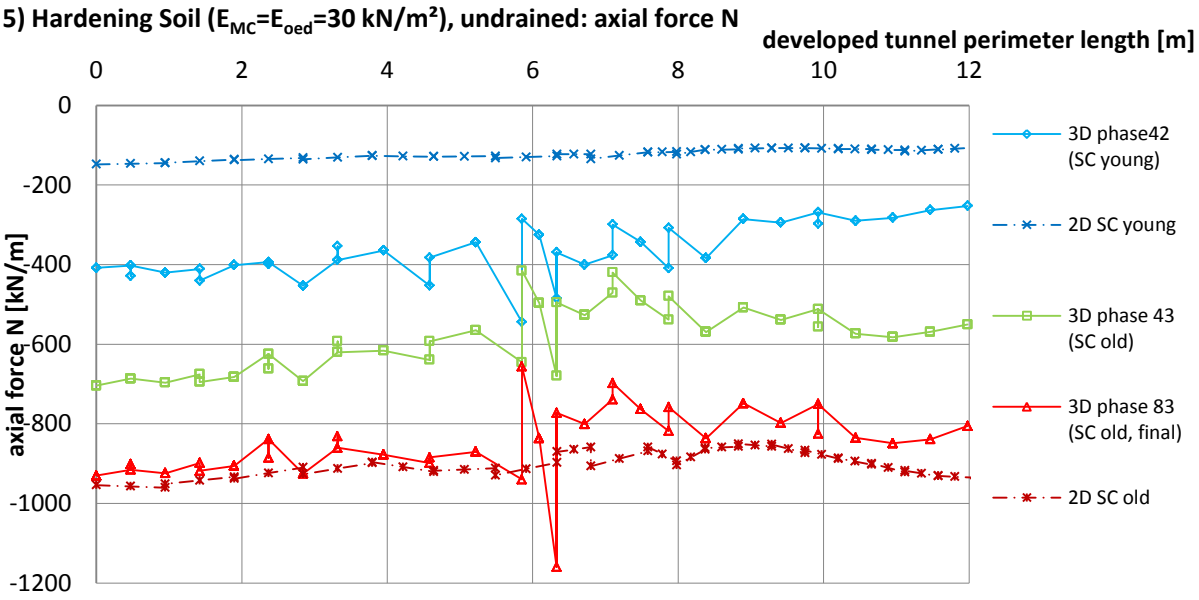

FIGURE 72: AXIAL FORCES FOR 3D AND 2D ANALYSIS WITH 5) HARDENING SOIL ($E_{MC}=E_{UR}$), UNDRAINED; CALIBRATION USING CROWN SETTLEMENTS IN STATION 69.5 M

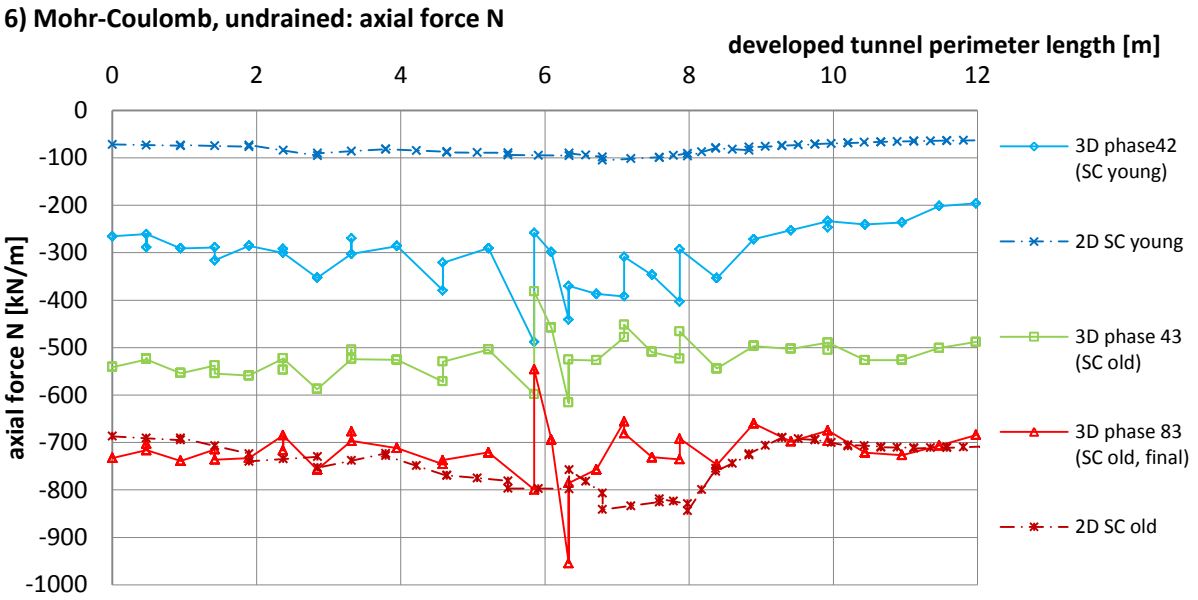

FIGURE 73: AXIAL FORCES FOR 3D AND 2D ANALYSIS WITH 6) MOHR-COULOMB, UNDRAINED; CALIBRATION USING CROWN SETTLEMENTS IN STATION 69.5 M

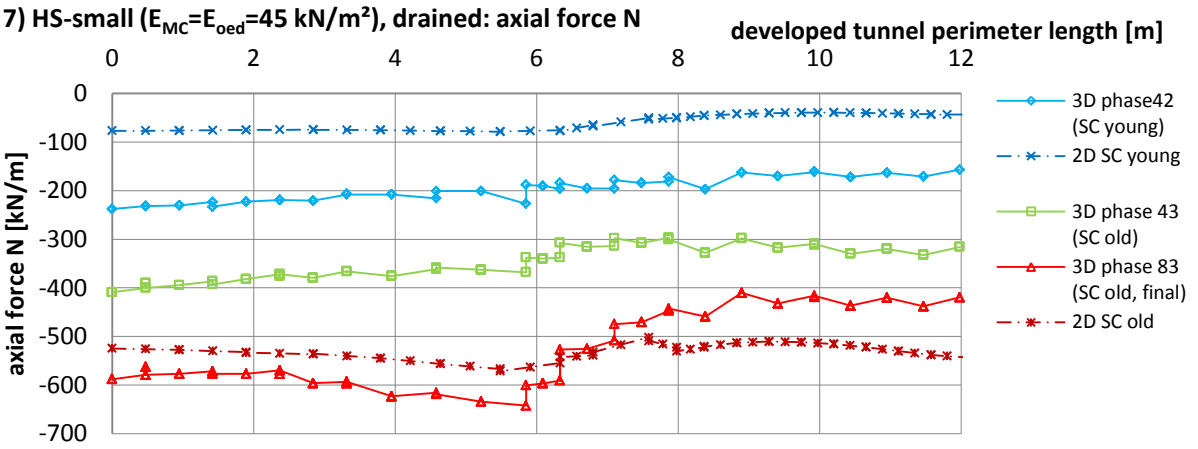

FIGURE 74: AXIAL FORCES FOR 3D AND 2D ANALYSIS WITH 7) HS-SMALL (E_{MC}=E_{OED}), DRAINED; CALIBRATION USING CROWN SETTLEMENTS IN STATION 69.5 M

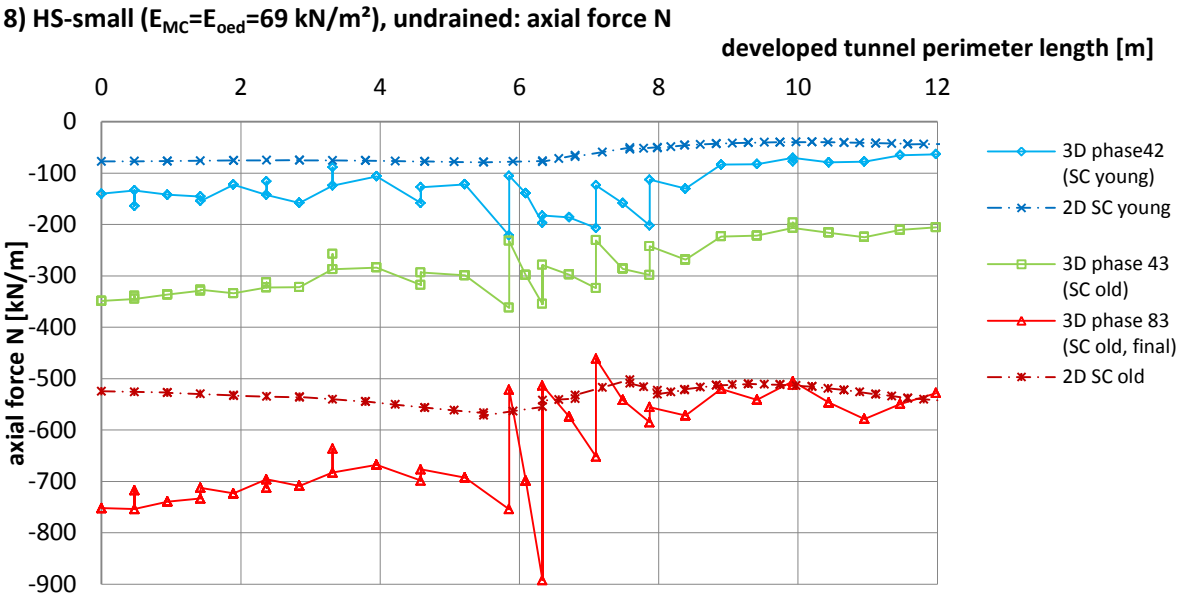

FIGURE 75: AXIAL FORCES FOR 3D AND 2D ANALYSIS WITH 8) HS-SMALL ($E_{MC}=E_{OED}$), UNDRAINED; CALIBRATION USING CROWN SETTLEMENTS IN STATION 69.5 M

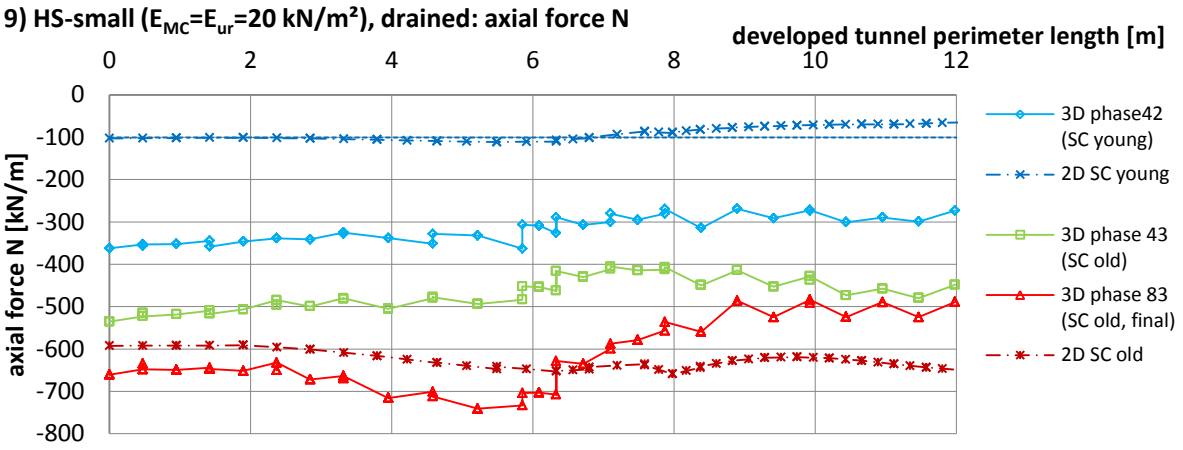

FIGURE 76: AXIAL FORCES FOR 3D AND 2D ANALYSIS WITH 9) HS-SMALL ($E_{MC}=E_{UR}$), DRAINED; CALIBRATION USING CROWN SETTLEMENTS IN STATION 69.5 M

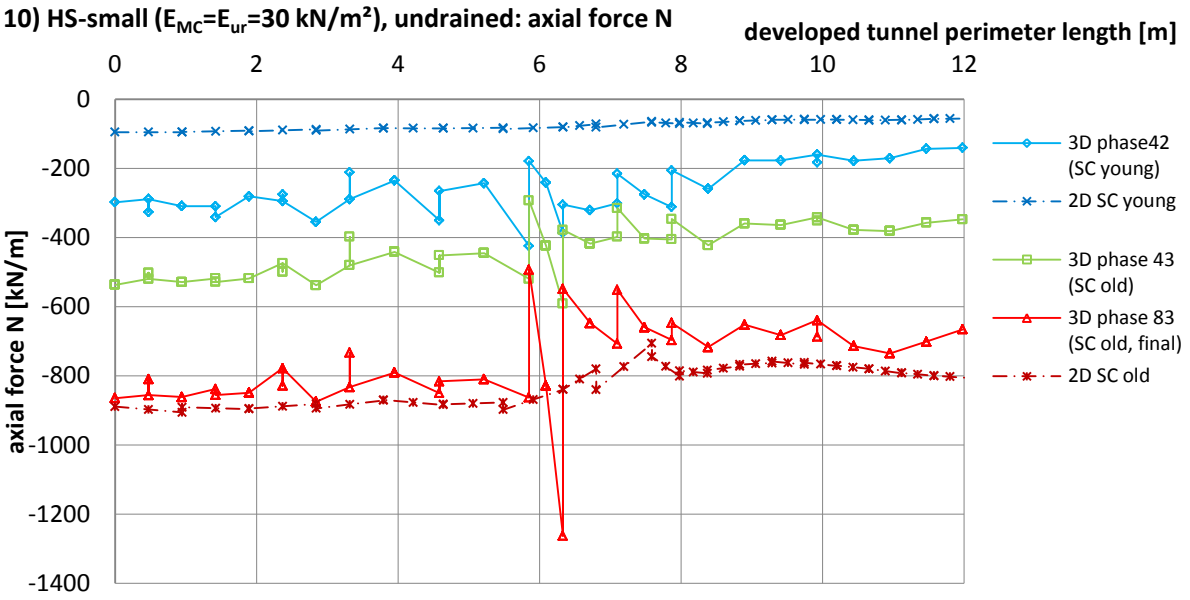

FIGURE 77: AXIAL FORCES FOR 3D AND 2D ANALYSIS WITH 10) HS-SMALL (E_{MC}=E_{UR}), UNDRAINED; CALIBRATION USING CROWN SETTLEMENTS IN STATION 69.5 M

The portion of axial forces carried by the young sprayed concrete lining is underestimated by the 2D analysis. Steady state conditions in 2D and 3D analysis are in better agreement, especially for drained analysis. Axial forces obtained from undrained 3D calculations show significant jumps in the area of the tunnel springline and are therefore not reliable. However, a good match is achieved at the tunnel shoulder and heel. The best match is obtained for calculation 1*) Mohr Coulomb drained*. Axial forces from calculation with the HS and HS-small model 2), 3), 7) and 9) are in good agreement at the tunnel spring line.

7.3.2 DETERMINATION OF β USING SURFACE SETTLEMENTS

For the calibration of 2D pre-relaxation factors surface settlements in station 71.0 m are compared. Due to a coarser FE-mesh at the model surface, the position has to be adapted. Station 71.0 m in phase 42 and 43 can be compared to station 69.5 m in phase 41 and 42. Steady state values of surface settlements in the middle of the FE-model are more or less uniform. Therefore, the exact position of the observation point is not important. The surface settlements are only evaluated in one node.

In Table 38 settlements from 3D and 2D calculation and the related *MStage*-values are listed.

TABLE 38: CROWN SETTLEMENTS IN 3D AND 2D WITH CORRESPONDING MSTAGE-VALUES

	pre-relaxation (Phase 42)			***SC young + anchors (Phase 43)***			***steady state/ SC old (Phase 83)***	
Station	*3D*	*2D*		*3D*	*2D*		*3D*	*2D*
	u_y *[mm]*	*Mstage*	u_y *[mm]*	u_y *[mm]*	*Mstage*	u_y *[mm]*	u_y *[mm]*	u_y *[mm]*
1) MC, drained								
71.0	-8.0	0.520	-8.0	-8.6	0.147	-8.6	-14.9	-13.0
2A) HS, $E_{MC}=E_{oed}$, drained, POP500, $K_0=0,7$								
71.0	-5.6	0.550	-5.6	-6.1	0.170	-6.1	-10.8	-8.5
2C) HS, $E_{MC}=E_{oed}$, drained, POP0, $K_0=0,7$								
71.0	-8.7	0.561	-8.8	-9.3	0.120	-9.3	-16.0	-13.0
3) HS, $E_{MC}=E_{ur}$, drained, POP500, $K_0=0,7$								
71.0	-12.1	0.544	-12.3	-13.1	0.155	-13.1	-22.5	-17.8
4A) HS, $E_{MC}=E_{oed}$, undrained, POP500, $K_0=0,7$								
71.0	-4.1	0.486	-4.1	-4.4	0.110	-4.4	-7.7	-6.3
4C) HS, $E_{MC}=E_{oed}$, undrained, POP0, $K_0=0,7$								
71.0	-6.2	0.471	-6.2	-6.9	0.170	-6.9	-13.0	-9.6
5) HS, $E_{MC}=E_{ur}$, undrained, POP500, $K_0=0,7$								
71.0	-8.5	0.471	-8.5	-9.1	0.150	-9.1	-15.7	-12.7
6) MC, undrained								
71.0	-6.9	0.467	-6.9	-7.4	0.150	-7.4	-12.3	-10.5
7) HSS, $E_{MC}=E_{oed}$, drained, POP500, $K_0=0,7$								
71.0	-2.3	0.610	-2.3	-2.5	0.130	-2.5	-4.8	-3.4
8) HSS, $E_{MC}=E_{oed}$, undrained, POP500, $K_0=0,7$								
71.0	-1.9	0.550	-1.9	-2.1	0.103	-2.1	-3.9	-3.1
9) HSS, $E_{MC}=E_{ur}$, drained, POP500, $K_0=0,7$								
71.0	-4.8	0.554	-4.8	-5.3	0.168	-5.3	-11.0	-7.1
10) HSS, $E_{MC}=E_{ur}$, undrained, POP500, $K_0=0,7$								
71.0	-5.5	0.544	-5.5	-5.9	0.140	-5.9	-10.8	-7.9

In the following figures the development of crown settlements in station 69.5 and 70.25 correlated to the position of the advancing tunnel face are displayed. The continuous lines show the result of 3D numerical calculation. The settlements obtained from the calibrated 2D model are displayed as small squares connected by a dashed line.

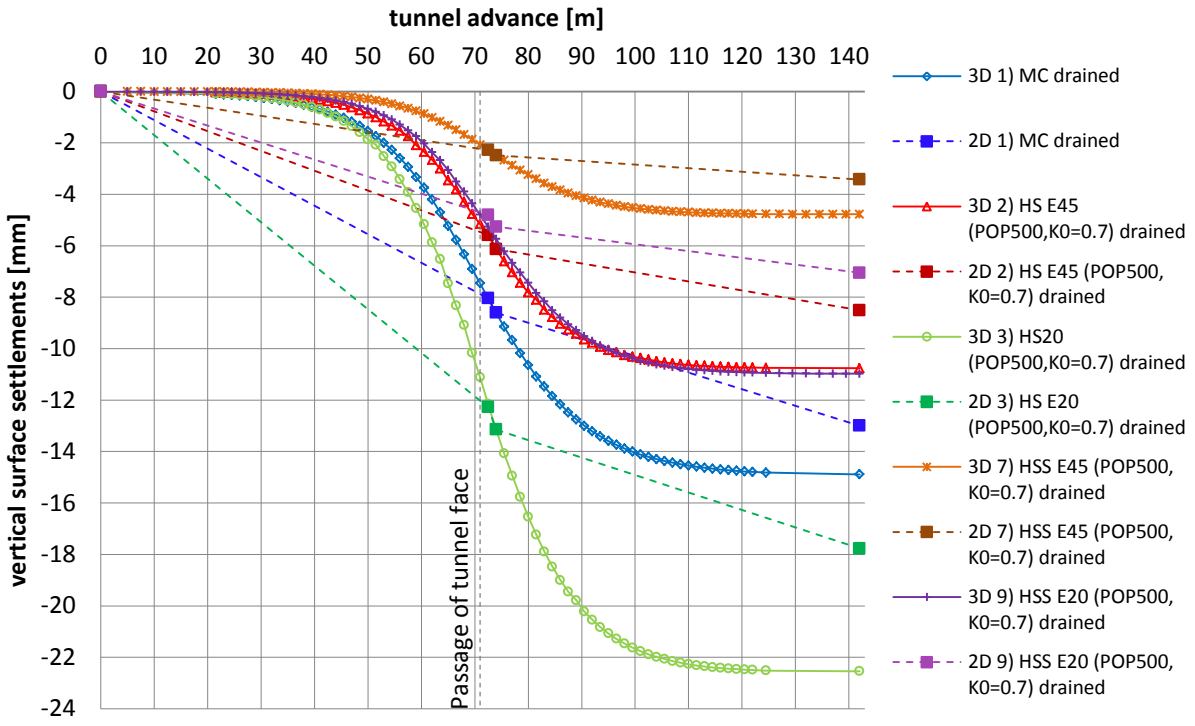

FIGURE 78: SURFACE SETTLEMENTS AT STATION 71.0 FOR 3D AND 2D DRAINED ANALYSIS

Deformations u_z at station 0/71.0/0 in drained conditions are under-predicted by 2D about 13-21%.

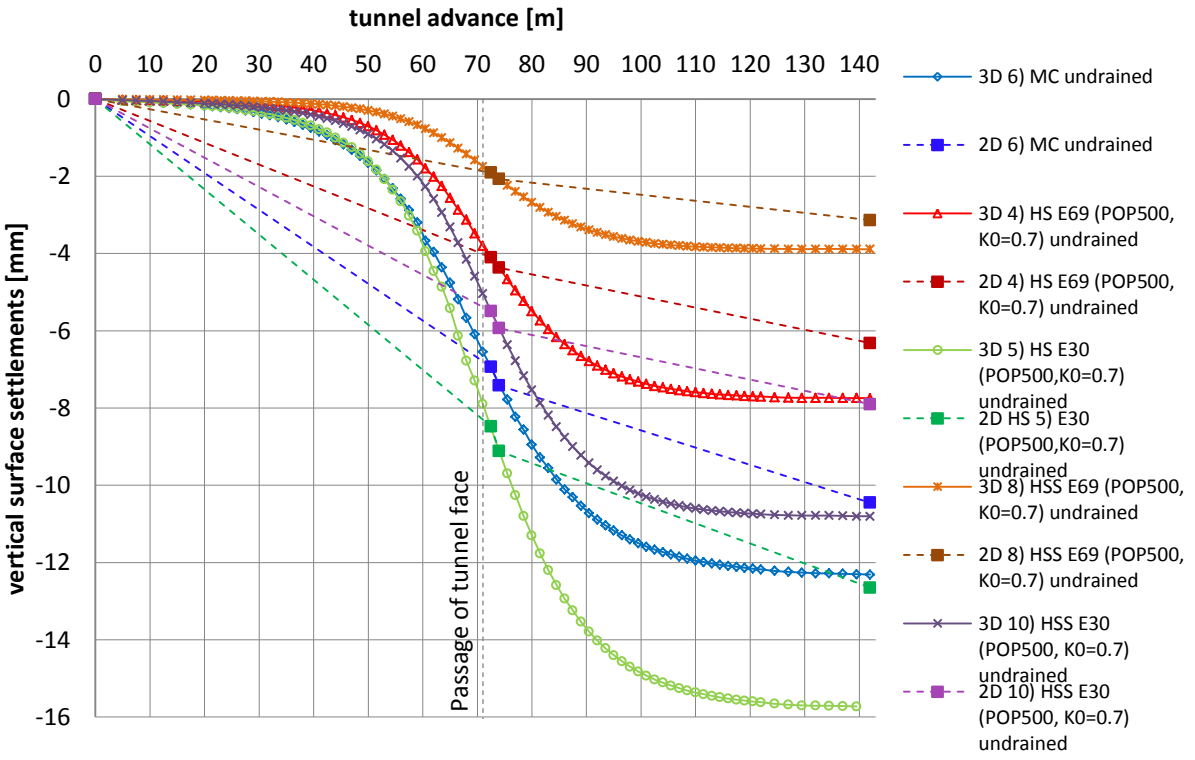

FIGURE 79: SURFACE SETTLEMENTS AT STATION 71.0 FOR 3D AND 2D UNDRAINED ANALYSIS

Deformations u_z at station 0/71.0/0 in drained conditions are under-predicted by 2D about 15-20%.

The final surface settlements predicted by 2D calculation do not match the related 3D deformations. It is concluded that surface settlements are not suitable for determination of load reduction factors in FE-analysis.

Because the influence of lining installation on surface deformations is small, a reliable determination of the second load reduction factor and the prediction of steady state settlements are not possible.

7.3.3 DETERMINATION OF β USING AXIAL FORCES IN THE LINING

Structural forces in the lining are of major interest in tunnel design. Using axial forces for calibration only one *MStage*-factor can be determined for the pre-relaxation phase. Lining forces in "*shotcrete young*" and "*shotcrete old*" are approximately the same, because no second load-reduction factor is introduced.

The lining internal forces obtained from 3D analysis are evaluated in the middle of the round length in station 70.25 m (central node of element) because the distribution of internal forces at the element margin shows a large scatter. As reference value the axial force at the tunnel springline (x_{min}) is used because maximum axial forces occur in this area. The extreme values resulting from jumps in the axial forces in PLAXIS 3D are not taken into account.

The normal forces of the 2D FE-analysis are fitted to match the results of the 3D calculation in phase 42 for the young shotcrete and phase 43 and 83 for the aged shotcrete for models 1) and 6). Because only the matching of the final internal forces (phase 83) gives useful results, calculation 2), 3), 4), 5), 7), 8), 9) and 10) are only calibrated at the final axial forces in phase 83.

7.3.3.1 AXIAL FORCES

The axial forces are displayed over the uncoiled tunnel perimeter length starting from the crown down to the invert in Figure 80 and Figure 81. The maximum value lies in the region of the tunnel springline.

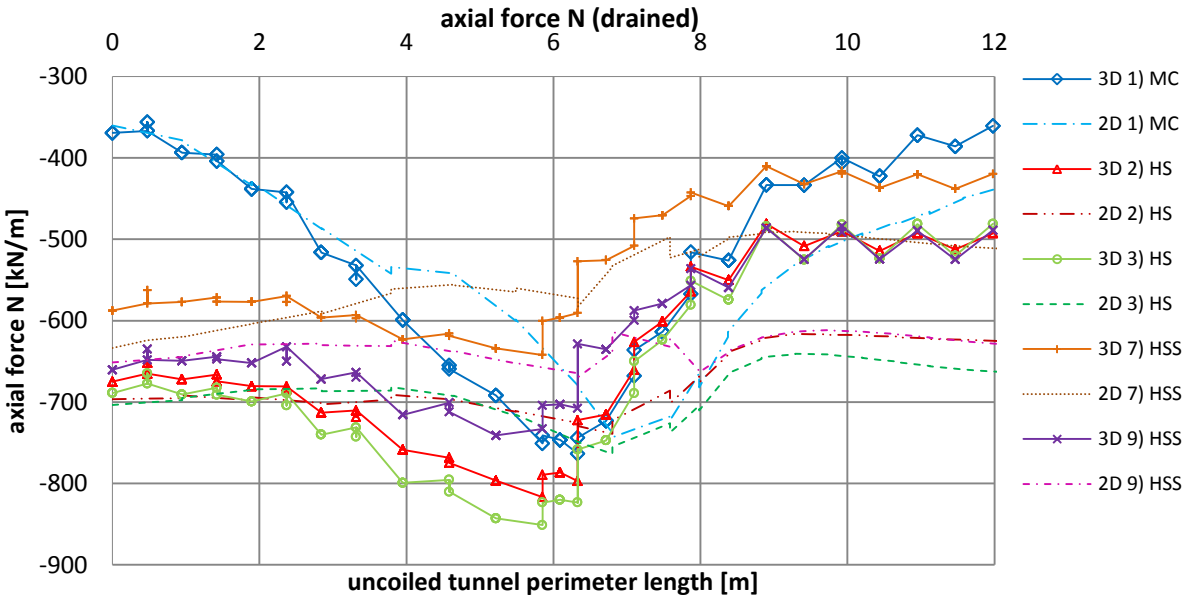

FIGURE 80: AXIAL FORCES IN 3D AND 2D (DRAINED ANALYSIS)

TABLE 39: AXIAL FORCES USED FOR CALIBRATION WITH CORRESPONDING MSTAGE-VALUES (DRAINED ANALYSIS)

	3D	2D	
	$N(x_{min})$ [kN/m]	MStage	$N(x_{min})$ [kN/m]
1)MC drained	-743.8	0.563	-743.1
2)HS E45 drained	-722.1	0.563	-722.6
3)HS E20 drained	-758.3	0.640	-754.8
7)HSS E45 drained	-527.0	0.635	-532.6
9)HSS E20 drained	-628.5	0.695	-549.1

As shown in Figure 80 the distribution of axial forces is not uniform in one plate element. To achieve a correlation between 2D and 3D results is, therefore, difficult. The *MStage*-values for drained analysis range from 0.56 to 0.70.

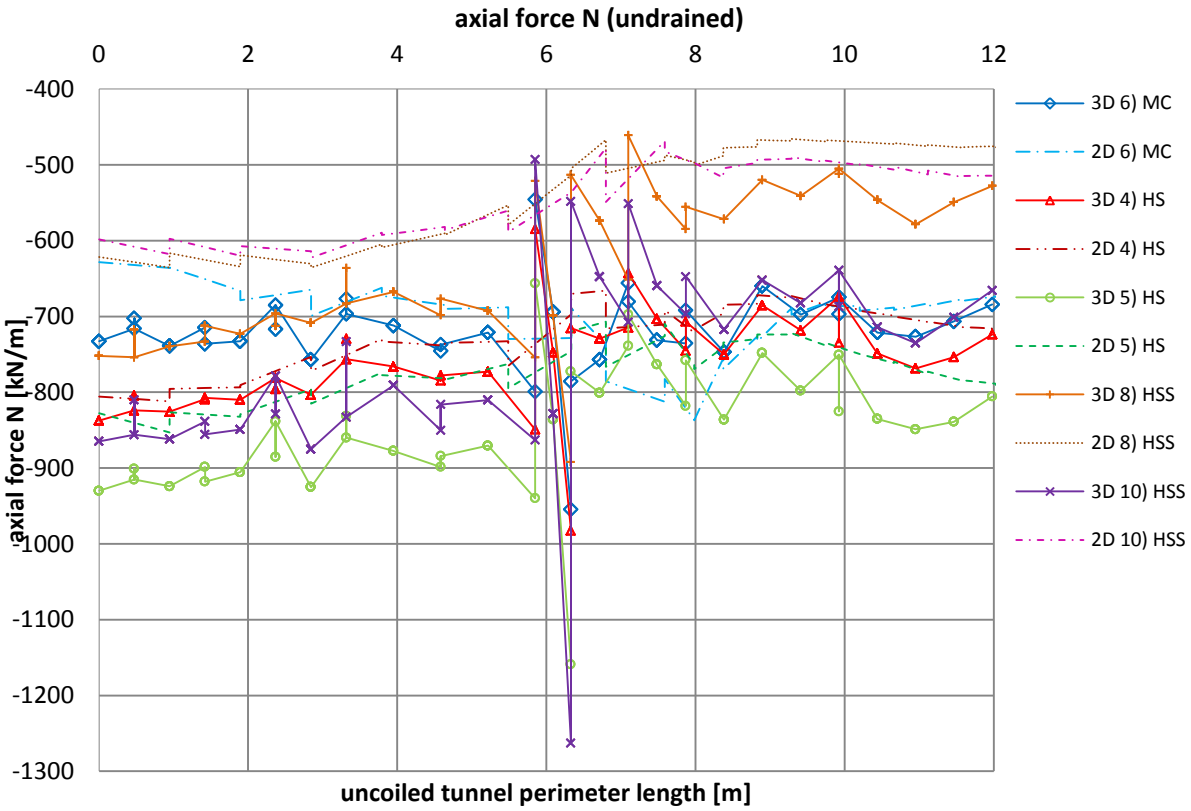

FIGURE 81: AXIAL FORCES IN 3D AND 2D (UNDRAINED ANALYSIS)

TABLE 40: AXIAL FORCES USED FOR CALIBRATION WITH CORRESPONDING MSTAGE-VALUES (UNDRAINED ANALYSIS)

	3D	2D	
	$N(x_{min})$ [kN/m]	MStage	$N(x_{min})$ [kN/m]
6)MC drained	-1575.4	0.540	-1575.8
4)HS E45 drained	-1474.9	0.660	-1473.0
5)HS E20 drained	-772.5	0.610	-766.5
8)HSS E45 drained	-513.3	0.720	-510.9
10)HSS E20 drained	-549.1	0.750	-549.1

Due to high excess pore water pressures, axial force distribution in undrained analysis is highly irregular. At the tunnel springline significant jumps in their distribution are developed independently of the used soil model. As shown in Figure 81 calibration using $N(x_{min})$ does not lead to reliable results. 3D axial forces exceed the corresponding 2D results in large parts of the lining. The least error results from calculations with the Mohr Coulomb model.

7.3.3.2 SURFACE AND CROWN SETTLEMENTS

Because only one load reduction factor is used in the 2D FE-analysis the results of calculation phase "*shotcrete young + anchors*" and "*shotcrete old*" are THE SAME. In 3D calculations there is a small difference between the settlements due to excavation (phase 41) and at the time of lining installation (phase 42). Hence, the settlements in calculation phase "*SC young + anchors*" cannot be expected to match 3D results. Only steady state settlements are compared.

TABLE 41: CROWN AND SURFACE SETTLEMENTS IN 3D AND 2D (DRAINED ANALYSIS)

	2D		3D			
	crown	*surface*	*crown*	*surface*	*crown*	*surface*
1) MC drained	-35.1 mm	-14.6 mm	-35.8 mm	-14.9 mm	98%	98%
2) HS E45 drained	-22.2 mm	-9.6 mm	-26.7 mm	-10.8 mm	83%	89%
3)HS E20 drained	-52.3 mm	-23.2 mm	-56.2 mm	-22.6 mm	93%	103%
7) HSS E45 drained	-12.0 mm	-4.4 mm	-19.9 mm	-7.7 mm	60%	57%
9) HSS E20 drained	-34.9 mm	-12.7 mm	-10.0 mm	-3.9 mm	349%	327%

TABLE 42: CROWN AND SURFACE SETTLEMENTS IN 3D AND 2D (UNDRAINED ANALYSIS)

	2D		3D			
	crown	*surface*	*crown*	*surface*	*crown*	*surface*
4)HS E69 undrained	-23.7 mm	-9.7 mm	-16.7 mm	-4.8 mm	142%	202%
5) HS E30 undrained	-50.5 mm	-21.6 mm	-41.4 mm	-11.0 mm	122%	197%
6) MC undrained	-28.7 mm	-12.5 mm	-28.1 mm	-12.3 mm	102%	101%
8) HSS E69 undrained	-28.9 mm	-13.4 mm	-36.8 mm	-15.7 mm	79%	85%
10) HSS E30 undrained	-111.5 mm	-57.1 mm	-27.3 mm	-10.8 mm	409%	528%

The calculated crown and surface settlements in 2D match the 3D-values quite well when using the Mohr-Coulomb model or the Hardening Soil model in a drained analysis without groundwater. In undrained analysis only steady state settlements obtained from calculations with the Mohr-Coulomb model are in good agreement. The HS model over predicts deformations. Surface settlements obtained from 2D FE-analysis are twice the corresponding values in 3D. When using the Hardening Soil-model small no useful prediction can be made.

As mentioned in previous chapters, internal lining forces in PLAXIS 3D 2011 are not reliable. Due to discretization of the curved lining by straight segments and the element formulation used, the obtained results have to be treated carefully. Singular extreme values resulting from sharp bends in the lining should not be considered. In undrained analysis the generated excess pore pressures have an additional negative influence on the calculated lining forces.

7.3.4 CONCLUSION

The load reduction factor β depends on ground conditions, tunnel geometry and construction processes [1]. The related input value in PLAXIS 2D is

$$MStage = 1 - \beta \tag{7.4}$$

Small β-factors indicate large excavation lengths and/or late installation of the tunnel lining. The applied fictive support pressure is small, resulting in relatively large ground deformations and small lining forces. [1]

The magnitude of the unloading factor has been investigated by several authors. However, a quantitative determination is very difficult, as it depends on numerous parameters. Möller [1] gave a qualitative overview of the influence of soil stiffness and strength (cohesion *c'* and friction angle φ') and excavation length. He concluded that the load reduction factor β decreases with increasing ground stiffness, decreasing cohesion and increasing round length. In a realistic range of 20° to 40° the friction angle has a very small influence on β. Internal lining forces are heavily influenced by the tunnel geometry. Therefore, a single load reduction factor for normal forces, bending moments and settlements is not recommended. [1]

In this study the influence of different soil models and pre-overburden pressure *POP* has been evaluated for different load reduction factors:

- Matching of crown settlements in two different positions of one excavation length

- Matching of surface settlement
- Matching of internal lining forces

For calibration of the 2D model with deformations two *MStage*-factors have been used. The second value is smaller than the factor used in the pre-relaxation phase. For the performed analysis values ranging from 0.10 to 0.35 were obtained. The largest values are obtained for matching crown settlements in the middle of the excavation length (station 70.25 m). Especially in drained analysis it exceeds the *MStage*-factors, obtained by matching other reference values, by 0.1. This is related to the sagging of the tunnel crown in 3D FE-analysis. The smallest values result from surface settlements because little influence of lining installation is noticeable at the surface. With respect to the applied constitutive model no distinct trend can be identified.

Further conclusions are valid for the load reduction factor *MStage* in pre-relaxation phase, referred to as pre-relaxation factor. It is expected that the magnitude of deformations used for calibration is related to the magnitude of the applied pre-relaxation factor.

In Figure 82 the obtained *MStage*-factors are summarized separately for drained and undrained analysis. They cannot be simply related because no groundwater is considered in the drained analyses. Differences may be caused by the drainage type or groundwater conditions. Generally *MStage* of drained calculations exceeds the values of undrained calculations because volumetric changes are restricted due to the incompressibility of the pore water.

Pre-relaxation factors for axial forces have to be treated carefully; especially in undrained analysis a calibration of the 2D model with lining forces from 3D calculations is not recommended. According to Möller [1] a conservative approach for structural forces would be $\beta = 0.5$ to 0.7 in soil. In this thesis the applied load reduction factor for axial forces is significantly lower. The investigated tunnel is constructed in ground specified as hard soil to soft rock.

The calibration of the 2D model using surface settlements results in the lowest pre-relaxation factors. At the surface a smaller proportion of settlements develop prior to the passage of the tunnel face compared to the crown. Because the influence of lining installation on surface deformations is small a reliable determination of the second pre-relaxation factor and the prediction of steady state settlements are not possible.

The largest deformations occur around the tunnel, while the influence of tunnel construction decreases at the surface. The deformations towards the cavity are largest in the middle of the slice/round length. Therefore, in drained analysis the highest *MStage*-values are obtained by matching crown settlements in the middle of the excavation length (station 70.25 m). The sagging of the tunnel crown is reduced in undrained analysis with a groundwater table 5.0 m below the surface. Volumetric changes are restricted due to incompressible pore water. In undrained analysis pre-relaxation factors calibrated in station 69.5 m are slightly higher than the corresponding values for station 70.25 m.

The Mohr Coulomb model gives lower *MStage*-values than the Hardening Soil model. The different stiffnesses used for the HS model have little influence on the obtained load-reduction factors unlike an existing pore-overburden pressure. *MStage*-values obtained from the calculations with *POP = 500 kN/m²* are larger than for the corresponding computations without *POP*. This does not match the assumption that calibration using larger deformation automatically results in higher *MStage*-values. Over-consolidated soils are subjected to smaller deformations than normal-consolidated soils with the same stiffness parameters. The HS-small model is very sensitive to variations of *MStage* in the pre-relaxation phase. This indicated that the computed shear strains are in a range, where the shear modulus is not constant. Even small changes of *MStage* lead to large differences in settlement results. *MStage*-values obtained from computations considering small strain stiffness are higher than from the corresponding standard Hardening Soil model.

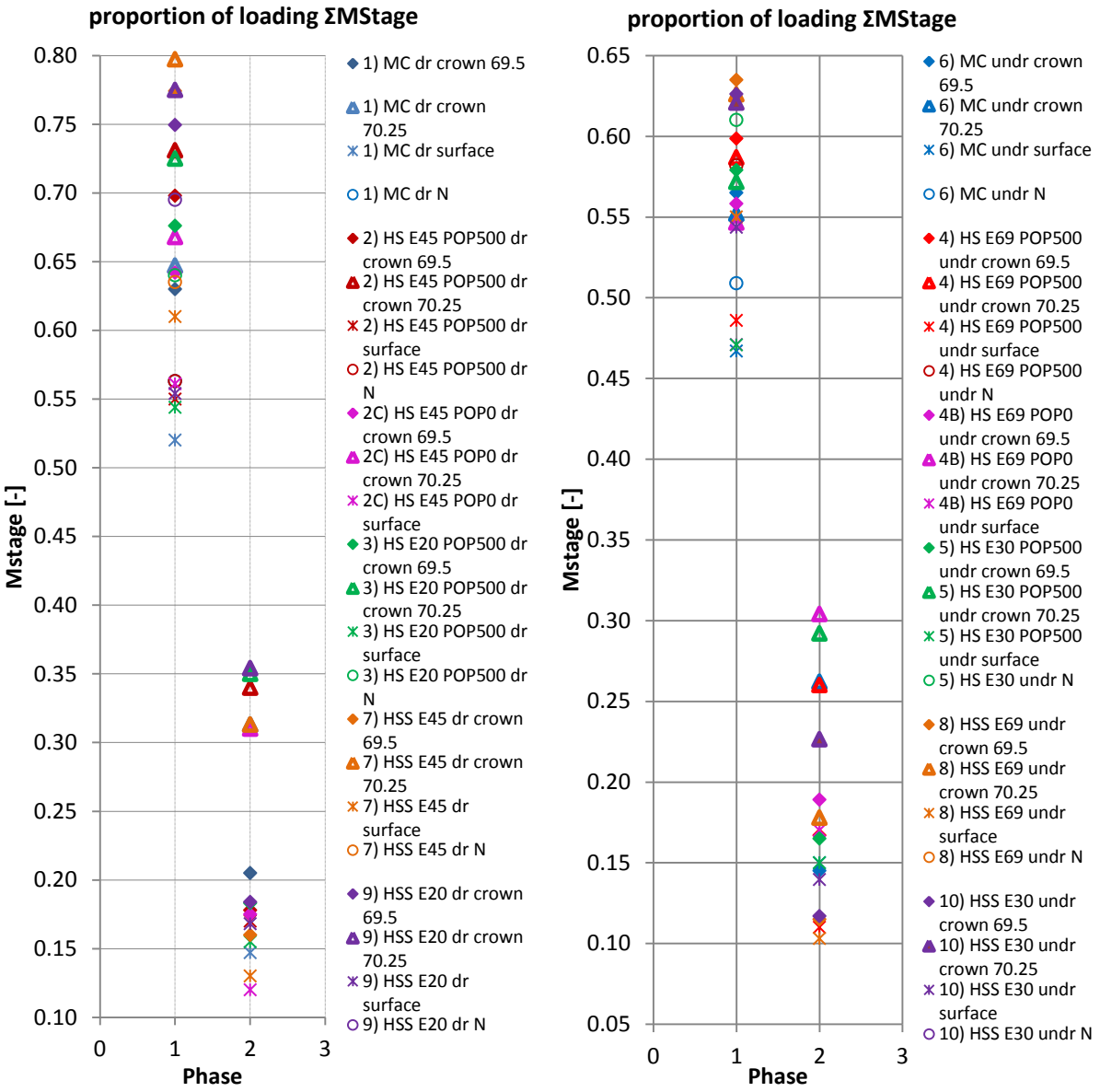

FIGURE 82: SUMMARY OF THE OBTAINED MSTAGE-VALUES FOR THE CALIBRATION OF THE 2D MODEL USING CROWN AND SURFACE SETTLEMENTS AND STEADY STATE VALUES OF AXIAL FORCES, LEFT: DRAINED CALCULATIONS, RIGHT: UNDRAINED CALCULATIONS

In Table 43 the maximum, minimum and mean values of the applied load reduction factors are summarized. *MStage*-values from calibration with axial forces are not included. For drained calculations *MStage* ranges from 0.52 to 0.80 in the pre-relaxation phase and 0.12 to 0.35 in phase "*SC young + anchors*". For undrained analysis *MStage* is generally smaller, ranging from 0.47 to 0.64 in phase 1 and 0.10 to 0.30 in phase 2.

TABLE 43: MAXIMUM, MINIMUM AND MEAN VALUES OF THE APPLIED LOAD REDUCTION FACTORS

MStage	Drained			Undrained		
	max	*min*	*mean*	*max*	*min*	*mean*
pre-relaxation	0.797	0.520	0.658	0.635	0.467	0.559
SC young + anchors	0.354	0.120	0.220	0.304	0.103	0.180

In Table 44 and Table 45 the *MStage*-values for the different calculations are summarized.

TABLE 44: MSTAGE-VALUES (CALIBRATION WITH SETTLEMENTS)

Mstage						
	MC drained			**MC undrained**		
	crown		*surface*	*crown*		*surface*
	69.50 m	*70.25 m*	*71.00 m*	*69.50 m*	*70.25 m*	*71.00 m*
Pre-relaxation	0.630	0.647	0.520	0.565	0.552	0.467
SC young + anchors	0.205	0.313	0.147	0.145	0.262	0.150
	HS E45 drained (POP500)			**HS E69 undrained (POP500)**		
	crown		*surface*	*crown*		*surface*
	69.50 m	*70.25 m*	*71.00 m*	*69.50 m*	*70.25 m*	*71.00 m*
Pre-relaxation	0.698	0.731	0.550	0.599	0.587	0.486
SC young + anchors	0.178	0.340	0.170	0.167	0.260	0.110
	HS E45 drained (POP0)			**HS E69 undrained (POP0)**		
	crown		*surface*	*crown*		*surface*
	69.50 m	*70.25 m*	*71.00 m*	*69.50 m*	*70.25 m*	*71.00 m*
Pre-relaxation	0.642	0.668	0.561	0.558	0.547	0.471
SC young + anchors	0.175	0.310	0.120	0.189	0.304	0.170
	HS E20 drained			**HS E30 undrained**		
	crown		*surface*	*crown*		*surface*
	69.50 m	*70.25 m*	*71.00 m*	*69.50 m*	*70.25 m*	*71.00 m*
Pre-relaxation	0.676	0.725	0.544	0.579	0.572	0.471
SC young + anchors	0.183	0.350	0.155	0.165	0.292	0.150
	HSS E45 drained (POP500)			**HSS E69 undrained (POP500)**		
	crown		*surface*	*crown*		*surface*
	69.50 m	*70.25 m*	*71.00 m*	*69.50 m*	*70.25 m*	*71.00 m*
Pre-relaxation	0.774	0.797	0.610	0.635	0.626	0.550
SC young + anchors	0.160	0.313	0.130	0.115	0.178	0.103
	HSS E20 drained			**HSS E30 undrained**		
	crown		*surface*	*crown*		*surface*
	69.50 m	*70.25 m*	*71.00 m*	*69.50 m*	*70.25 m*	*71.00 m*
Pre-relaxation	0.750	0.775	0.554	0.626	0.621	0.544
SC young + anchors	0.184	0.354	0.168	0.117	0.227	0.140

TABLE 45: MSTAGE-VALUES (CALIBRATION WITH AXIAL FORCES)

	1) MC	**2) HS E45**	**3) HS E20**	**7) HSS E45**	**9) HSS E20**
Pre-relaxation	0.563	0.563	0.640	0.635	0.695
	6) MC	**4) HS E69**	**5) HS E30**	**8) HSS E69**	**10) HSS E30**
Pre-relaxation	0.540	0.660	0.610	0.720	0.750

8 COMPARISON WITH ANALYTICAL METHODS

The construction of a tunnel in soft rock/hard soil inevitably causes ground movements. Depending on the construction techniques different support measures are installed to guarantee the stability of the cavity and reduce deformations.

In recent years the use of sprayed concrete linings for tunnelling in relatively soft ground became more common, particularly for tunnels of shorter length and non-circular cross-section. For a tunnel constructed using the NATM, the main causes of settlements can be specified as: [1]

1) *Movement of the ground towards the unsupported tunnel heading*
2) *Radial ground movement towards the deforming lining*
3) *Radial ground movement towards the lining due to consolidation*

By reducing the unsupported round length and installing additional support measures, e.g. anchors, the ground movement can be reduced, but due to the initially ductile shotcrete lining radial deformations towards the tunnel remain relatively large. [1]

Especially for shallow tunnels in urban environment the ground deformations have to be reduced to a minimum, because surface settlements may affect nearby infrastructure.

The tunnel analysed in this thesis is an exploratory tunnel with a non-circular cross section. It is excavated as the top heading of the final tunnel. Hence, the primary shotcrete lining is the sole mean of support for a significant period. The average overburden is about 25 m (D/C = 7.8/25 = 3.12). Because the tunnel passes under some nearby buildings and infrastructures, the determination of deformations is of prime importance. The adjacent structures are not considered in FE-analysis.

For a single tunnel in “green-field-conditions” the development of the surface settlements can be described by a Gaussian distribution. The assumption of “green-field-conditions” for tunnels in urban areas implies a conservative approach. [15]

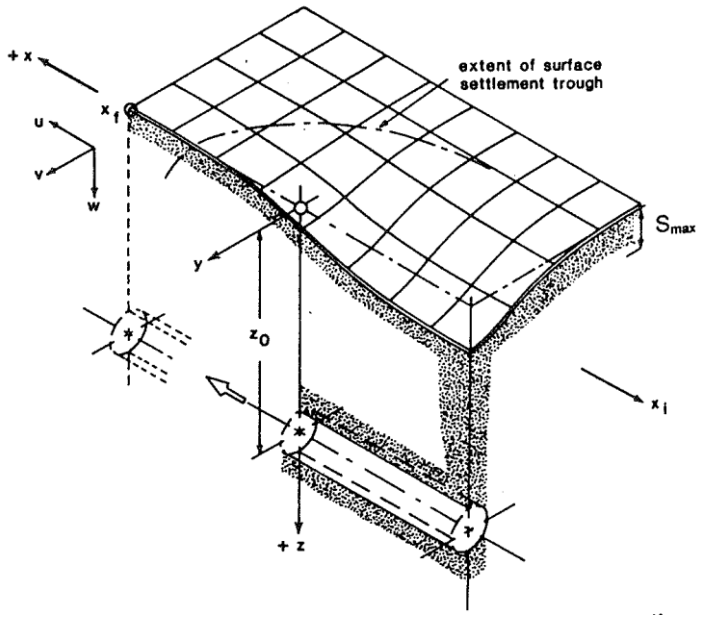

FIGURE 83: SETTLEMENT TROUGH ABOVE ADVANCING TUNNEL HEADING (ATTWELL ET AL, 1986) [15]

8.1 TRANSVERSAL SURFACE SETTLEMENT TROUGH

Peck [17] was the first to show, that the shape of the transverse settlement trough immediately after tunnel construction is well described by a Gaussian distribution curve:

$$S = S_{max} \cdot e^{-\frac{y^2}{2 \cdot i^2}} \tag{8.1}$$

S settlement
S_{max} maximum settlement above the tunnel axis
y horizontal distance from the tunnel centre line
i horizontal distance from the tunnel centre line to the point of inflection of the settlement trough

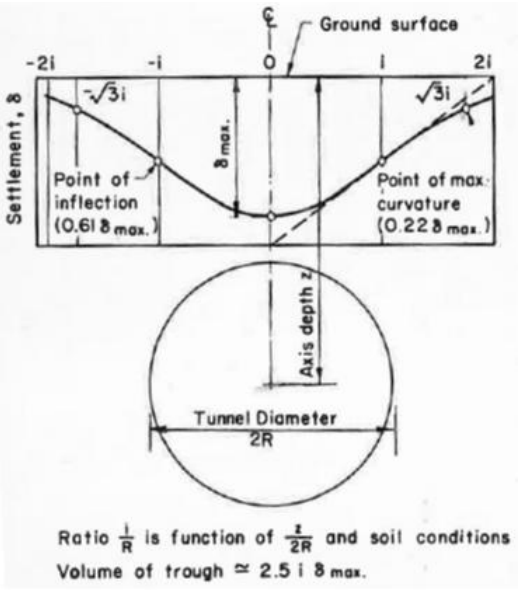

FIGURE 84: GAUSSIAN DISTRIBUTION CURVE FOR TRANSVERSE SURFACE SETTLEMENT PROFILE (PECK, 1969) [17]

The volume of the settlement trough per unit length of tunnel V_s, can be calculated by integrating Equation (2.17).

$$V_s = \int S_v(y)\, dx = \sqrt{2 \cdot \pi} \cdot i \cdot S_{max} \tag{8.2}$$

For tunnelling in clays the volume of the surface settlement trough V_s is more or less the same as the amount of ground lost in the region close to the tunnel, referred to as volume loss or ground loss V_t, because no volumetric change occurs in undrained conditions. When tunnelling in drained conditions, the settlement volume tends to be a little bit smaller than the corresponding volume loss due to dilatation and swelling. The differences remain small and $V_s \approx V_t$. The amount of ground lost in the region close to the tunnel depends on the soil type and the method of construction. It is controlled by ground stiffness and initial stresses. For a NATM tunnel round length and size of the excavation are significant influencing factors. The volume of the surface settlement trough is usually expressed as percentage of the area of the excavated tunnel. [15]

$$GLR = \frac{V_t}{A_t} \approx \frac{V_s}{A_t} \tag{8.3}$$

GLR ground loss ratio
A_t area of excavated tunnel

Mair (1996) concluded that for open face tunnelling in stiff clays (e.g. London Clay) ground loss is generally between 1 % and 2 %. When using sprayed concrete linings (NATM) the value varies between 0.5 % and 1.5 % in London Clay. [15]

The determination of the horizontal distance from the tunnel axis to the point of inflection of the settlement trough has been subject to many investigations. O'Reilly and New (1982) suggested that *i* is a linear function of the tunnel depth [15]. It is broadly independent of the tunnel diameter or the method of construction, except for very shallow tunnels with *C/D < 1.0*. *i* can be expressed by the simple approximate relationship: [15]

$$i = K \cdot z_0 \tag{8.4}$$

K trough width parameter: *K ≈ 0.5* for tunnels in clay and *K ≈ 0.25* for tunnels in sands and gravels

z_0 tunnel depth

The approach has been confirmed by Mair and Tylor (1997), who presented a large variety of tunnel case histories for tunnels in clays and tunnels in sands and gravel [15].

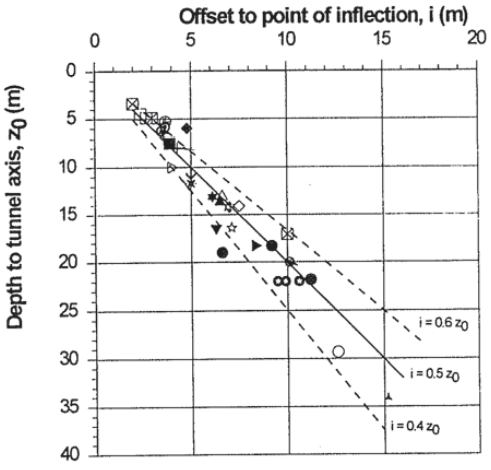

FIGURE 85: VARIATION IN SURFACE SETTLEMENT TROUGH WIDTH PARAMETER WITH TUNNEL DEPTH FOR TUNNELS IN CLAYS [15]

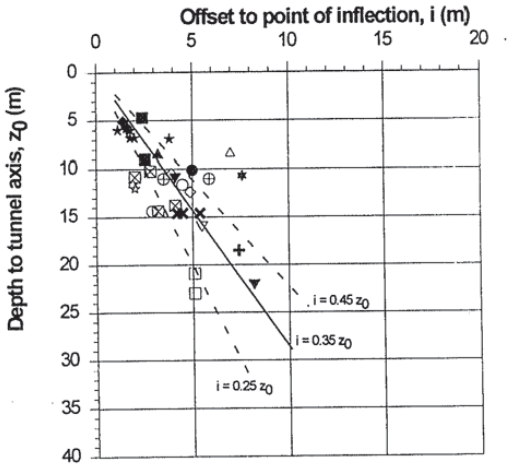

FIGURE 86: VARIATION IN SURFACE SETTLEMENT TROUGH WIDTH PARAMETER WITH TUNNEL DEPTH FOR TUNNELS IN SANDS [15]

The surface settlement profiles obtained from 3D and 2D FE-analysis are compared to the probability functions of the empirical method. It is valid for the immediate settlements related to tunnel construction [18]. Consolidation is not taken into account.

The shape of the transversal settlement trough is governed by volume loss, respectively the maximum settlements above the tunnel centre line, and the point of inflection. According to literature the trough width parameter *K* can be taken as 0.5 for tunnels in clays. Tunnel depth z_0 is 30 m.

TABLE 46: POINT OF INFLECTION FOR DIFFERENT TROUGH WIDTH PARAMETERS

K	i
0,5	15
0,4	12
0,6	18

The settlement profiles obtained from FE-analysis are displayed as continuous lines and the associated Gaussian functions as dashed lines. The results of the FE-analysis for the transversal settlement trough are shown in the figures below.

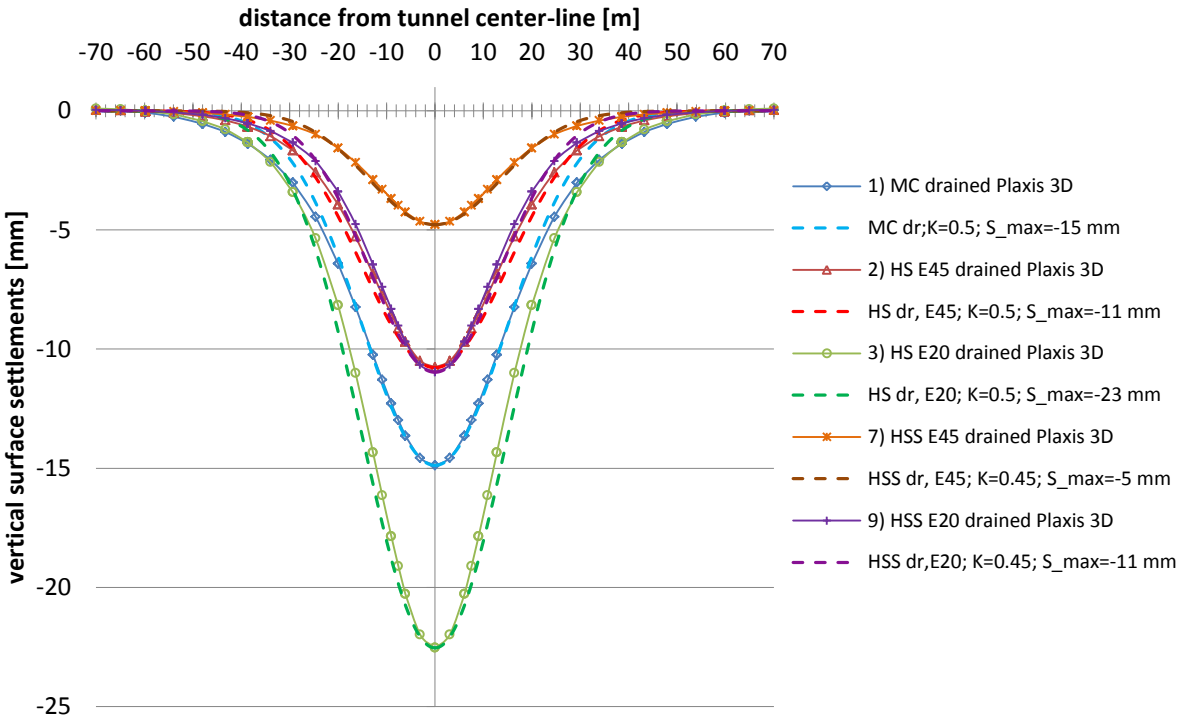

FIGURE 87: TRANSVERSAL SETTLEMENT TROUGH FOR DRAINED ANALYSIS

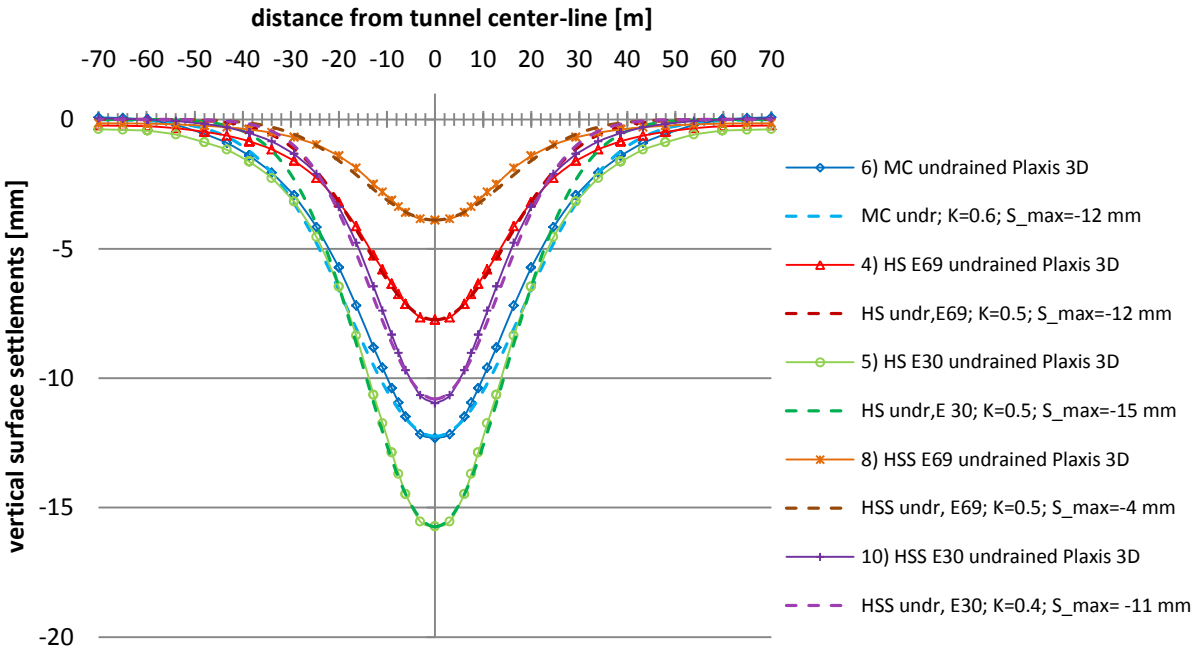

FIGURE 88: TRANSVERSAL SETTLEMENT TROUGH FOR UNDRAINED ANALYSIS

The shape of the surface settlement trough obtained from FE-analysis is matched quite well by the Gaussian distribution curve with a width parameter *K = 0.5*. The HS models 2) and 4) cause a narrower settlement profile compared to the MC model and the HS model with lower stiffness parameters. Generally undrained analysis leads to a wider surface settlement trough. Consideration of small-strain stiffness results in a narrower and steeper settlement trough and is better matched using a width parameter *K = 0.45* for drained analysis. In undrained analysis the settlement profiles resulting from calculations with the Hardening Soil model are wider than predicted by the Gaussian distribution curve.

For FE-analysis with the Hardening Soil model the influence of the initial stresses on the development of the transversal surface settlement trough is investigated and the trough width parameter is adapted to match numerical calculation.

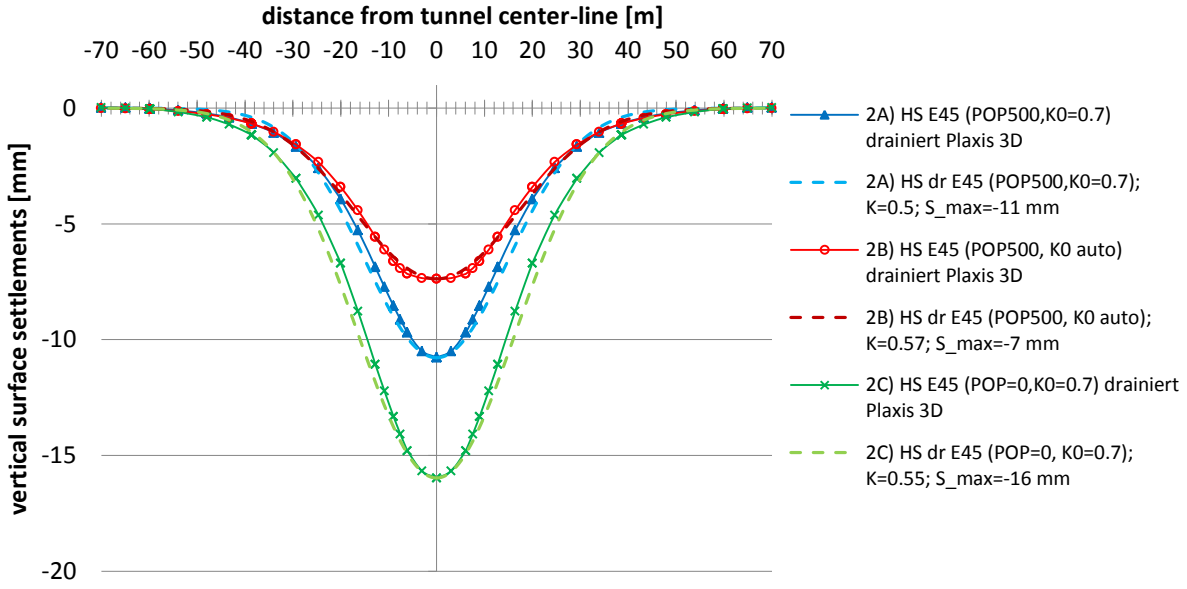

FIGURE 89: INFLUENCE OF INITIAL STRESSES ON THE DEVELOPMENT OF THE TRANSVERSAL SETTLEMENT PROFILE

The deepest and widest settlement trough is generated in the case of no pre-overburden pressure and constant K_0. For *POP = 500 kN/m²* the model with K_0 varying with depth (calculation 2B) leads to a shallower settlement trough compared to a constant value of K_0 (calculation 2A). To match the results of 3D FE-analysis the trough width parameter is adapted, for calculation 2B) *i* is 0.57 and for 2C) *i* is 0.55. Ng and Lee [20] investigated the influence of the initial coefficient of earth pressure at rest K_0 and the stiffness ratio $n=E'_h/E'_v$ on ground deformations and stress-transfer mechanisms in open-face tunnelling. They concluded that a lower initial K_0 for a given *n* leads to a deeper and narrower computed settlement trough [20].

The surface settlements of 2D analyses depend on the used pre-relaxation factors.

In the table below the volume of the surface settlement trough calculated with the maximum settlements above the tunnel axis are compared with the volume of the surface settlement trough generated by the three-dimensional FE-analysis. The volume of the settlement trough obtained from FE-analysis exceeds the respective volume calculated by integration of the Gaussian distribution. The value depends on the horizontal distance from the tunnel axis to the point of inflection *i*, respectively the trough width parameter *K*. In all calculations *K* was assumed to be 0.5. To obtain a wider settlement profile the value has to be increased.

TABLE 47: VOLUME OF THE SURFACE SETTLEMENT TROUGH OBTAINED FROM FE-ANALYSIS COMPARED TO THE RESULT OF THE INTEGRATED GAUSSIAN FUNCTION

	$V_s = \frac{\sqrt{(2 \cdot \pi) \cdot i \cdot S_{max}}}{V_{exc}}$			*Plaxis 3D*		
	GLR	V_s *[m³/m]*	S_{max} *[mm]*	*GLR*	V_s *[m³/m]*	S_{max} *[mm]*
1) MC drained	-1.12%	-0.56	-14.88	-1.21%	-0.61	-16.09
2) HS E45 drained	-0.81%	-0.41	-10.78	-0.99%	-0.49	-13.15
3) HS E20 drained	-1.69%	-0.85	-22.54	-1.65%	-0.82	-21.89
4) HS E69 undrained	-0.58%	-0.29	-7.74	-0.65%	-0.33	-8.68
5) HS E30 undrained	-1.18%	-0.59	-15.73	-1.31%	-0.65	-17.39
6) MC undrained	-0.92%	-0.46	-12.24	-1.06%	-0.53	-14.06
7) HSS E45 drained	-0.36%	-0.18	-4.78	0.33%	0.17	-4.44
8) HSS E69 undrained	-0.29%	-0.15	-3.90	-0.31%	-0.16	-4.18
9) HSS E20 drained	-0.83%	-0.41	-11.00	-0.74%	-0.37	-9.90
10) HSS E30 undrained	-0.81%	-0.41	-10.80	-0.79%	-0.39	-10.50
HS E45 drained POP0, K0=0,7	-1.20%	-0.60	-15.97	-1.27%	-0.63	-16.87
HS E45 drained POP500, K0 auto	-0.55%	-0.28	-7.37	-0.63%	-0.32	-8.41

The results of the undrained calculation with the Hardening Soil model 4) are the best fit of the volume of the surface settlement trough at station MQ1146. For the calculation the unsymmetrical profile from field measurements was used.

TABLE 48: MEASURED VOLUME OF THE SURFACE SETTLEMENT TROUGH AT STATION MQ1146

Field data MQ1146	*GLR*	0,63	%
	V_s	0,32	m³/m
	S_{max} *[mm]*	-7,00	mm

8.2 LONGITUDINAL SURFACE SETTLEMENT TROUGH

Beside the transversal settlement profile, the development of the longitudinal surface settlement trough is important for the prediction of three-dimensional influences of settlements on structures close or directly above the tunnel axis. Attwell and Woodman [18] concluded from several field studies that the longitudinal settlement trough above the tunnel centre line follows a cumulative probability function. Long-term processes, e.g. consolidation, are not considered. [18]

$$S_y = \frac{V_s}{\sqrt{2 \cdot \pi \cdot i}} \cdot \exp\left(-\frac{y^2}{2 \cdot i^2}\right) \cdot \left[G\left(\frac{x - x_i}{i}\right) - G\left(\frac{x - x_f}{i}\right)\right] \quad \textbf{(8.5)}$$

V_s volume loss
i point of inflection of the settlement trough
y transverse distance from the tunnel centre line
x_i start point of the tunnel
x_f final position of the tunnel phase
G probability function $G(\alpha) = \frac{1}{\sqrt{2 \cdot \pi}} \int_{-\infty}^{\alpha} exp\, \frac{-\beta}{2} d\beta$

The results of the probability function *G(α)* can be obtained from standard probability tables or a statistics program. The point of inflection can be assumed to be the same as for the transversal settlement trough. It can

be estimated directly from measurements or adopted from comparable case histories. Values of volume loss are obtained from measurements, case histories or numerical analysis.

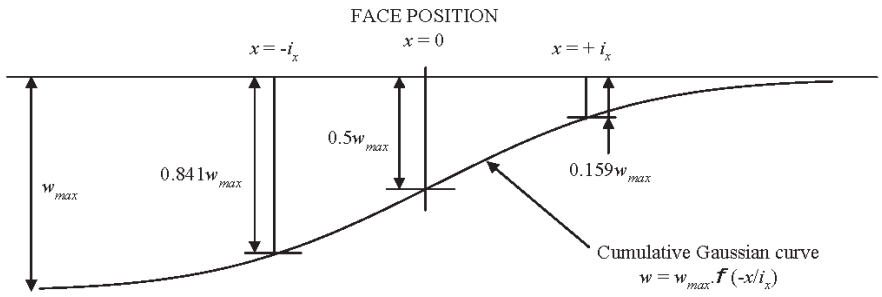

FIGURE 90: CUMULATIVE PROBABILITY FORM OF THE LONGITUDINAL SURFACE SETTLEMENT PROFILE [21]

The settlement directly above the tunnel face is about 50 % of the maximum settlement in the case of open face tunnelling. If significant face support is provided (close face tunnelling) the settlements ahead of the tunnel face are reduced. Mair and Tylor [15] concluded that for shield tunnelling the majority of settlements are associated with the tail void and the settlements above the tunnel face are reduced to 25 % - 30 % of the maximum settlements. For NATM tunnels the magnitude of surface settlements is governed by the length of the unsupported span and placement and hardening of the shotcrete lining. [20]

For the calculation of the longitudinal settlement trough the volume loss obtained from FE-analysis is used. The tunnel was considered semi-infinite to eliminate the influence of boundary conditions. In the figure below, the distribution for a finite and a semi-infinite tunnel by means of the cumulative probability function according to Attwell and Woodman [18] are compared with the results of FE-analysis.

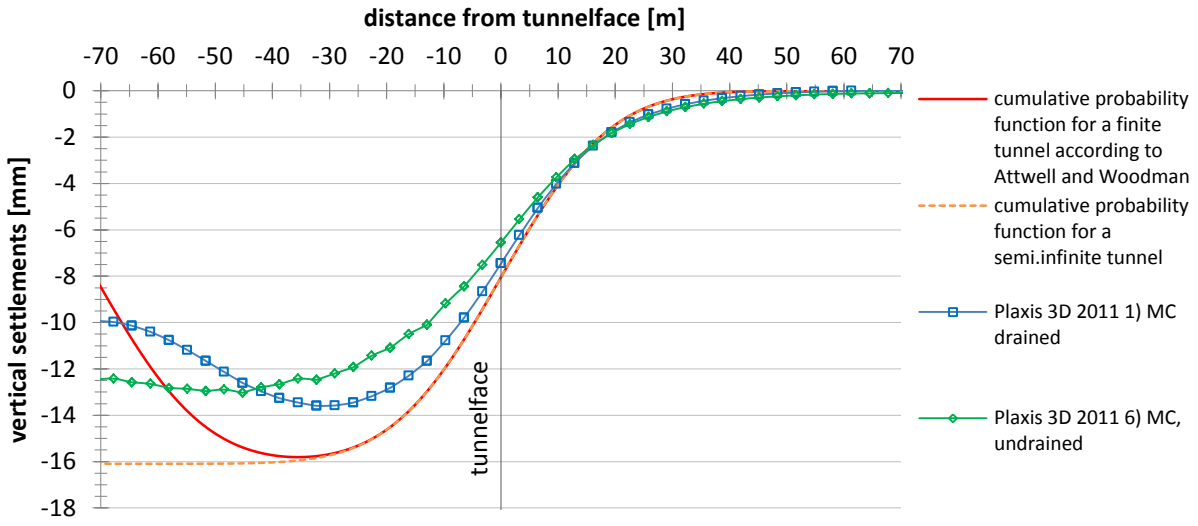

FIGURE 91: INFLUENCE OF BOUNDARY CONDITIONS ON THE SHAPE OF THE CUMULATIVE PROBABILITY FUNCTION

In Figure 91 it is shown, that the definition of a “wished-in-place” area at the beginning and end of the FE-model in drained analyses results in a decrease of surface settlements at the boundaries of the model. In undrained analyses sequential excavation is carried out for the whole tunnel.

The calculation of the longitudinal surface settlement profile with the cumulative probability function according to Attwell and Woodman [18] over-predicts the surface settlements ahead of the tunnel face. The undrained analysis using the Hardening Soil model is the best fitting of the theoretical distribution.

Field data for the development of surface settlements during tunnel construction show a large range in the evaluated section. Hence, a comparison with the results of empirical and FE analysis is not realistic. The tunnel face passes the considered measuring cross-section MQ 1015 on the 25.10.2005 and MQ 1146 on the 16.11.2005. In the figure below the surface settlement trough developed at the time of passage of the tunnel face as well as the settlements at the respective station for the position of the advancing face are displayed.

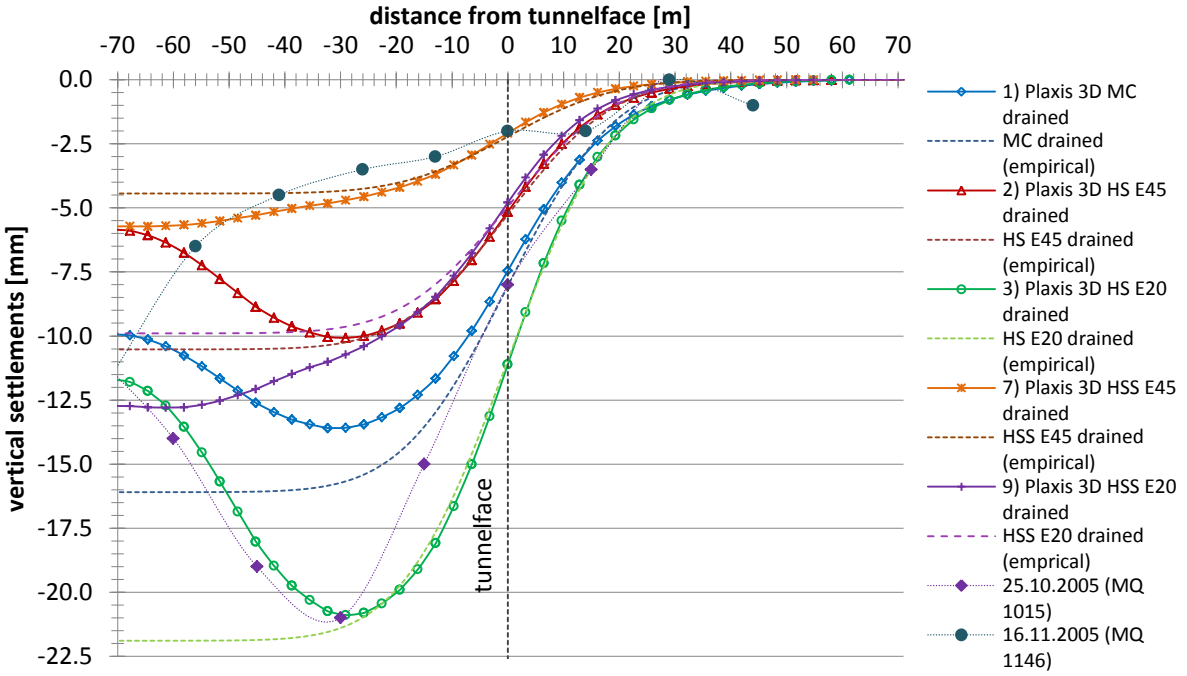

FIGURE 92: LONGITUDINAL SURFACE SETTLEMENT TROUGH FOR DRAINED ANALYSIS

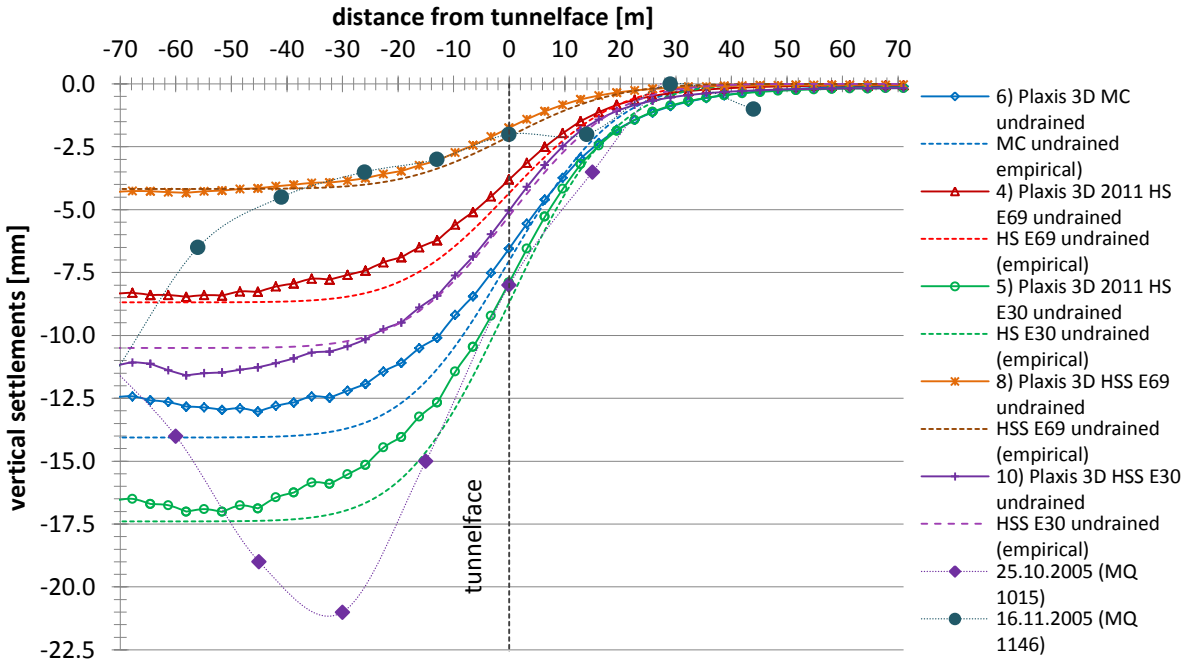

FIGURE 93: LONGITUDINAL SURFACE SETTLEMENT TROUGH FOR UNDRAINED ANALYSIS

The influence of the initial stress distribution on the development of the longitudinal settlement trough corresponds to the influence on the transversal settlement profile. For undrained analyses the cumulative probability curves are a better fit to the longitudinal surface settlement profile in 3D due to sequential excavation also at the tunnel start.

9 COMPARISON WITH FIELD MEASUREMENTS

The results of the numerical calculation are compared with field measurements. Measuring points were installed every 10 - 15 meters at the tunnel cross section and at the surface above the tunnel axis. For the comparison an almost homogeneous section between station 1016 and 1187.5 is chosen with the dominant rock type silt- and claystone and uniform support measures.

The vertical settlements obtained from the three-dimensional numerical calculations and from measurements are summarized in the tables below.

TABLE 49: CROWN AND SURFACE SETTLEMENTS FROM FE-ANALYSIS IN TUNNEL AXIS AT THE BEGINNING/MIDDLE/END OF ONE EXCAVATION LENGTH

	Eoed,ref	*E50,ref*	*Eur,ref*	***crown***			***surface***	
	[MN/m²]	*[MN/m²]*	*[MN/m²]*	*74.00 m*	*74.75 m*	*75.50 m*	*71.00 m*	*74.23 m*
DRAINED								
1) MC	*E=135 MN/m²*			-36 mm	-39 mm	-36 mm	-15 mm	-15 mm
2) HS E45	*45*	*45*	*135*	-27 mm	-32 mm	-27 mm	-11 mm	-11 mm
3) HS E20	*20*	*20*	*60*	-56 mm	-67 mm	-56 mm	-23 mm	-23 mm
7) HSS E45	*45*	*45*	*135*	-17 mm	-21 mm	-17 mm	-5 mm	-5 mm
9) HSS E20	*20*	*20*	*60*	-41 mm	-52 mm	-41 mm	-11 mm	-11 mm
UNDRAINED								
6) MC	*E=135 MN/m²*			-28 mm	-29 mm	-28 mm	-12 mm	-12 mm
4) HS E69	*69*	*69*	*208*	-20 mm	-21 mm	-20 mm	-8 mm	-8 mm
5) HS E30	*30*	*30*	*90*	-40 mm	-42 mm	-39 mm	-16 mm	-16 mm
8) HSS E69	*69*	*69*	*208*	-10 mm	-10 mm	-10 mm	-4 mm	-4 mm
10) HSS E30	*30*	*30*	*90*	-27 mm	-28 mm	-27 mm	-11 mm	-11 mm

TABLE 50: CROWN AND SURFACE SETTLEMENTS FROM ON-SITE MEASUREMENTS IN TUNNEL AXIS

MEASUREMENTS approximately 2 months after the passage of the tunnel face			
SURFACE		**CROWN**	
Station	$u_{y,surface}$ *[mm]*	*Station*	$u_{y,crown}$ *[mm]*
1000	-19	998	-17
1015	-15	1015	-11
1030	-15	1030	-14
1045	-17	1044	-19
1060	-17	1059	-14
1075	-14	1076	-14
1090	-10	1090	-8
1105	-8	1104	-7
1120	-5	1119	-11
1133	-6	1134	-13
1146	-7	1150	-9
1160	-7	1164	-13
1175	-10	1176	-9

Between station 1145 and 1155 the tunnel passes under a mixed water channel, a street and a water pipe. [8] The existing installations could be a possible reason for the unsymmetrical settlement profile. At the building "Seebacher" located near station 1040 maximum settlements of the structure of 2 mm were measured. [8]

In Figure 95 the results of 3D FE-analysis are displayed as the difference between steady state crown settlements and deformations at the time of the passage of the tunnel face.

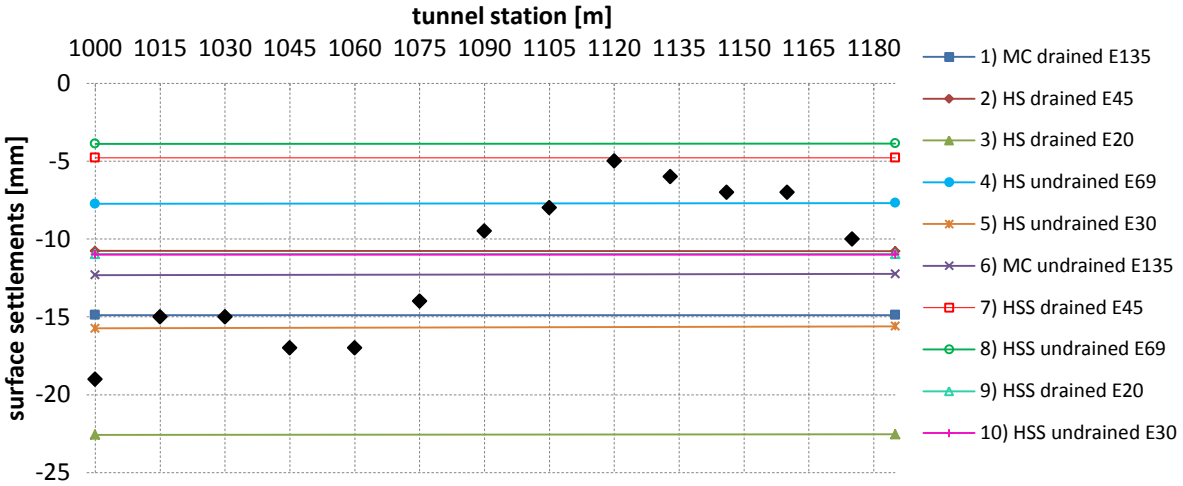

FIGURE 94: COMPARISON OF SURFACE SETTLEMENTS FROM NUMERICAL CALCULATIONS WITH ON-SITE MEASUREMENTS

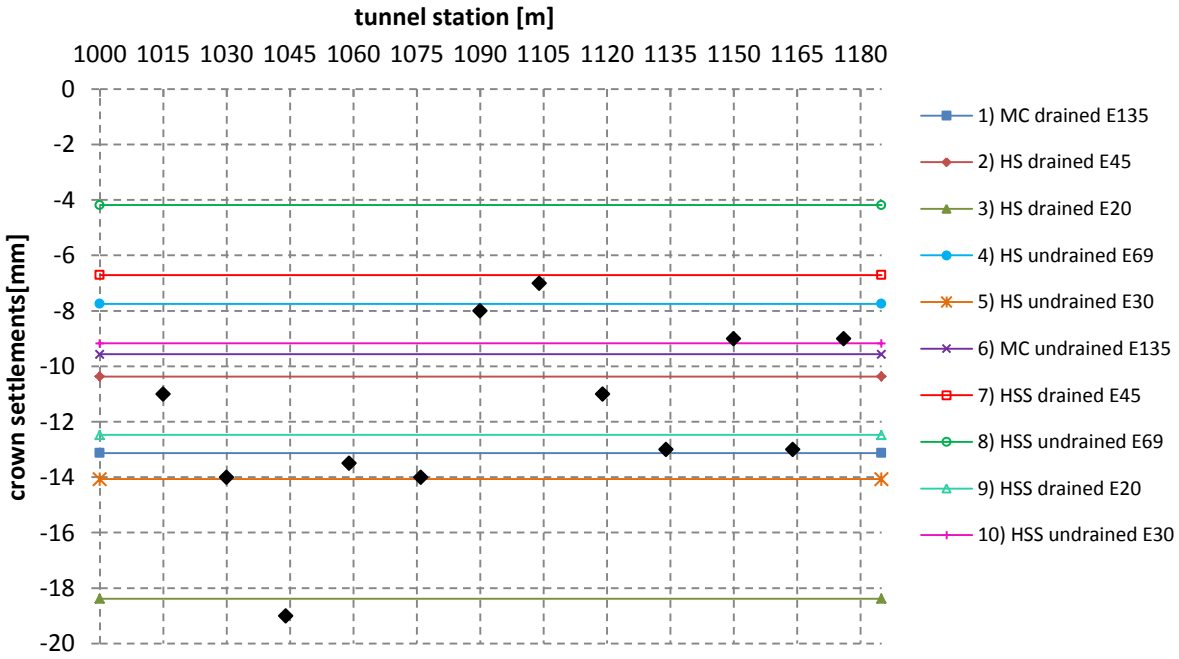

FIGURE 95: COMPARISON OF CROWN SETTLEMENTS FROM NUMERICAL CALCULATIONS WITH ON-SITE MEASUREMENTS

Although the considered section is assumed to be homogeneous along the tunnel axis, measurements of surface settlements and crown settlements are clearly not uniform. The measured surface settlements are between -5 and -19 mm. Crown settlements range from -7 to -19 mm. For all calculation models the predicted surface and crown settlements are within the measured range. Due to the wide scatter of measurements further conclusions are not possible.

10 CONCLUSION

The objective of this thesis was to compare 3D and 2D FE-analysis and empirical methods for the assessment of tunnel induced settlements and internal lining forces. The purpose was to achieve a better understanding of the influencing factors for the determination of the load reduction factor β to account for three-dimensional effects in 2D FE-analysis. The influence of different reference values, constitutive models and the initial stress state was of main interest.

The investigated tunnel "*Mitterpichling Ost*" is an exploratory tunnel with a non-circular cross section. It is excavated as the top heading of the final tunnel using the New Austrian Tunnelling Method. Although ground conditions were assumed homogenous, field measurements of deformations showed a wide scatter. All used soil parameter sets predict settlements within the measured range. It is concluded that in reality ground conditions are inhomogeneous and/or the behaviour is influenced by stratification and discontinuities.

Surface settlements obtained from Finite Element analysis are in good agreement with the empirical distribution by Peck (1969) and Attwell and Woodman (1982).

In 2D FE-analysis two different *MStage*-factors for the pre-relaxation phase and for the installation of the shotcrete lining were used. The load reduction factors were obtained by matching results in 2D and 3D analysis. The load reduction factor *MStage = 1* – β used in the 2D pre-relaxation phase is highly influenced by the used reference value:

- For calibration with crown settlements, steady state conditions are predicted with ± 5%.
- Matching crown settlements in the middle of the excavation length results in large *MStage*-values, 0.65 – 0.80 in drained analysis and 0.55 – 0.63 in undrained analysis. It is influenced by the sagging of the tunnel crown in 3D calculations. The predicted surface settlements are overestimated.
- By matching crown settlements at the end of the excavation length the predicted steady state surface settlements and axial forces are in good agreement with the result of 3D analysis. The applied MStage-values range from 0.63 to 0.78 in drained analysis and 0.56 and 0.64 in undrained analysis.
- The calibration of the 2D model using surface settlements results in the lowest pre-relaxation factors. Because the influence of lining installation on surface deformations is small, a reliable determination of the second pre-relaxation factor and the prediction of steady state settlements are not possible.
- When matching axial forces in 2D and 3D only one *MStage*-value can be determined. The determination of the maximum axial force for calibration is difficult due to the uneven distribution of lining forces in PLAXIS 3D 2011. Reliable results are only obtained for calibration with the final axial forces. Predicted crown and surface settlements are in good agreement for drained analysis.

Generally *MStage* of drained calculations exceed the values of undrained calculations, because volumetric changes are restricted due to incompressible pore water and the applied load reduction factor is related to the magnitude of reference settlements.

The constitutive model influences the load reduction factor. The use of the Mohr-Coulomb model results in lower *MStage*-values than the Hardening Soil model. *MStage* obtained from computations considering small strain stiffness (HS-small) is higher than the corresponding values from the standard HS model. The HS-small model is very sensitive to changes of *MStage*. Different stiffness parameters have little influence on the obtained load-reduction factors unlike an existing pre-overburden pressure. *MStage*-values obtained from the calculations using the HS model with *POP = 500 kN/m²* are larger than for the corresponding computations without *POP*. Stiffer soils result in slightly higher *MStage*-values.

The second load reduction factor is significantly smaller. It is highly influenced by the used reference value in drained analysis. For matching axial forces no second *MStage* can be determined. For matching crown settlements in the middle of the excavation length the values are between 0.30 and 0.35, for all other reference values between 0.10 and 0.20. In undrained analysis the calibrated values range from 0.10 to 0.30.

11 REFERENCES

[1] S. Möller, *Tunnel induced settlements and structural forces in linings,* Bd. Mitteilung 54 des Instituts für Geotechnik, P. Vermeer, Hrsg., Universität Stuttgart, 2006.

[2] Plaxis bv, *PLAXIS 3D 2011 Manual,* Delft, The Netherlands, 2011.

[3] T. Schanz, P. A. Vermeer und P. Bonnier, *The hardening soil model: Formulation and verification,* Rotterdam, The Netherlands: Balkema, 1999.

[4] P. W. Rowe, „The stress-dilatiancy relation for static equilibrium of an assembly of particles in contract," *Proceeding of the Royal Society A. 296,* pp. 500-527, 9 October 1962.

[5] T. Benz, *Small-Strain Stiffness of Soils and its Numerical Consequences,* Bd. Mitteilung 55 des Instituts für Geotechnik, P. Vermeer, Hrsg., Universität Stuttgart, 2007.

[6] H. F. Schweiger, *Computational Geotechnics - Lecture Notes,* Graz: Institute for Soil Mechanics and Foundation Engineering, 2011.

[7] B. Moritz, H. Goldberger und P. Schubert, „Application of the Observational Method in Heterogeneous Rock Mass with Low Overburden," *Felsbau 24,* Nr. 1, pp. 62-72, 2006.

[8] H. Meißner, „Tunnelbau unter Tage, Empfehlungen des Arbeitskreis 1.6 "Numerik in der Geotechnik" Abschnitt 2," *Geotechnik 19,* pp. 99-108, 1996.

[9] GEOCONSULT ZT GmbH, *Geotechnische Dokumentation - Tunnelbau, B1260 Erkundungstunnel Mitterpichling,* ÖBB Bau AG, 2009.

[10] GEOCONSULT ZT GmbH, *Geomechanische Prognose - B1258 Erkundungstunnel Paierdorf,* 2003.

[11] Plaxis bv, *Plaxis 2D 2011 Manual,* Delft, The Netherlands, 2011.

[12] M. Wohlfahrt, *Diplomarbeit: Anhang- Erkunndungstunnel Mitterpichling Ost,* Graz: Institut für Bodenmechanik und Grundbau, 2010.

[13] M. Wehnert, *Ein Beitrag zur drainierten und undrainierten Analyse in der Geotechnik,* Mitteilung 53 des Institut für Geotechnik Hrsg., P. Vermeer, Hrsg., Universität Stuttgart, 2006.

[14] H. F. Schweiger, „Some remarks on Pore Pressure Parameters A and B in Undrained Analyses with the Hardening Soil Model," *Plaxis Bulletin 12,* pp. 6 - 8, 2002.

[15] R. J. Mair und T. R. N., *Theme lecture: Bored tunneling in the urban enviroment,* Hamburg: 14th ISSMFE, 1997.

[16] R. N. Hwang, C. B. Fan und G. R. Yang, „Consolidation settlements due to tunneling," *Proceedings of South East Asian Symposium on Tunneling and Underground Space Development,* pp. 79-86, 18-19 January 1995.

[17] R. B. Peck, „Deep Excavations and Tunneling in Soft Ground," *Proceedings of the 7th International Conference on Soil Mechanics and Foundation Engineering,* pp. 225-290, 1969.

[18] P. B. Attewell und J. P. Woodman, „Predicting the dynamics of ground settlements and its derivatives

caused by tunneling in soil," *Ground Engeneering,* pp. 13-22, November 1982.

[19] K. Schikora und T. Fink, „Berechnungsmethoden moderner bergmännischer Bauweisen beim U-Bahn-Bau," *Bauingenieur 57,* pp. 193-198, 1982.

[20] C. W. W. Ng und G. T. K. Lee, „Three-dimensional ground settlements and stress-transfer mechanisms due to open-face tunnelling," *Canadian Geotechnical Journal 42,* pp. 1015-1029, 2005.

[21] A. G. Bloodworth, *Three-dimensional Analysis of Tunneling Effects on Structures to Develop Design Methods,* University of Oxford, 2002.

[22] G. R. Dasari, C. G. Rawlings und M. D. Bolton, *Numerical Modelling of NATM Tunnel Construction in London Clay,* J. R. Mair und R. N. Taylor, Hrsg., Rotterdam, 1996, pp. 491-496.

12 LIST OF FIGURES

Figure 1: stress-strain relation of an linear-elastic perfectly plastic model [2] 2
Figure 2: Mohr-Coulomb yield surface in principal stress space for cohesionless soil [2] 2
Figure 3: hyperbolic stress-strain relation in a standard drained triaxial test [2] 3
Figure 4: yield surfaces of the Hardening soil model in two-dimensional p'-q plane - activation of deviatoric and volumetric yield surface 4
Figure 5: shear hardening flow rule - mobilization of friction 5
Figure 6: yield contour of the Hardening soil model in three-dimensional principal stress space for cohesionless soil [2] 6
Figure 7: small-strain stiffness reduction curve in the Hardening soil-small model [5] 6
Figure 8: stiffness parameters of the Hardening soil model with small strain stiffness in a triaxial test [2] 7
Figure 9: numerical model 8
Figure 10: cross-section of the tunnel 9
Figure 11: geological profil from station 1100 to 1200 [8] 10
Figure 12: stiffness parameters 11
Figure 13: coefficient of lateral earth pressure at rest K_0 with POP = 500 kN/m² 14
Figure 14: vertical pre-consolidation stress σp in relation to vertical in-situ stress σ [10] 14
Figure 15: initial vertical and horizontal stresses 15
Figure 16: over-consolidation ratio (OCR) 16
Figure 17: 10-noded tetrahedral soil elements (3D) [2] 17
Figure 18: 3D Finite element mesh 18
Figure 19: mesh quality 18
Figure 20: 6-noded soil elements (2D) [5] 19
Figure 21: 2D Finite element mesh 19
Figure 22: sequential excavation in 3D 20
Figure 23: sequential excavation in 2D 20
Figure 24: ratio G/ G_{ur} For drained "wished-in-place" computations using the HS-small model (PLAXIS 2D 2010) 24
Figure 25: LEFT- plastic points for calculation 2) with K_0=0.7 and POP=500 kN/m²; RIGHT - plastic points for calculation 2b) with K_0=0.7 and POP=0 kN/m² 25
Figure 26: position of nodes 25
Figure 27: LE, WIP: distribution excess pore pressures over tunnel length 26
Figure 28: MC, undrained, WIP: distribution excess pore pressures over tunnel length 27
Figure 29: 2D 2010: MC, undrained, WIP: excess pore pressure 27
Figure 30: 3D 2011 (y=71m): MC, undrained, WIP: excess pore pressure 27
Figure 31: 2D 2010: 4) HS, undrained, WIP: excess pore pressure 28
Figure 32: 2D 2010: 8) HSS undrained, WIP: excess pore pressure 28
Figure 33: 2D 2010: 5) HS, undrained, WIP: excess pore pressure 28
Figure 34: 2D 2010: 10) HSS undrained, WIP: excess pore pressure 28
Figure 35: longitudinal effective stresses at the tunnel face for HS-small under drained conditions 31
Figure 36: comparison of the transversal surface settlement trough at station 1015, 1040, 1067 and 1146 with the results of the numerical drained calculations in station 71 32
Figure 37: comparison of the development of surface settlements at station 1015 and 1146 with the results of the numerical drained calculations in station 71 33
Figure 38: development of crown settlement in longitudinal direction for drained FE-analysis 34
Figure 39: comparison of the development of crown settlements at station 1015 and 1146 with the results of the numerical drained calculations in station 71 35
Figure 40: axial forces (drained analysis) 36
Figure 41: bending moments (drained analysis) 36
Figure 42: effective stress paths For undrained analysis with the Mohr-Coulomb model [2] 38
Figure 43: longitudinal total stresses at the tunnel face under undrained conditions 39

Figure 44: comparison of the transversal surface settlement trough at station 1040, 1067 and 1146 with the results of the numerical undrained calculations in station 71 40
Figure 45: comparison of the development of surface settlements at station 1015 and 1146 with the results of the numerical undrained calculations in station 71 41
Figure 46: development of crown settlements in longitudinal direction for undrained FE-analysis 42
Figure 47: comparison of the development of crown settlements at station 1015 and 1146 with the results of the numerical undrained calculations in station 71 43
Figure 48: axial forces (undrained anAlysis) 44
Figure 49: bending moments (undrained anAlysis) 45
Figure 50: development of excess pore pressures over time for consolidation at the end of the excavation (30 days) 47
Figure 51: development of consolidation settlements at the tunnel crown in station 71.0 m (passage of tunnel face in phase 41) 48
Figure 52: development of consolidation settlements at the surface in station 71.0 m (passage of tunnel face in phase 41) 48
Figure 53: comparison crown settlements for undrained analysis after consolidation 49
Figure 54: influence of consolidation on the transversal surface settlement trough 49
Figure 55: MC, undrained: magnitude of settlements resulting from tunnel construction 50
Figure 56: MC, undrained: magnitude of settlements resulting from consolidation 50
Figure 57: development of crown settlements due to coupled consolidation analysis at point (0/26.75/-25) with passage of the tunnel face on day 11/12 50
Figure 58: three-dimensional arching around the unsupported tunnel heading 52
Figure 59: schema of the stress-reduction method [8] 52
Figure 60: schema of stress-reduction method using two β –factors 53
Figure 61: excavation phases for the calibration of the 2D-model using crown settlements 54
Figure 62: crown settlements at station 69.5 for 3D and 2D drained analysis 56
Figure 63: crown settlements at station 69.5 for 3D and 2D undrained analysis 56
Figure 64: crown settlements at station 70.25 for 3D and 2D drained analysis 57
Figure 65: crown settlements at station 70.25 for 3D and 2D undrained analysis 57
Figure 66: comparison of the settlement profile above the tunnel axis from the tunnel crown to the surface obtained from 2D and 3D calculation with the Hardening soil model (E=45 kN/m², drained) 58
Figure 67: over-consolidation ratio above the tunnel axis obtained from 2D and 3D calculation with the Hardening soil model (E=45 kN/m², drained) considering pre-overburden pressure POP 59
Figure 68: axial forces for 3D and 2D analysis with 1) Mohr-Coulomb, drained; calibration using crown Settlements in Station 69.5 m 60
Figure 69: axial forces for 3D and 2D analysis with 2) Hardening soil ($E_{MC}=E_{oed}$), drained; calibration using crown Settlements in Station 69.5 m 60
Figure 70: axial forces for 3D and 2D analysis with 3) Hardening soil ($E_{MC}=E_{ur}$), drained; calibration using crown Settlements in Station 69.5 m 60
Figure 71: axial forces for 3D and 2D analysis with 4) Hardening soil ($E_{MC}=E_{oed}$), undrained; calibration using crown Settlements in Station 69.5 m 61
Figure 72: axial forces for 3D and 2D analysis with 5) Hardening soil ($E_{MC}=E_{ur}$), undrained; calibration using crown Settlements in Station 69.5 m 61
Figure 73: axial forces for 3D and 2D analysis with 6) Mohr-Coulomb, undrained; calibration using crown Settlements in Station 69.5 m 62
Figure 74: axial forces for 3D and 2D analysis with 7) HS-small ($E_{MC}=E_{oed}$), drained; calibration using crown Settlements in Station 69.5 m 62
Figure 75: axial forces for 3D and 2D analysis with 8) HS-small ($E_{MC}=E_{oed}$), undrained; calibration using crown Settlements in Station 69.5 m 63
Figure 76: axial forces for 3D and 2D analysis with 9) HS-small ($E_{MC}=E_{ur}$), drained; calibration using crown Settlements in Station 69.5 m 63

Figure 77: axial forces for 3D and 2D analysis with 10) HS-small (E_{MC}=E_{ur}), undrained; calibration using crown Settlements in Station 69.5 m 64
Figure 78: surface settlements at station 71.0 for 3D and 2D drained analysis 66
Figure 79: surface settlements at station 71.0 for 3D and 2D undrained analysis 66
Figure 80: Axial forces in 3D and 2D (drained analysis) 67
Figure 81: Axial forces in 3D and 2D (undrained analysis) 68
Figure 82: summary of the obtained MStage-values for the calibration of the 2D model using crown and surface settlements and steady state values of axial forces, LEFT: drained calculations, RIGHT: undrained calculations 71
Figure 83: settlement trough above advancing tunnel heading (Attwell et al, 1986) [15] 73
Figure 84: Gaussian distribution curve for transverse surface settlement profile (Peck, 1969) [17] 74
Figure 85: Variation in surface settlement trough width parameter with tunnel depth for tunnels in clays [15] 75
Figure 86: Variation in surface settlement trough width parameter with tunnel depth for tunnels in Sands [15] 75
Figure 87: transversal settlement trough for drained analysis 76
Figure 88: transversal settlement trough for undrained analysis 76
Figure 89: Influence of initial stresses on the development of the transversal settlement profile 77
Figure 90: cumulative probability form of the longitudinal surface settlement profile [21] 79
Figure 91: influence of boundary conditions on the shape of the cumulative probability function 79
Figure 92: longitudinal surface settlement trough for drained analysis 80
Figure 93: longitudinal surface settlement trough for undrained analysis 80
Figure 94: comparison of surface settlements from numerical calculations with on-site measurements 82
Figure 95: comparison of crown settlements from numerical calculations with on-site measurements 82

13 LIST OF TABLES

Table 1: input parameters tunnel cross-section 9
Table 2: Material parameters gathered from geological report from Exploration Tunnel Paierdorf [7] 10
Table 3: soil parameters without consideration of groundwater 12
Table 4: soil parameters with consideration of groundwater 12
Table 5: Material Parameters Lining 16
Table 6: soil parameters without consideration of groundwater 21
Table 7: soil parameters with consideration of groundwater 21
Table 8: WIP, settlements: 1) MC, drained 22
Table 9: WIP, settlements: 2) HS, $E_{MC} = E_{oed}$, drained 22
Table 10: WIP, settlements: 3) HS, $E_{MC} = E_{ur}$, drained 22
Table 11: WIP, settlements: 4) HS, $E_{MC} = E_{oed}$, undrained 22
Table 12: WIP, settlements: 5) HS, $E_{MC} = E_{ur}$, undrained 22
Table 13: WIP, settlements: 6) MC, undrained 22
Table 14: WIP, settlements: 7) HSS, $E_{MC} = E_{oed}$, drained 22
Table 15: WIP, settlements: 8) HSS, $E_{MC} = E_{oed}$, undrained 22
Table 16: WIP, settlements: 9) HSS, $E_{MC} = E_{ur}$, drained 23
Table 17: WIP, settlements: 10) HSS, $E_{MC} = E_{ur}$, undrained 23
Table 18: WIP: Hardening soil vs. HS-small 23
Table 19: ratio of "wished-in-place" settlements: Hardening Soil vs. HS-small ($E_{MC}=E_{oed}$) 24
Table 20: ratio of "wished-in-place" settlements: Hardening Soil vs. HS-small ($E_{MC}=E_{ur}$) 24
Table 21: versions for “wished-in-place” calculation using Linear-Elastic model 26
Table 22: MC, undrained, WIP: excess pore pressures 27
Table 23: soil parameters without consideration of groundwater 30
Table 24: surface settlements from drained FE-analysis 31
Table 25: Crown settlements from drained FE-analysis 33
Table 26: difference between crown settlements at the passage of the tunnel face and steady state crown settlements 34
Table 27: Internal lining forces (drained analysis) 35
Table 28: soil parameters with consideration of groundwater 39
Table 29: surface settlements from undrained FE-analysis 40
Table 30: crown settlements from undrained FE-analysis 42
Table 31: difference between crown settlements at the passage of the tunnel face and steady state crown settlements 43
Table 32: Internal lining forces (undrained analysis) 44
Table 33: relation of excess pore pressures generated by 2D and 3D analysis 47
Table 34: comparison of Surface and crown settlements for undrained analysis and consolidation 48
Table 35: crown settlements due to tunnel excavation and consolidation 51
Table 36: Crown settlements in 3D and 2D with corresponding MStage-values 55
Table 37: surface settlements of 2D calculation calibrated with crown settlements 58
Table 38: Crown settlements in 3D and 2D with corresponding MStage-values 65
Table 39: Axial forces used for calibration with corresponding MStage-values (drained analysis) 67
Table 40: Axial forces used for calibration with corresponding MStage-values (undrained analysis) 68
Table 41: crown and surface settlements in 3D and 2D (drained analysis) 69
Table 42: crown and surface settlements in 3D and 2D (undrained analysis) 69
Table 43: maximum, minimum and mean values of the applied load reduction factors 71
Table 44: MStage-values (Calibration with settlements) 72
Table 45: MStage-values (Calibration with axial forces) 72
Table 46: point of inflection for different trough width parameters 75
Table 47: volume of the surface settlement trough obtained from FE-analysis compared to the result of the integrated Gaussian function 78

Table 48: measured volume of the surface settlement trough at station MQ1146 78
Table 49: crown and surface settlements from FE-analysis in tunnel axis at the beginning/middle/end of one excavation length 81
Table 50: crown and surface settlements from on-site measurements in tunnel axis 81